DIPLOMARBEIT

Westfälische-Wilhelms-Universität Münster

Black Hole Initial Data by a Kerr-Schild Approach

Florian Beyer

2003

Anmerkung

In der vorliegenden Version wurden einige Druckfehler und inhaltliche Ungenauigkeiten beseitigt, so dass sie sich geringfügig von der offiziellen Version unterscheidet, die beim Prüfungssekretariat eingereicht wurde.

Table of Contents

List of Figures

Part I

Introduction

0.1 Introduction & Outline

An isolated system of two interacting bodies has been a fundamental model in many fields of physics. In classical mechanics it is completely integrable for some special types of interactions and gives for example rise to the understanding of the motion of planets around the sun. In quantum mechanics it is the two body hydrogen atom whose theoretical investigation has been the key to understand bound states and it was the starting point to approach even more complicated systems like molecules and crystals. Eventually unbound relativistic two body scattering processes could be investigated which lead to the standard model of particle physics.

All those theories describe the physics in a given flat background spacetime – the Minkowski spacetime (or the Euclidean space plus time as its low velocity approximation). In the general theory of relativity, published by Einstein in 1915, the curvature of spacetime (gravity) itself takes part in the dynamics because it is coupled to the energy and momentum density of all other physical fields (gravity) in *both directions*: spacetime tells the fields how to propagate and the fields tell spacetime how to curve. Hence black holes which are singularities in the curvature surrounded by horizons are not *bodies* in the usual sense; their dynamics are rather those of a continuous non linear medium. Nevertheless one calls the binary black hole system the *two body problem of general relativity* although it is not a very good name. *Bodies* in other theories can be characterized by their individual energies, linear and angular momenta and in special cases one can formulate conservation laws for them which simplifies the integration of the orbits of the bodies. This cannot be done for black holes with the exceptions of infinite separations, if they are very close or if there are Killing fields on the horizons due to a newly developed formalism that assigns energies and momenta to horizons quasi-locally [6]. Notions of energy etc. in general only exist for the whole spacetime, not quasi-locally. So it is very difficult to distinguish between the individual black holes and further gravitational waves and the analysis of the dynamics of a black hole system is very complicated. Only for some highly symmetric and simple cases the curvature spacetime can be integrated analytically, otherwise approximation methods or numerics have to be applied.

To simplify the analysis one considers *vacuum systems* that neglect the influence of all physical fields except for curvature of spacetime itself.

Investigating and hopefully eventually understanding the two body system of general relativity is not only of fundamental theoretical but also of astrophysical interest. Mergers of two black holes are assumed to be one of the strongest and thus most promising sources of gravitational waves which could be detected with (near) future gravitational wave detectors, e.g. GEO600, LIGO and VIRGO [3]. Observations suggest that binary black hole systems are quite frequent in the observable universe, some of them as final products of star evolution, others as super massive objects in the centers of galaxies. However, it is expected that there are many binary black hole systems mostly in circular orbit around each other, slowly getting closer and closer due to the loss of angular momentum (gravitational waves). The wave forms measured by terrestrial detectors should contain some characteristics of the binary black hole system like masses, distances and orbital periods. How the wave forms encode this information can in principle be answered by full numerical binary black hole simulations.

In numerical relativity one wants to solve the binary black hole problem as an initial

value problem. Einstein's equations do not only govern the evolution with time but additionally put certain constraints on the initial data. These constraint equations are mathematically complicated and their character depends very much on the choice of the free part of the initial data. In the current approaches to construct initial data this free part does not only involve the two physical degrees of freedom of gravity but additional gauge degrees. This problem will remain until one is able to find a procedure to identify the physical degrees in general; without this one needs many very different initial data sets to find at least qualitative characteristics, obtain systematic comparisons and interpret the physical content of the constructed data. In this Diploma Thesis I try a new approach to construct binary black hole initial data.

In the first part of the thesis I give a brief introduction to differential geometry, general relativity, the general relativistic initial value problem and the currently most important approaches to the binary black hole initial data problem. In the second part I describe Bishop's ansatz to construct black hole initial data after having introduced Kerr-Schild metrics in general. Then I describe my new idea to construct the free part of these Kerr-Schild initial data, which was worked out only in limited cases before, and discuss the problems with the associated Kerr-Schild constraint equations, problems which are not mentioned in Bishop's original paper. Then I follow two directions to make use of the Kerr-Schild approach. On the one hand this is the linear regime in part three where I apply my ansatz to a specific binary black hole system in first order perturbation theory and discuss evolution of these data, waveforms, masses, apparent horizons etc. Eventually this will lead to a publication together with Edward Seidel and Peter Diener. On the other hand in part four I describe a modification of this Kerr-Schild ansatz invented by Bishop which solves some of the obstacles. With Nigel Bishop I applied it to a special perturbation of the Schwarzschild metric, obtained numerical solutions of the constraint equations and was able to prove that these data are not conformally flat. This part of the work has already been published by Bishop, Michael Koppitz and me. In the last part I summarize and conclude.

Chapter 1

Differential Geometry and General Relativity

1.1 Riemannian Geometry

This section is a very brief and not complete summary of differential geometry. More details can be found e.g. in [52].

I will use Greek indices $\mu, \nu, \ldots$ running from $0, \ldots, n-1$ for an n-dimensional manifold using the Einstein summation convention. The signature of the metric will be assumed to be $(-,+,\ldots,+)$. Sometimes tensorial objects will be referred to by their *abstract* name printed in boldface or if there is no risk of confusion by the components with respect to some coordinate basis.

A **differentiable manifold** M is a topological space which is locally homeomorphic to $\mathbb{R}^n$ (giving rise to local coordinate maps) and has a differentiable structure. Each point $p \in M$ is equipped with a **tangent vector space** $T_p(M)$ and an associated **cotangent space** $T_p^*(M)$ which are n-dimensional vector spaces. With the tensor product it is possible additionally to define **tensor spaces** in each point of M.

A tangent vector defined in $T_p(M)$ for all $p \in U \subset M$ is called a **tangent vector field**, the same for covectors and tensors. To compare the vector field in different points of M one must define a transport from the vector space in one point to the vector space in another point. Assume there is a family of curves $\gamma : [a,b] \to M$ and a one-parameter family of diffeomorphisms $\Theta_t : M \to M$ mapping the point $\gamma(t)$ to $\gamma(t=0)$ with the tangent vector $\mathbf{V} = d\gamma/dt$. The **Lie derivative** is defined as

$$\mathcal{L}_{\mathbf{V}}\mathbf{U} = \lim_{t\to 0} \frac{(\Theta_t)^*\mathbf{U}(t) - \mathbf{U}(0)}{t}$$

where $(\Theta_t)^*$ is the **push-forward**. It turns out that in a coordinate basis this can be written as

$$(\mathcal{L}_{\mathbf{V}}\mathbf{U})^\mu = U^\mu_{,\nu}V^\nu - V^\mu_{,\nu}U^\nu$$

for an arbitrary vector field U where a comma represents the partial derivative with respect to the associated coordinate direction. The Lie derivative behaves like a vector field.

Another way of comparing the vector spaces in each point is to use a **linear connection** which is a linear map $\Gamma : T_p(M) \to T_q(M)$. In terms of this the **covariant derivative** is

defined as

$$U^{\mu}_{;\nu} = U^{\mu}_{,\nu} + \Gamma^{\mu}_{\rho\nu} U^{\nu}.$$

The connection coefficients $\Gamma^{\mu}_{\rho\nu}$ are called **Christoffel symbols** in case of a coordinate basis.

On the manifold we may define a **metric tensor field** $g_{\mu\nu}$ which is a non-degenerate bilinear map $T_p(M)\times T_p(M) \to \mathbb{R}$, the inverse metric $g^{\mu\nu}$ is a bilinear map $T^*_p(M)\times T^*_p(M) \to \mathbb{R}$. The metric can also be regarded as a one-one map $T_p(M) \to T^*_p(M)$, i.e. for each tangent vector field it uniquely defines an associated covector field. The metric gives rise to a scalar product, although it is not necessarily positive definite e.g. in the case of the Lorentzian spacetime manifold.

If the linear connection above is supposed to define a *parallel transport* one has to postulate that $g_{\mu\nu;\rho} = 0$ because this ensures that lengths and relative angles of vectors transported with vanishing covariant derivative along a curve are unchanged. Such a connection is referred to as being **metric**. If one additionally assumes that the connection is **torsion free**, i.e. $\Gamma^{\mu}_{\rho\nu} = \Gamma^{\mu}_{\nu\rho}$ then one obtains

$$\Gamma^{\mu}_{\nu\rho} = \frac{1}{2} g^{\mu\sigma} \left(g_{\nu\sigma,\rho} + g_{\sigma\rho,\nu} - g_{\nu\rho,\sigma} \right). \tag{1.1}$$

On curved manifolds one finds that second covariant derivatives do not necessarily commute but on uncurved ones they do. This defines the **Riemann tensor** (also called curvature tensor) which can then be expressed in terms of the Christoffel symbols. This expression is not important for this work, but can be found in [52]. To formulate the general relativistic field equations, see below, we only need its first contraction, the **Ricci tensor**

$$R_{\mu\nu} = \Gamma^{\alpha}_{\mu\nu,\alpha} - \Gamma^{\alpha}_{\mu\alpha,\nu} + \Gamma^{\alpha}_{\beta\alpha}\Gamma^{\beta}_{\mu\nu} - \Gamma^{\alpha}_{\beta\nu}\Gamma^{\beta}_{\mu\alpha}. \tag{1.2}$$

1.2 General Theory of Relativity

The general theory of relativity (GR) is a generalization of special relativity by considering spacetime as an in general curved pseudo-Riemannian 4-dimensional manifold; the metric is of Lorentzian signature $(-,+,+,+)$. In this document the following physical units will be used

$$c = 1 \quad G = 1$$

with c the velocity of light and G the Newtonian gravity constant.

A dynamical curvature leads to a variation in the physical distance between two events and the shortest curve between them, the geodesic, is not necessarily a straight line – as it is in Minkowski space in Cartesian coordinates – even if there are no forces. This effect is interpreted as gravity. So force free particles take the shortest curves – geodesics – in spacetime

$$u^{\mu}_{;\nu} u^{\nu} = 0$$

with u^{μ} the 4-velocity of a particle; gravity is thus not a force. In a small neighborhood of an event in spacetime, curvature can be neglected and coordinates can be chosen such that a force free particle propagates on a straight world line. Hence special relativity is valid in small – but only in small – regions of spacetime.

Curves $x^\mu(\tau)$ with tangent vector field $V^\mu = dx^\mu/d\tau$ are called

timelike	$g_{\mu\nu}V^\mu V^\nu < 0$
null	$g_{\mu\nu}V^\mu V^\nu = 0$
spacelike	$g_{\mu\nu}V^\mu V^\nu > 0$

Particles with mass bigger than zero travel on timelike curves whereas massless particles like photons follow null curves. Points connected by timelike or null curves are called **causally connected**.

On the other hand all masses and energies create curvature locally satisfying **Einstein's field equations**

$$G_{\mu\nu} = 8\pi T_{\mu\nu} \tag{1.3}$$

with $G_{\mu\nu}$ the **Einstein tensor**

$$G_{\mu\nu} = R_{\mu\nu} - \frac{1}{2}g_{\mu\nu}R$$

and

$$R = g^{\mu\nu}R_{\mu\nu}$$

the **Ricci scalar**. $T_{\mu\nu}$ is called **energy-momentum tensor**. It describes the energy densities and momentum fluxes of all physical fields (other than gravity), e.g. swarms of particles, fluids, electromagnetic fields etc. Because for this document it will be assumed that there are no fields in spacetime, i.e. vacuum, the energy momentum tensor is not be described here, see for instance [37].

1.3 Surfaces and Horizons

1.3.1 Hypersurfaces

Classification Let again M be a n-dimensional differentiable manifold with a metric $\mathbf{g}$ of Lorentzian signature $(-,+,\ldots,+)$. A **hypersurface** [26] is a submanifold Σ with an embedding $\Theta : \Sigma \to M$. The **induced metric** of Σ is the pull-back $\Theta_*\mathbf{g}$.

There exists a form (a covariant vector field) $\mathbf{n} \in T_q^*(M)$, called normal form of Σ, and an associated tangent vector field $N^\mu = g^{\mu\nu}n_\nu$ such that

$$\mathbf{g}(\mathbf{N}, \Theta^*\mathbf{X}) = 0 \quad \forall \mathbf{X} \in T_p(\Sigma).$$

Σ is a $(n-1)$-dimensional hypersurface. It is called a **timelike hypersurface** if $\mathbf{n}$ is spacelike, a **spacelike hypersurface** if $\mathbf{n}$ is timelike and a **null hypersurface** if $\mathbf{n}$ is null. In [26] it is shown that the induced metric of a spacelike hypersurface is positive definite (Riemannian), of a timelike one is Lorentzian (also called pseudo-Riemannian) and of a null hypersurface is degenerated. This means that on a spacelike hypersurface there exists the usual notion of positive definite *lengths*. On null hypersurfaces the normal N^μ is actually tangent to the hypersurface.

Induced metric of spacelike Hypersurfaces Let M be 4-dimensional and Σ spacelike. In each point $q \in \Theta(\Sigma)$ one can find a basis of the tangent space, e.g. $(\mathbf{N}, \mathbf{E}^1, \mathbf{E}^2, \mathbf{E}^3)$ with $\mathbf{E}^1, \mathbf{E}^2, \mathbf{E}^3 \in \Theta^* T_p(\Sigma)$. $\mathbf{N}$ is timelike and $\mathbf{E}^1$, $\mathbf{E}^2$ and $\mathbf{E}^3$ are spacelike and without loss of generality orthonormalized. Assume normalization $g_{\mu\nu}N^\mu N^\nu = -1$. As it is always the case

the metric can also be represented in terms of a basis tetrad and not in terms of a coordinate basis (notation from and more about the tetrad formalism e.g. in [16]), here

$$(g_{(\mu)(\nu)}) = \begin{pmatrix} -1 & 0 & 0 & 0 \\ 0 & 1 & 0 & 0 \\ 0 & 0 & 1 & 0 \\ 0 & 0 & 0 & 1 \end{pmatrix}.$$

This can also be written in the following way, again with respect to a coordinate basis

$$g_{\mu\nu} = -n_\mu n_\nu + E^1_\mu E^1_\nu + E^2_\mu E^2_\nu + E^3_\mu E^3_\nu.$$

Then the induced metric of $\Theta(\Sigma)$ is

$$\gamma_{\mu\nu} = E^1_\mu E^1_\nu + E^2_\mu E^2_\nu + E^3_\mu E^3_\nu = g_{\mu\nu} + n_\mu n_\nu.$$

Raising one index with $g_{\mu\nu}$ gives

$$\gamma^\mu{}_\nu = \delta^\mu{}_\nu + N^\mu n_\nu \tag{1.4}$$

which is a projection operator onto the tangent space of $\Theta(\Sigma)$. Especially $\gamma^\mu{}_\nu N^\nu = 0$.

In the following if there is no risk of confusion, I will not distinguish between $\Theta(\Sigma)$ and Σ anymore, the same for the associated local vector spaces. This makes sense because Θ is an embedding.

Covariant Derivative Because Σ is a differentiable manifold on its own, one can also define a covariant derivative D_μ on it using the same formalism as before. In contrast the covariant derivative on M will be written either with a semicolon or as ∇_μ. For $\mathbf{V} \in T^*_p(\Sigma)$ one finds

$$D_\mu V_\nu = \gamma^\rho{}_\mu \gamma^\sigma{}_\nu \nabla_\rho V_\sigma.$$

Extrinsic Curvature To describe the geometry of the embedded hypersurface Σ, the induced metric related to the geometry from the *intrinsic point of view* is not sufficient for the general relativistic initial value problem, but also not in simpler situations. For instance the 2-cylinder embedded into $\mathbb{R}^3$ is flat in terms of the induced metric. But from the *extrinsic point of view* it is curved because its normal vector changes its direction from point to point. Hence one defines the **extrinsic curvature** (or second fundamental form) of a hypersurface as

$$K_{\mu\nu} = -D_\mu n_\nu.$$

The extrinsic curvature is symmetric, for the position of a hypersurface is determined by the roots of a function $f : M \to \mathbb{R}$ with $n_\mu = (df)_\mu$. Then

$$K_{\mu\nu} = -D_\mu D_\nu f = -D_\nu D_\mu f$$

using the fact that covariant derivatives of a scalar function always commute. The symmetry implies that

$$K_{\mu\nu} = -D_{(\mu} n_{\nu)} = -\frac{1}{2} \mathcal{L}_{\mathbf{n}} \gamma_{\mu\nu} \tag{1.5}$$

where the notation as in eq. (1.7) and **Killing's relation** [52] has been used.

The trace of the extrinsic curvature K, which is defined with respect to $\gamma_{\mu\nu}$,

$$K := -\gamma^{\mu\nu} D_\mu n_\nu = -\gamma^{\mu\nu} \nabla_\mu n_\nu \tag{1.6}$$

is the Σ-divergence of the normal vector field. In adapted coordinates of the space-time-split, see section 2.2.3, it becomes obvious that $\gamma^{\mu\nu}$ is a three-by-three tensor with only *spatial* components and K is the **mean curvature** of Σ. In general a surface with extremal volume has vanishing mean curvature, thus hypersurfaces with $K = 0$ are called **maximal slices**.

1.3.2 Spacelike 2-Surfaces

The intersection S of two unequal null hypersurfaces in a 4-dimensional manifold M is called a **spacelike 2-surface**, i.e. it has two non-vanishing linearly independent null normals $\mathbf{n}_1$, $\mathbf{n}_2$. Assume the normalization $g^{\mu\nu} n_{1\mu} n_{2\nu} = -1$. Then as above

$$g_{\mu\nu} = -2(n_{1(\mu} n_{2\nu)}) + E^1_\mu E^1_\nu + E^2_\mu E^2_\nu$$

using the usual short notation

$$n_{1(\mu} n_{2\nu)} := \frac{1}{2}(n_{1\mu} n_{2\nu} + n_{1\nu} n_{2\mu}). \tag{1.7}$$

The induced metric of S

$$q_{\mu\nu} = E^1_\mu E^1_\nu + E^2_\mu E^2_\nu = g_{\mu\nu} + 2(n_{1(\mu} n_{2\nu)})$$

is positive definite.

1.3.3 Trapped Surfaces and Apparent Horizons

As S is always embedded into a spacelike hypersurface Σ which in turn is embedded into M, either the pull-back of $\mathbf{n}_1$ to Σ or the pull-back of $\mathbf{n}_2$ to Σ is an outgoing normal of S with respect to Σ, the other one an ingoing normal. One defines the **outgoing and ingoing divergence** (in analogy with the trace of the extrinsic curvature of a spacelike hypersurface eq. (1.6)) of a spacelike 2-surface S as

$$\Theta_1 := \frac{1}{2} q^{\mu\nu} n_{1\mu;\nu}, \quad \Theta_2 := \frac{1}{2} q^{\mu\nu} n_{2\mu;\nu}.$$

respectively. If $\Theta_1 < 0$ and $\Theta_2 < 0$ then Σ is called a **trapped surface**. If the divergence of the outgoing null normal vanishes (i.e. S is as above a surface of extremal volume, a **minimal surface**) and that of the ingoing one is negative then Σ is a **marginally trapped surface**. If S on Σ is the outermost marginally trapped surface it is an **apparent horizon**.

If again we assume coordinates adapted to the space-time-split, see section 2.2.3, the outgoing normal of S with $\gamma_{ij} n^i n^j = 1$ has to fulfill the following equation [54]

$$D_i n^i - K_{ij} n^i n^j + K = 0 \tag{1.8}$$

on a given spatial hypersurface Σ with Latin spatial indices running from 1 to 3. There exists a function $f : \Sigma \to \mathbb{R}$ such that $S = \{p \in \Sigma | f(p) = 0\}$. Then eq. (1.8) is an elliptic equation for f and can be used to numerically find marginally trapped surfaces on each spacelike hypersurface during an evolution [49].

(Marginally) trapped surfaces are of great importance not only from the numerical point of view. They also define a local concept of horizons and find an application in the singularity theorems of Penrose and Hawking [26].

1.4 Black holes and Horizons

Stationary isolated black hole solutions of Einstein's field equations eq. (1.3) in vacuum $T_{\mu\nu} = 0$ were found by Schwarzschild (static, spherically symmetric) and Kerr (stationary, axisymmetric), see [16]. Solutions of the coupled Maxwell-Einstein equations lead to charged black holes. Because a macroscopic body, especially a star after gravitational collapse, should have zero net charge, we will only consider black holes without an electromagnetic field. Historically the Schwarzschild solution was the first solution of Einstein's field equations found. It represents a non-rotating black hole and is the unique spherical symmetric solution due to Birkhoff's Theorem. The Kerr solution is axisymmetric, stationary and algebraically special which was the way it was found by Kerr [28]. In case of axisymmetry there is no uniqueness theorem but there is a conjecture by Penrose that eventually all gravitational collapses settle down to the Kerr metric. This is one of the arguments which lead Penrose to the so-called **Penrose inequality** [40].

In general non stationary spacetimes one needs a generalized definition of black holes. Both the Schwarzschild and the Kerr metric possess a horizon which *sucks all light* so indeed they are *black* from a point of view of an observer at infinity. In general dynamic situations black holes are hence defined by the existence of such horizons.

An important horizon concept is the apparent horizon defined in Section 1.3.3. It represents a spacelike 2-surface having an outgoing null normal with vanishing divergence. As was stated above it can be found on each spacelike hypersurface (if it exists) by means of eq. (1.8). Singularity theorems state that the existence of a trapped surface on one spacelike hypersurface leads to a singularity on a future spacelike hypersurface under certain conditions [26].

Another (more famous) notion of a horizon is the **event horizon**. It is defined as the border of that region of spacetime M that is causally connected with null infinity $\mathcal{J}^+$. This means that light rays originating from outside the event horizon can reach $\mathcal{J}^+$ and from inside cannot. Hawking [26] was able to show that the volume of an event horizon always increases to the future. To find the intersection of the event horizon and a spacelike hypersurface one needs the metric of the full spacetime in principle up to $\mathcal{J}^+$ and follow light rays to see if they can reach $\mathcal{J}^+$. Recently more sophisticated techniques to find event horizons were developed and applied [20].

One can show that apparent horizons always lie inside (or in the stationary case coincide with) the intersection of an event horizon with a given spacelike hypersurface. Hence the first ones can be considered as a stronger indicators of an gravitational collapse. As an example, a (marginally) trapped 2-surface can be thought of as a closed constant phase surface of an electromagnetic wave at a given instant of time which was sent outwards but

nevertheless immediately (marginally) shrinks. Having the same picture in mind in the case of a spatial section of an event horizon then it means that the electromagnetic wave is able to propagate outwards some finite distance and then collapses, never reaching $\mathcal{J}^+$.

Chapter 2

The General Relativistic Initial Value Problem

2.1 Initial Value Problems in Physics

A dynamical system given in terms of a system of partial differential equations can be treated as an **initial value problem** which is a special form of the **Cauchy problem** [27]. Therefore one has to choose an initial surface Σ_0 together with **initial data** (also called Cauchy data) which describe the initial state of the system completely. For the **initial value problem** where **time** is the evolution parameter, Σ_0 is necessarily spacelike. If Σ_0 is sufficient to determine the data one the whole spacetime by means of **evolution equations** it is called a **Cauchy surface**. In this chapter I will not discuss the mathematics of the Cauchy problem which can be found in [27], but rather the physics.

Following [55] the simplest initial value problem in physics is that of classical mechanics. In the Hamiltonian formulation the data describing the state of the system at a given time (i.e. on a given Cauchy surface) are the generalized positions and the conjugate momenta of the bodies. There may be constraints for the data, e.g. a gas which is confined to a box, but there are no further *principle* constraints on the possible states of the system. The equations of motion which guide the evolution of the system with time are Hamilton's equations.

Equivalent is the Lagrangian formulation. The state of the system is described by generalized positions and their first time derivatives of each body. One can also say that one has to know the position of each body in the system at a time $t = t_0$ and at $t = t_0 + dt$. Hence one also calls the Lagrangian formulation **thin sandwich initial value problem** because data has to be specified on two very close hypersurfaces. The equations of motion which govern the evolution are the Lagrange equations.

Another equivalent approach is to define an action function $S = \int_{t_0}^{t_1} L dt$. The principle of least action (**Hamilton's principle**) states that a systems evolves such that the action is extremal. Here like in the thin sandwich approach the state of the system is given by the generalized positions of each body at the times t_0 and t_1. In the limit $t_1 = t_0 + dt$ we recover the thin sandwich approach.

An example of a theory with *fundamental* constraints on the data and gauge freedoms is the following formulation of electrodynamics in Minkowski space. The problem can be

simplified by looking at vacuum electrodynamic fields $\rho = j^i = 0$. At the initial time t_0, i.e. the initial Cauchy surface Σ_0, let the data be $\mathbf{E}, \phi, \mathbf{A}$ where $\mathbf{E}$ is the electric field, ϕ is the scalar potential and $\mathbf{A}$ is the vector potential. The constraint

$$\text{div}\mathbf{E} = 0$$

must be satisfied for all points in Σ_0. The evolution equations are

$$\partial_t \mathbf{E} = \Delta \mathbf{A} - \text{grad div}\mathbf{A} \quad \text{Maxwell eq.}$$
$$\partial_t \mathbf{A} = -\mathbf{E} - \text{grad}\phi \quad \text{Definition of the potentials.}$$

There is no evolution for ϕ until one fixes the residual gauge freedom. For example one can choose the Lorentz gauge

$$0 = \partial_\mu A^\mu = \partial_t \phi - \text{div}\mathbf{A}.$$

So in principle one can integrate from one spacelike hypersurface to the next. The constraint propagates due to the evolution equations, i.e.

$$\partial_t \text{div}\mathbf{E} = 0.$$

2.2 The Initial Value Problem in General Relativity

2.2.1 Foliation

Let M be the spacetime manifold together with the metric $g_{\mu\nu}$. General relativistic equations are invariant under general coordinate transformations (diffeomorphisms). So one is free to choose a one parameter family of spacelike hypersurfaces

$$\Sigma_{t'} := \{p \in M_4 | t(p) = t'\}$$

with a function $t : M \to \mathbb{R}$. This means that $(dt)_\mu$ is timelike. Such a differentiable global time function exists if and only if the spacetime is stably causal [52]. Define

$$n_\mu = -\alpha (dt)_\mu$$

with the **lapse function** α such that

$$g^{\mu\nu} n_\mu n_\nu = -1.$$

Furthermore we define another timelike vector field **t** by

$$t^\mu (dt)_\mu = 1$$

so that in general it can be written as

$$t^\mu = \alpha n^\mu + \beta^\mu$$

with the **shift vector** field β tangent to the slice

$$\beta^\mu n_\mu = 0$$

and $n^\mu = g^{\mu\nu} n_\nu$.

2.2.2 Gauß-Codacci-equations

The in- and extrinsic geometric quantities of a spacelike hypersurface Σ are directly connected with the geometry of the embedding spacetime M. This is what the **Gauß-Codacci-equations** [26] state

$$\begin{aligned}
\gamma^{\mu'}_{\ \mu}\gamma^{\nu'}_{\ \nu}\gamma^{\rho'}_{\ \rho}\gamma^{\sigma'}_{\ \sigma}\,{}^4R_{\mu'\nu'\rho'\sigma'} &= {}^3R_{\mu\nu\rho\sigma} + K_{\rho\mu}K_{\sigma\nu} - K_{\sigma\mu}K_{\rho\nu} \\
\gamma^{\mu'}_{\ \mu}\gamma^{\nu'}_{\ \nu}\gamma^{\rho'}_{\ \rho}n^{\sigma}\,{}^4R_{\mu'\nu'\rho'\sigma} &= D_\nu K_{\mu\rho} - D_\mu K_{\nu\rho} \\
\gamma^{\mu'}_{\ \mu}n^{\nu}\gamma^{\rho'}_{\ \rho}n^{\sigma}\,{}^4R_{\mu'\nu\rho'\sigma} &= \mathcal{L}_{\mathbf{n}}K_{\mu\nu} + \frac{1}{\alpha}D_\mu D_\nu\alpha + K_{\mu\rho}K^{\rho}_{\ \nu}.
\end{aligned} \tag{2.1}$$

All other contractions vanish.

2.2.3 Adapted coordinates

For practical purposes it is convenient to introduce coordinates which are adapted to the foliation. One chooses the parameter t of the family of the spacelike hypersurfaces Σ_t as the time coordinate and uses arbitrary coordinates x^i independent of t with $i = 1, 2, 3$ as spatial coordinates on each Σ_t.

Then

$$(n_\mu) = (-\alpha, 0, 0, 0).$$

From $t^\mu\nabla_\mu t = 1$ we get $t^\mu = (1, t^i)$ and as a special choice of coordinates we set

$$(t^\mu) = (1, 0, 0, 0).$$

From $n_\mu\beta^\mu = 0$ we obtain

$$(\beta^\mu) = (0, \beta^i).$$

The projection operator eq. (1.4) has the property

$$\gamma^\mu_{\ i} = \delta^\mu_i + n_i n^\mu = \delta^\mu_i$$

and the induced metric is

$$\gamma_{ij} = g_{ij}.$$

From $n_\mu = g_{\mu\nu}n^\nu$ it is obtained that

$$(g_{\mu\nu}) = \begin{pmatrix} -\alpha^2 + \beta^2 & \beta_1 & \beta_2 & \beta_3 \\ \beta_1 & \gamma_{11} & \gamma_{12} & \gamma_{13} \\ \beta_2 & \gamma_{21} & \gamma_{22} & \gamma_{23} \\ \beta_3 & \gamma_{31} & \gamma_{32} & \gamma_{33} \end{pmatrix}. \tag{2.2}$$

The inverse metric tensor is

$$(g^{\mu\nu}) = \begin{pmatrix} -\frac{1}{\alpha^2} & \frac{\beta^1}{\alpha^2} & \frac{\beta^2}{\alpha^2} & \frac{\beta^3}{\alpha^2} \\ \frac{\beta^1}{\alpha^2} & \gamma^{11} - \frac{\beta^1\beta^1}{\alpha^2} & \gamma^{12} - \frac{\beta^1\beta^2}{\alpha^2} & \gamma^{13} - \frac{\beta^1\beta^3}{\alpha^2} \\ \frac{\beta^2}{\alpha^2} & \gamma^{21} - \frac{\beta^2\beta^1}{\alpha^2} & \gamma^{22} - \frac{\beta^2\beta^2}{\alpha^2} & \gamma^{23} - \frac{\beta^2\beta^3}{\alpha^2} \\ \frac{\beta^3}{\alpha^2} & \gamma^{31} - \frac{\beta^3\beta^1}{\alpha^2} & \gamma^{32} - \frac{\beta^3\beta^2}{\alpha^2} & \gamma^{33} - \frac{\beta^3\beta^3}{\alpha^2} \end{pmatrix} \tag{2.3}$$

which follows most easily from $n^\mu = g^{\mu\nu}n_\nu$. There we used

$$\beta_i := \gamma_{ij}\beta^j, \quad \beta^2 := \gamma_{ij}\beta^i\beta^j.$$

Hence the line element can be written as

$$ds^2 = -\alpha^2 dt^2 + \gamma_{ij}\left(dx^i + \beta^i dt\right)\left(dx^j + \beta^j dt\right).$$

On a given Σ_t, i.e. $dt = 0$, it is thus confirmed that the metric is fully given by γ_{ij}. Hence it is also called the **spatial metric** or simply **3-metric**. The meaning of the shift vector becomes clear from Fig. 2.1. If an observer travels from coordinate position (t, x^i) to $(t + dt, x^i)$,

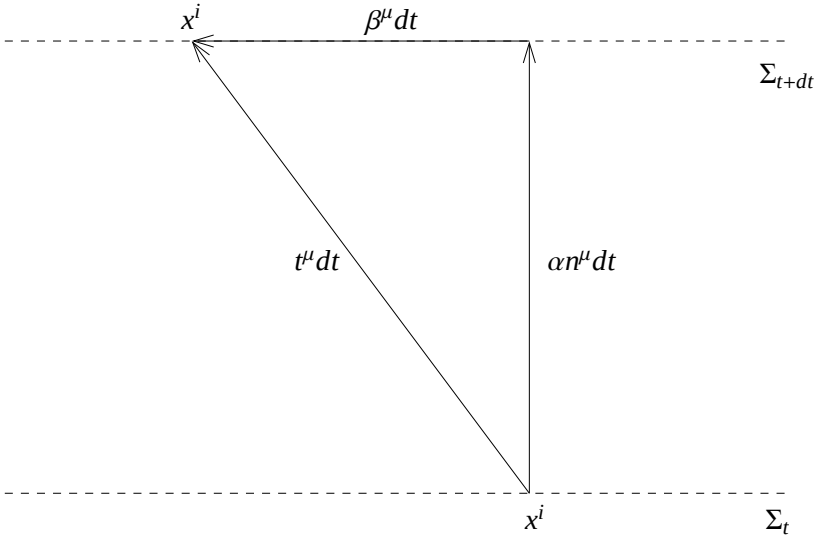

Figure 2.1: Meaning of the shift vector β

his spatial position changes by $\beta^i dt$ with respect to an observer traveling along n^μ. That is where the name of the shift vector comes from. If he travels from (t, x^i) to $(t + dt, x^i - \beta^i dt)$, i.e. along n^μ (so $dx^i = -\beta^i dt$), it takes the proper time αdt which clarifies the meaning of the lapse function.

The extrinsic curvature eq. (1.5) becomes (linearity of the Lie derivative)

$$K_{ik} = -\frac{1}{2}\left(\mathcal{L}_{\frac{1}{\alpha}\mathbf{t}}\gamma_{ik} - \mathcal{L}_{\frac{1}{\alpha}\beta}\gamma_{ik}\right)$$

and one can show that this is

$$K_{ik} = \frac{1}{2\alpha}\left(\mathcal{L}_\beta\gamma_{ik} - \partial_t\gamma_{ik}\right). \tag{2.4}$$

2.2.4 3+1-Decomposition of the Vacuum Einstein Equations

By means of the Gauß-Codacci-equations eq. (2.1), it is possible to construct the 3+1-decomposition of the Ricci tensor and thus of the vacuum Einstein's field equations eq. (1.3).

We assume adapted coordinates as described in the last section. From the equation ${}^4G^{00} = {}^4R^{00} = 0$ and ${}^4G^{0i} = {}^4R^{0i} = 0$ respectively we get four equations

- **Hamiltonian constraint:**
$$ {}^3R + K^2 - K^{ik}K_{ik} = 0 \tag{2.5} $$
- **Momentum constraints:**
$$ D_j\left(K^{ij} - \gamma^{ij}K\right) = 0 \tag{2.6} $$

which are constraints on the data on a spacelike hypersurface because they only contain first time-derivatives. From ${}^4R^{ij} = 0$ one obtains six evolution equations for the extrinsic curvature

$$ \begin{aligned} \partial_t K_{ik} = {} & \mathcal{L}_\beta K_{ik} - D_i D_k \alpha \\ & + \alpha\left({}^3R_{ik} + KK_{ik} - 2K_{ij}K^j{}_k\right) \end{aligned} \tag{2.7} $$

and from eq. (2.4) additionally six evolution equations for the 3-metric

$$ \partial_t \gamma_{ik} = \mathcal{L}_\beta \gamma_{ik} - 2\alpha K_{ik}. \tag{2.8} $$

The evolution equations allow to integrate the data from one slice to the next in time. In eq. (2.5) to (2.8) all indices are lowered and raised with γ_{ik}.

Thus for the general relativistic Cauchy problem we can take γ_{ik}, K_{ik}, α and β^i as the data. On the initial hypersurface Σ_0 these data have to fulfill the four constraint equations eq. (2.5) and eq. (2.6). Then eq. (2.7) and eq. (2.8) can be used to integrate γ_{ik} and K_{ik} to Σ_{dt}. On Σ_{dt} the **Bianchi Identities** [52] guaranty that the constraints are fulfilled again, i.e. like in electrodynamics the constraints propagate [55]. But Einstein equations do not evolve α and β^i; as in electrodynamics we have to invent further **gauge conditions** for these quantities. The simplest would be **geodesic gauge**

$$ \alpha = 1, \quad \beta^i = 0 $$

which turns out to be a bad choice in practice. In general we must choose $\alpha = \alpha(t, x^i)$ and $\beta = \beta(t, x^i)$ to obtain the complete data on all slices.

It is not obvious from the beginning what the physical content of a data set is. It is mostly not clear how and if at all the curvature of spacetime changes if specific components of γ_{ij} or K_{ij} are varied. This is the case because in the twelve components of a data set there are not only the two physical degrees of freedom but further gauge degrees: on each slice there is the freedom of arbitrary spatial coordinate transformations and the choice of a foliation.

2.3 Variational Principle and ADM-Energy

In [19] and more detailed in [52] they show that Einstein's field equations (especially in the case of vacuum) can be derived using a variational principle by means of the Lagrangian density

$$ \mathcal{L}_G = \sqrt{-g}R $$

where g is the determinant of the spacetime metric $g_{\mu\nu}$. With this and the Euler equations, Einstein's vacuum field equations can be obtained straight forwardly.

The 3+1-split obtained in Section 2.2.4 can now be derived by means of the Hamiltonian formalism. After having chosen a foliation of spacetime, with the Gauß-Codacci equations eq. (2.1) the dynamical relevant part of the Lagrange density is

$$\mathcal{L}_G = \sqrt{\gamma}\alpha({}^3R + K^2 - K^{ik}K_{ik})$$

with the dynamical variables γ_{ij}, $\partial_t\gamma_{ij}$, α and β_i. As usual one can show that total divergence terms can be discarded because they lead to integrals over the boundaries of the considered spacetime region with Gauß's Theorem and converge to zero for boundaries at infinity if there is a certain fall-off rate, see [52] for deeper discussion. The conjugate momentum of γ_{ij} turns out to be

$$\pi^{ij} = \frac{\partial\mathcal{L}_G}{\partial(\partial_t\gamma_{ij})} = \sqrt{\gamma}(K^{ij} - K\gamma^{ij}),$$

the conjugate momenta of α and β^i vanish identically. Then the Hamiltonian density is given by

$$\mathcal{H}_G = \pi^{ij}\partial_t\gamma_{ij} - \mathcal{L}_G.$$

The canonical equations are equivalent to the evolution equations (2.7) and (2.8)

$$\dot{\gamma}_{ij} = \frac{\partial\mathcal{H}_G}{\partial\pi^{ij}} \quad \text{and} \quad \dot{\pi}^{ij} = -\frac{\partial\mathcal{H}_G}{\partial\gamma_{ij}}$$

and the variations of $\mathcal{H}_G$ with respect to α and β_i lead to the constraint equations (2.5) and (2.6) respectively. For the dynamical fields $\gamma_{ij}(x^i, t)$ and $\pi^{ij}(x^i, t)$ as solution of the evolution equations, it turns out that $\mathcal{H}_G$ vanishes identically and thus cannot be interpreted as an energy density of spacetime. In [19] they point out that the main reason for this difference to other dynamical theories in physics are the second spatial partial derivatives of the dynamical variables in the Lagrange density which can be eliminated by partial integration if the fields vanish outside some finite domain. This is not the case in gravity and for the total integrated energy the following surface integral is left

$$E = \lim_{r\to\infty} \oint \alpha\,\sqrt{\gamma}\,\gamma^{ij}\left(\gamma_{ik,j} - \gamma_{ij,k}\right) dS^k \tag{2.9}$$

in asymptotically flat Cartesian Minkowski coordinates. It is easy to check that it is equal to the mass of an isolated source, e.g. a Schwarzschild black hole. Moreover the total energy is a conserved quantity of evolution. There is no notion of total energy in spacetimes which are not asymptotically flat.

In [38] they found the same result for the energy of spacetime but used the linearized field equations in the asymptotically flat region far away from the sources to change the volume integral of the total energy into a surface integral in analogy with Minkowski electrodynamics. To honor the authors of this article, one calls E the **ADM-energy**. They were also able to define ADM-momentum and ADM-spin analogously.

Chapter 3

Black Hole Initial Data

The aim of this diploma thesis is the construction of black hole initial data for the general relativistic initial value problem. This chapter gives a brief overview of existing methods and solutions of this problem, more details and further references are given in [17].

3.1 Basic aspects

Above it was described how to set up the initial value problem in general relativity. To summarize, we have to choose a foliation of spacetime where the spacelike hypersurfaces are labeled by a time function t. So there is a unique identification of the initial spacelike hypersurface Σ_0 on which we want to give initial data. On all Σ_t one picks adapted coordinates, i.e. spacelike coordinates independent of time. As initial data we give the 3-metric γ_{ij} and the extrinsic curvature K_{ij} fulfilling the constraint equations (2.5) and (2.6) on Σ_0.

As was described before, the first problem arises already at this point beside the formal difficulty of the constraint equations: It is not clear which of the twelve components of γ_{ij} and K_{ij} are to be specified freely and which are to be taken as solutions of the constraint equations to obtain physically relevant initial data sets. The mathematically elegant **York-Lichnerowicz conformal decomposition** described in the next section gives a recipe for this and has been used more or less for all black hole initial data types currently existing. Bishop [10] introduced a different method which will be used in this thesis and will be described in Part II.

In principle all initial data sets where trapped surfaces or apparent horizons exist at given positions and one can show asymptotical flatness are *valid* black hole initial data sets. In analogy with multiple body problems in other physical theories, one additionally wants to control the physical parameters of each *body*, e.g. masses, momenta and spins. In general relativity this is not possible in general as was mentioned before because there is no clear definition of quasi-local properties of spacetime. But at least one wants some approximated control if the black holes are separated some finite coordinate distance and exact control if the separation is infinite. In the case of black holes there is the hope that the dynamical horizon framework [6] can guide a way out of this dilemma because at least if there are Killing fields present on the horizons, one can give a meaning to energies and spins of horizons quasi-locally. But it seems to take some time until these ideas are accepted in the numerical relativity community.

In practical numerical computations, the black holes must be set not too far away from each other because of the limited grid space in the computer memory and not too close because otherwise one misses the interesting non-linear dynamical phase. But this means that in general one does not have full control over the physics of the initial data sets one wants to construct. Especially it is an unsolved question how *artificial* an initial data set is compared to astrophysically realistic scenarios. One believes that in an *astrophysically relevant* spacetime there are stationary black holes orbiting each other in a large orbit, losing energy by weak gravitational waves, getting closer and finally plunging to form a Kerr black hole. Initial data sets in numerical relativity are supposed to model this system *somewhere in the middle* of the evolution for the reasons given above. If it is not possible to find such initial data sets there is little hope that the computed gravitational waveforms are related to those that will be measured by the gravitational wave detectors.

3.2 York-Lichnerowicz Conformal Decomposition

As was described before the conformal decomposition is a mathematically elegant way of choosing the free part of the initial data and obtaining the rest from the constraint equations. It will only be described very briefly here because I will not use it for this thesis. Further details are in [55] and [17].

The basic idea is to write the 3-metric as

$$\gamma_{ij} = \psi^4 \overline{\gamma}_{ij} \tag{3.1}$$

with the **conformal metric** (also called **background metric**) $\overline{\gamma}_{ij}$ and the **conformal factor** ψ. The constraints can be expressed by means of conformal quantities alone; for example the Hamiltonian constraint eq. (2.5) becomes

$$\overline{\Delta}\psi - \frac{1}{8}\psi\overline{R} - \frac{1}{8}\psi^5 K^2 + \frac{1}{8}\psi^5 K_{ij}K^{ij} = 0 \tag{3.2}$$

where quantities with a bar mean quantities defined by the conformal metric. This is a quasi-linear elliptic equation for ψ if K_{ij} is a known function on the initial slice, e.g. in the case of time-symmetry, see below. So if one chooses the conformal metric as the free part of the initial data one obtains an equation which can be solved as a boundary value problem for the conformal factor ψ. In more general situations one must find an additional conformal decomposition of the extrinsic curvature, see [17].

3.3 Conformally flat black hole initial data

The most simple non-trivial ansatz for $\overline{\gamma}_{ij}$ is the Euclidean 3-metric

$$\overline{\gamma}_{ij} = \mathrm{diag}(1, 1, 1)$$

in *Cartesian coordinates* and this ansatz has been used in most existing initial data sets up to now. Initial data with this property are called **conformally flat**.

3.3.1 Time-symmetric black hole initial data

The trivial solution of the momentum constraints at $t = 0$ is $K_{ij} = 0$, **time-symmetry**. Then one is left with the Laplace equation for ψ for which existence and uniqueness of solutions were proved for von-Neumann and Dirichlet boundary conditions [27]. The spherically symmetric solution on the domain $\mathbb{R}^3 - \{0\}$ with $\psi \to 1$ for $r \to \infty$ is

$$\psi(r) = 1 + \frac{M}{2r}.$$

Hence the physical induced metric γ_{ik} of the initial slice can be computed using eq. (3.1) and with $K_{ik} = 0$ and additional choices of the gauge functions the full Cauchy data on the initial slice is known. It is the $t = 0$-slice of the Schwarzschild solution in isotropic coordinates [17] and the line element of the induced metric can be written as

$$ds_3^2 = \left(1 + \frac{M}{2r}\right)^4 \left(dr^2 + r^2 d\theta^2 + r^2 \sin^2\theta d\phi^2\right). \tag{3.3}$$

Such slices – sometimes calls isotropic slices – are isometric under the transformation

$$r \to \left(\frac{m}{2}\right)^2 \frac{1}{r}$$

which is a reflection on the 2-sphere $r = m/2$, called **throat** or **Einstein-Rosen bridge** [21]. Fig. 3.1 shows the embedding diagram of eq. (3.3) holding ϕ fixed. So isotropic slices is are

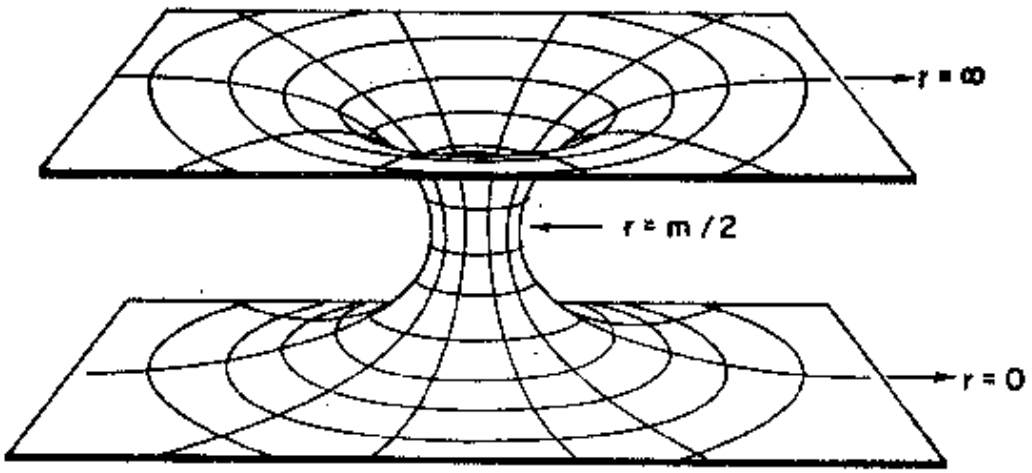

Figure 3.1: Isometric embedding of eq. (3.3) with $d\phi = 0$ into $\mathbb{R}^3$, taken from [15]

not simply connected and consist of two isometric asymptotically flat ends for $r \to \infty$ and $r \to 0$.

Because Laplace's equation is linear and homogeneous

$$\psi(r) = \sum_{i=1}^{N} \left(1 + \frac{M_i}{2|\mathbf{r} - \mathbf{r}_i|}\right)$$

is a solution of eq. (3.2) for $K_{ik} = 0$ on the domain $\mathbb{R}^3 - \{\mathbf{r}_1, \ldots, \mathbf{r}_n\}$ and one obtains multiple black hole initial data, called **Brill-Lindquist-data** [15]. Multiple Brill-Lindquist black holes have the property that each black hole has a throat, i.e. the metric gets asymptotically flat in the limit $\mathbf{r} \to \mathbf{r}_i$, but there is no isometry on each of the $N + 1$ parts (if there are N black holes). Misner [37] constructed time-symmetric data which only consist of two isometric asymptotically flat pieces.

Hence, what may seem surprising at the beginning, conformally flat slices with their mathematical simplicity are adapted to black holes, at least in the case of time-symmetry.

3.3.2 Maximal Initial Data

One wants to go beyond time-symmetry and chooses maximal slices (Section 1.3.1), i.e. $K = 0$, with conformally flat 3-metrics. One is left with an elliptic equation for ψ eq. (3.2) and the momentum constraints which are linear in the conformal extrinsic curvature without any ψ-terms, see [17]. Bowen and York [12] found an explicit solution of the momentum constraints for the conformal extrinsic curvature in terms of parameters which reduce to the associated ADM-quantities for large separations. Due to the linearity of the momentum constraints these solutions for K_{ij} can be superposed analogously to Misner data and one obtains the same topology, specifying isometry conditions at the throats of each black hole as boundary conditions.

Those spherical boundaries are complicated to implement numerically. **Puncture data** (found by Brandt, Brügmann [13]) use the same solution of the conformal momentum constraint, but a simpler superposition of the solutions for K_{ij}, eventually constructing data with the same topology as the Brill-Lindquist ones. Due to the so called *puncture trick* to solve the Hamiltonian constraint eq. (3.2), i.e. separating singular parts of the conformal factor from regular ones, one is left on the one hand with a regular elliptic equation and on the other hand one does not need a boundary condition at the punctures at all – where the whole asymptotically flat end of each black hole is compactified.

3.3.3 Problems

Up to now conformally flat black hole initial data sets are those which are used most intensively for black hole evolutions. But there are a lot of problems. Conformally flat initial data work quite well in the time-symmetric case where for large separations each black hole becomes Schwarzschild. But [17] it turns out that isolated black holes with non-vanishing Bowen-York spin are not stationary. Following a conjecture by Penrose gravitational collapse eventually leads to a Kerr black hole. If this is true Bowen-York initial data cannot represent black holes arising from an isolated gravitational collapse and are thus not astrophysically realistic. Further more Garat and Price [23] showed that – at least under certain assumptions – there exist no conformally flat slices of the Kerr metric. So one states that black holes with a Bowen-York spin have an artificial gravitational wave content. It is not known if it is significant or maybe leaves the computational grid quickly. Nevertheless, systematic comparisons can only be done if several initial data sets exist with similar features but very different ways of construction.

3.4 Other approaches

Since conformal flatness of black hole initial slices does not seem to be applicable to general situations people invented other approaches.

An important first step was in [14] where a not conformally flat slice of the Kerr metric was superposed with a Brill wave according to the York-Lichnerowicz conformal decomposition. These data were evolved and analyzed.

Furthermore there are Post-Newtonian methods that treat the black holes as point particles taking post-Newtonian corrections to the Newtonian gravitational potential and orbits into account [50]. It was shown that there are deviations from conformal flatness already in second post-Newtonian order, see e.g. [18]. The post-Newtonian approximation is certainly valid if the holes are far separated, that is in the early phase of a binary inspiral, but breaks down for close orbits.

Another class of initial data leading to not conformally flat data naturally is based on Kerr-Schild metrics and is the topic of this diploma thesis. The construction procedure introduced in this thesis is a generalization of an ansatz invented by Bishop et al. [10]. It uses an alternative approach to the standard York-Lichnerowicz conformal decomposition (Section 3.2) to hopefully obtain significantly different data than the currently mostly used ones and learn about black hole initial data sets in general by systematic comparisons. That is why I decided to not work on Matzner's Kerr-Schild approach [36] which constructs Kerr-Schild initial data by means of the conformal decomposition.

Part II

Kerr-Schild Initial Data for Black Holes

Chapter 4

Kerr-Schild metrics

4.1 Definition

Let M be a differentiable manifold. In 1962, Trautmann [51] considered metrics of the type

$$g_{\mu\nu} = \eta_{\mu\nu} - 2Vl_\mu l_\nu \tag{4.1}$$

with a null vector field $l_\mu =: g_{\mu\nu}l^\mu$, i.e.

$$l^\mu l_\mu = g_{\mu\nu}l^\mu l^\nu = 0, \tag{4.2}$$

a scalar function V and $\eta_{\mu\nu}$ the metric of (flat) Minkowski space. Metrics of the type (4.1) are called **Kerr-Schild metrics** and in this chapter we will explore its algebraic, geometric and physical properties. More details can be found in [31] and [25]. In the next chapter this knowledge will be used to construct black hole initial data. If **g** is given then one can choose coordinates with respect to **g** on M such that e.g.

$$(\eta_{\mu\nu}) = \mathrm{diag}(-1, 1, 1, 1)$$

which will be called (Cartesian) **Kerr-Schild coordinates** (t, x, y, z) (or sloppily Cartesian coordinates). In later applications we will often use spherical Kerr-Schild coordinates (t, r, θ, ϕ) where $(\eta_{\mu\nu}) = \mathrm{diag}(-1, 1, r^2, r^2 \sin^2\theta)$.

Kerr-Schild metrics are adapted to black hole physics because the Kerr solution of Einstein's vacuum equations (Section 4.4) can be brought to the Kerr-Schild form and Kerr-Schild metrics are invariant under Lorentz boosts. Furthermore they have nice algebraic and geometric features.

4.2 Algebraic Features of Kerr-Schild Metrics

In [31] they list the following relations which I have checked by straight forward computations. First it is

$$l_\mu = g_{\mu\nu}l^\nu = \eta_{\mu\nu}l^\nu, \tag{4.3}$$

which implies that

$$0 = l^\mu l_\mu = g_{\mu\nu}l^\mu l^\nu = \eta_{\mu\nu}l^\mu l^\nu \tag{4.4}$$

so that indices of l_μ can be raised and lowered by both metrics with the same result and it is a null vector field with respect to both. Furthermore we have

$$g^{\mu\nu} = (\eta^{-1})^{\mu\nu} + 2Vl^\mu l^\nu$$

where $g^{\mu\nu}$ is the inverse tensor of $g_{\mu\nu}$ and $(\eta^{-1})^{\mu\nu}$ is the inverse tensor of $\eta_{\mu\nu}$, i.e.

$$(\eta^{-1})^{\mu\nu}\eta_{\nu\rho} = \delta^\mu_\rho.$$

From this one finds

$$\det g = \det \eta \tag{4.5}$$

so in Cartesian Kerr-Schild coordinates the determinant is -1. These relations are helpful for algebraic calculations, for instance computing the Kerr-Schild Ricci tensor. One the one hand many terms drop out because l_μ is a null vector field, on the other hand it is $\Gamma^\mu{}_{\nu\mu} = 0$ due to eq. (4.5) in the case of Cartesian Kerr-Schild coordinates.

4.3 Geometry of the null vector field l_μ

As before let $(M, g_{\mu\nu})$ be a spacetime with a Kerr-Schild metric $g_{\mu\nu}$ with Cartesian Kerr-Schild coordinates x^μ. Relative angles and lengths of the tangents vectors of the coordinate lines in each points are given by $\mathbf{g}$. Let $(\tilde{M}, \eta_{\mu\nu})$ be Minkowski space in Cartesian Minkowski coordinates $\tilde{x}^\mu$, i.e. the coordinates are defined by η in the same way.

On $\tilde{M}$ introduce a vector field $\tilde{l}_\mu$ such that on $\tilde{M}$ with respect to $\tilde{x}^\mu$ it has the same components as the Kerr-Schild null vector field l_μ on M with respect to x^μ.

It can be shown by simple algebra that for the 4-acceleration of l_μ one gets

$$a_\mu = l_{\mu;\nu}l^\nu = \tilde{l}_{\mu,\nu}\tilde{l}^\nu$$

where a semicolon represents the covariant derivative with respect to $g_{\mu\nu}$ and a comma that with respect to $\eta_{\mu\nu}$ which in these coordinates reduces to a partial derivative. A vector field is called geodesic if $a_\mu = 0$. Thus l_μ is geodesic in M if and only if $\tilde{l}_\mu$ is geodesic in $\tilde{M}$. The **divergence** is

$$\Theta := \frac{1}{2}l^\mu_{;\mu} = \frac{1}{2}\tilde{l}^\mu_{,\mu},$$

twist

$$\omega^2 := \frac{1}{2}l_{[\mu;\nu]}l^{\mu;\nu} = \frac{1}{2}\tilde{l}_{[\mu,\nu]}\tilde{l}^{\mu,\nu}$$

and **shear**

$$\sigma^2 := \frac{1}{2}l_{(\mu;\nu)}l^{\mu;\nu} - \Theta^2 = \frac{1}{2}\tilde{l}_{(\mu,\nu)}\tilde{l}^{\mu,\nu} - \Theta^2$$

where the last equality only holds if l_μ is geodesic; for the meaning of these geometric quantities see [52]. In summary the geometry of l_μ in M is very closely related to the geometry of $\tilde{l}_\mu$ in $\tilde{M}$. This fact will be used later for the construction of Kerr-Schild initial data. If there is no risk of confusion I will write l_μ instead of $\tilde{l}_\mu$ and speak of l_μ in M and l_μ in $\tilde{M}$ respectively.

The relations above hold without any field equations. If the Kerr-Schild metric additionally fulfills the vacuum Einstein equations $R_{\mu\nu} = 0$ it can be shown that l_μ is geodesic, shear free and it is a double degenerate principal null congruence of the Weyl tensor, i.e.

$$C_{\mu\nu\rho[\sigma}l_{\tau]}l^\nu l^\rho = 0$$

in agreement with the Goldberg-Sachs-Theorem [31]. This implies that spacetimes with Kerr-Schild metrics fulfilling Einstein's vacuum equations are of Petrov Type II or Petrov Type D.

4.4 Kerr solution

Kerr-Schild metrics are interesting for black hole physics because the Kerr solution can be brought to this form by means of a coordinate transformation. The Kerr solution represents a stationary rotating black hole and is – following a conjecture by Penrose – believed to be the final state of any gravitational collapse.

In ingoing Kerr-Schild coordinates (see [37], Exercise 33.8) it is

$$g_{\mu\nu} = \eta_{\mu\nu} - 2Vl_\mu l_\nu$$

with the (flat) Minkowski metric

$$(\eta_{\mu\nu}) = \mathrm{diag}(-1, 1, 1, 1),$$

the scalar function

$$V = -\frac{MR^3}{R^4 + a^2z^2}, \tag{4.6}$$

the Kerr-Schild null vector field

$$(l_\mu) = \left(-1, -\frac{Rx + ay}{R^2 + a^2}, -\frac{Ry - ax}{R^2 + a^2}, -\frac{z}{R}\right) \tag{4.7}$$

using the radial functions

$$R = \sqrt{\frac{1}{2}\left(\rho^2 - a^2 + \sqrt{(\rho^2 - a^2)^2 + 4a^2z^2}\right)} \tag{4.8}$$

and

$$\rho = \sqrt{x^2 + y^2 + z^2}.$$

In fact, R is the Boyer-Lindquist radial coordinate. The Kerr solution in Boyer-Lindquist coordinates can be found in [37].

4.5 Kerr-Schild Slices

Use again the notation: $i = 1, 2, 3$ spatial components, 0 time component of a tensor.

A **Kerr-Schild slice** is a 3-dimensional hypersurface defined by constant Kerr-Schild time. Using the normalization $l^0 = 1$ it is spacelike as long as

$$g^{\mu\nu}(dt)_\mu(dt)_\nu = g^{00} = -1 + 2V(l^0)^2 = -1 + 2V < 0$$

which is the case if $V < 1/2$ (fulfilled for instance in eq. (4.6)).

In the case of the Schwarzschild metric the relation of Kerr-Schild slices and slices of constant Schwarzschild time can be demonstrated in the Kruskal diagram, see [38] (Chapter 31) and Fig. 4.1. Slices of constant Schwarzschild time are straight lines through the origin

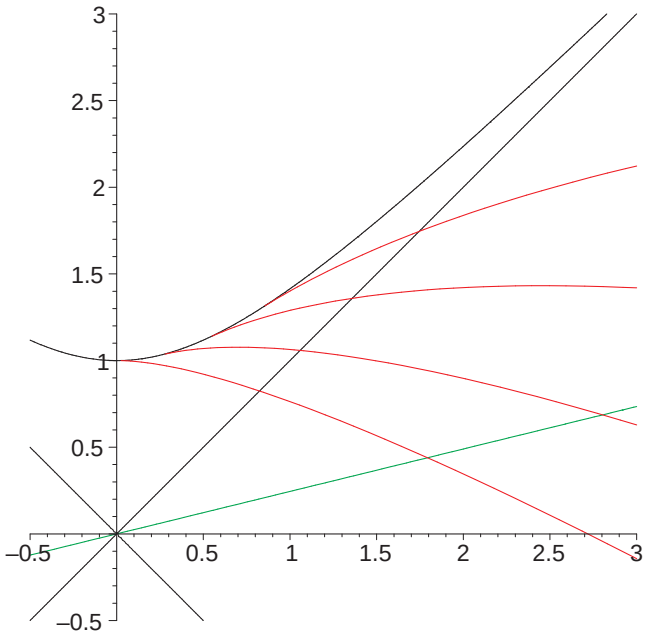

Figure 4.1: Kerr-Schild and Schwarzschild slicings of Schwarzschild metric in Kruskal Coordinates

of the Kruskal coordinate frame, i.e. they avoid the singularity whereas Kerr-Schild slices hit the singularity. The latter ones do not have two asymptotically flat ends as for instance maximal slices (Section 3.3.2). So a Kerr-Schild ansatz does not allow to cover the whole black hole manifold but rather its *astrophysically relevant* part associated with gravitational collapse [37].

The induced metric on a Kerr-Schild slice is (eq. (2.2))

$$\gamma_{ik} = g_{ik} = d_{ik} - 2V l_i l_k, \tag{4.9}$$

where in Cartesian Kerr-Schild coordinates x^i

$$(d_{ik}) = \mathrm{diag}(1, 1, 1)$$

is the Euclidean metric. If one defines

$$\tilde{l}^i := (d^{-1})^{ij} l_j$$

with $(d^{-1})^{ij}$ the inverse tensor of d_{ij} one obtains for the inverse tensor of γ_{ik}

$$(\gamma^{-1})^{ij} = (d^{-1})^{ij} + \frac{2V}{1-2V} \tilde{l}^i \tilde{l}^j.$$

When we set

$$\overline{l^i} := (\gamma^{-1})^{ij} l_j$$

then we find

$$\overline{l}^i = \frac{1}{1-2V}\tilde{l}^i$$

and (assuming again that $l^0 = 1$)

$$\overline{l}^i l_i = \frac{1}{1-2V}, \quad \tilde{l}^i l_i = 1. \tag{4.10}$$

From eq. (2.3) it follows for the lapse

$$g^{00} = -\frac{1}{\alpha^2} \quad \Leftrightarrow \quad \alpha = \frac{1}{\sqrt{1-2V}} \tag{4.11}$$

which is always well defined if $V < 1/2$, i.e. the Kerr-Schild slice is spacelike, see above. From the same equation one infers that

$$g^{0i} = \frac{\beta^i}{\alpha^2} \quad \Leftrightarrow \quad \beta^i = \frac{2V}{1-2V}\, l^i \tag{4.12}$$

where again

$$l^i = g^{i\mu} l_\mu.$$

Eq. (2.8) can then be used to compute the extrinsic curvature K_{ik} on the Kerr-Schild slice; the result is in [39] for instance.

Chapter 5

Kerr-Schild Initial data

5.1 Basic Idea

In Chapter 3 important examples of multiple black hole initial data were discussed. Here I describe an ansatz leading to a significantly different type of initial data. It was created by Bishop et al. [10] and was generalized by Moreno et al. [39]. I invented a modification to construct the free part of the initial data for general multiple black hole systems and worked it out in this thesis.

Suppose we have a 4-dim. manifold $(M, g_{\mu\nu})$ representing multiple black holes which can be covered with a single coordinate map. Ignoring possible problems with that, it is clear that it is too restrictive to assume that $g_{\mu\nu}$ is of the Kerr-Schild type for all times. Instead Bishop et al. in [10] made the following ansatz for the metric and coordinates

$$g_{\mu\nu}(t, x^i) = \underbrace{\eta_{\mu\nu}(x^i) - 2V(t, x^i) l_\mu(t, x^i) l_\nu(t, x^i)}_{\text{Kerr-Schild part}} + t^2 \sum_{s=0}^{\infty} t^s j^{(s)}_{\mu\nu}(x^i) \tag{5.1}$$

with $j^{(0)}_{\mu\nu}(x^i) \neq 0$. This implies that the spacelike hypersurface Σ_0 defined as the $t = 0$-surface – the initial slice – is a Kerr-Schild slice (Section 4.5) and the Cauchy data on it, i.e. both the induced 3-metric γ_{ik} and the extrinsic curvature K_{ik}, are determined by the Kerr-Schild part of $g_{\mu\nu}$ alone. This is the case because the metric eq. (5.1) deviates in second order of t. Thus there are no j-terms in the constraint equations on Σ_0 and we are left with a Kerr-Schild initial data problem, (hopefully) benefiting from those algebraic simplifications and nice geometric and physical properties described in Section 4.2. Consequently as soon as the data and coordinates on the initial slice are fixed, the initial lapse and shift are also determined by this ansatz. Anyway, because these are only gauge functions one is free to choose anything else.

It is not clear if Σ_0 is a Cauchy surface, i.e. if the data on Σ_0 determines the data in the whole spacetime M uniquely. It is even unknown if M is globally hyperbolic, i.e. if this spacetime admits a Cauchy surface at all. It is a further assumption that Σ_0 is a Cauchy surface otherwise it is of no or limited meaning to look for initial data on Σ_0. For further discussions on that see [52].

Following [10] the idea is to specify the Kerr-Schild null vector field l_μ at $t = 0$ as the free part of the initial data because there is hope that it is sufficient alone to determine the

physics of Σ_0 a priori in some sense. These are two free functions because on the one hand one has the freedom to normalize l_μ such that $l^0 = 1$ and on the other hand there is the null condition $\eta_{\mu\nu} l^\mu l^\nu = 0$ or equivalently

$$d_{ij} l^i l^j = 1. \tag{5.2}$$

The constraint equations then turn out to be sufficient in principle to compute V, $\partial_t l_\mu$ and $\partial_t V$ so that γ_{ik} and K_{ik} on Σ_0 can be obtained (Section 4.5). This is true because there are only four unknown functions V, $\partial_t V$ and two components of $\partial_t l_i$ because $\partial_t l^0 = 0$ and

$$d_{ij} l^i \partial_t l^j = 0, \tag{5.3}$$

where eq. (5.2) was used and because in adapted coordinates the Euclidean metric d_{ij} is always time independent.

In all initial data construction procedures there is the further freedom of how to choose boundary conditions for the constraint equations, see below, and hence the same free part of the initial data – here l_μ – can lead to different initial data eventually.

5.2 Coordinates and Auxiliary Spaces

There exists a conceptional problem not only with this specific Kerr-Schild ansatz which is to be discussed now.

When one wants to construct initial data on an initial slice Σ_0 (not limited to Kerr-Schild slices at the moment) one has to specify free parts of the initial data and has to use the constraint equations to obtain the rest. This free part consists of components of tensor fields – in my case the Kerr-Schild null vector field l_μ – which are defined with respect to some coordinates x^μ. But these coordinates on Σ_0 are undefined until the induced metric γ_{ik} on Σ_0 is known. The metric γ_{ik} in turn is not known until the full initial data problem is solved. So in summary, independently of the actual construction procedure, the free part of the initial data is always given in a *meaningless* way at the beginning; not before the full initial data problem is solved one can check if the ansatz makes sense.

So how to deal with this dilemma? For example in the description of puncture data [13] they talk of "a problem in $\mathbb{R}^3$" and mean that they take the three spatial coordinates which will later cover the initial slice in the black hole manifold as a triple of numbers in the auxiliary space $\mathbb{R}^3$ without physical meaning at the beginning. For the Kerr-Schild ansatz there is a similar way. As was described in Sec. 4.3 the Kerr-Schild null vector field has analogous geometric properties in the Kerr-Schild spacetime $(M, g_{\mu\nu})$ and in Minkowski spacetime $(\tilde{M}, \eta_{\mu\nu})$. For the ansatz eq. (5.1) this correspondence only holds on the initial slices Σ_0 in M and $\tilde{\Sigma}_0$ in $\tilde{M}$ respectively (and maybe for some very small times $t \ll 1$). So to prescribe the free part of the Kerr-Schild initial data we give l_μ on the 3-manifold $\tilde{\Sigma}_0 \subset \tilde{M}$ with coordinates x^i with respect to the induced metric $(d_{ik}) = \mathrm{diag}(1, 1, 1)$. The reason why we stay in the 4-dimensional picture and talk of $\tilde{\Sigma}_0$ in Minkowski space and not simply of $\mathbb{R}^3$ as in [13] is that we want to give a 4-dimensional construction procedure for l_μ, see below. Once l_μ is given on $\tilde{\Sigma}_0$ with the metric d_{ik} one solves the constraint equations to obtain γ_{ik} and K_{ik} and interprets the spatial part of the Minkowski coordinates as the spatial part of the Kerr-Schild coordinates on Σ_0 defined by γ_{ik}.

5.3 Further Remark

It is clear that in eq. (5.1) it would not be desirable to let the metric deviate from the initial Kerr-Schild form too fast, i.e. with t, because then in the constraint equations we would also have j-terms. But for a multiple black hole metric it is also not good to let it deviate too slow, for example with t^3. This would imply that the full Einstein equations at $t = 0$ would be fulfilled by the Kerr-Schild part of the metric alone and as described in Section 4.3, the Weyl tensor belonging to that metric would be of Petrov-Type II/D. So l_μ would be a geodesic shear free double degenerate principal null direction at $t = 0$ which would be too restrictive for general black hole systems.

5.4 Construction of the Kerr-Schild null vector field l_μ

As was described before, we want to construct l_μ first on $\tilde{\Sigma}_0$, the initial slice in the auxiliary Minkowski space, as the free part of a n black hole initial data set. Of course there is no unique way to do this; in principle the only restriction is that eventually one must be able to prove existence of trapped surfaces or apparent horizons on Σ_0 and asymptotical flatness.

The null field l_μ should be constructed by means of parameters m_i, $\mathbf{P}_i$, $\mathbf{S}_i$ which should at least converge to the associated ADM-quantities mass, momentum and spin (Section 2.3) of the i-th black hole respectively if the coordinate separations go to infinity. In this limit we want that a region around each black hole in Σ_0 has the same geometry as the initial Kerr-Schild slice of a single Kerr black hole modulo global coordinate shifts, rotations and Lorentz boosts.

In [10] this was done for unboosted ($\mathbf{P}_i = 0$) non-spinning ($\mathbf{S}_i = 0$) black holes; in [39] this was generalized for unboosted spinning black holes. In this thesis I generalize (or better said modify) their ansatz and implicitly fix the spin-spin-interaction function which in [39] was introduced only in the close limit.

5.4.1 The new Idea

My procedure is motivated by Lind and Newman [35] who discovered an analogy of principal null vector fields of algebraically special metrics with eigenvector fields of associated Maxwell tensors in Minkowski space. To describe this analogy would be beyond the scope of this document. After straight forward but lengthy computations done with Mathematica, I additionally found that the Kerr-Schild null vector field of the Kerr metric (spin in z-direction) in Cartesian coordinates with $(x_1, x_2, x_3) = (x, y, z)$ eq. (4.7) can be obtained as an eigenvector of the matrix

$$(F^\mu{}_\nu) = \begin{pmatrix} 0 & x & y & z \\ x & 0 & -a & 0 \\ y & a & 0 & 0 \\ z & 0 & 0 & 0 \end{pmatrix} \tag{5.4}$$

associated with the eigenvalue $-1/R$. This tensor in Minkowski space can be interpreted as being proportional to the electromagnetic field tensor of a spinning charge at rest in Cartesian Minkowski coordinates (although not a magnetic dipole), see [33]. So in addition to [35] this result shows a deep connection between black hole physics and Minkowski electrodynamics.

The electromagnetic field tensor (5.4) is not the only one for which the eigenvalue equation

$$F^\mu{}_\nu l^\nu = \lambda l^\mu$$

is solved by the null field l_μ of the Kerr metric. I made the following more general ansatz

$$(F^\mu{}_\nu) = \begin{pmatrix} 0 & x & y & z \\ x & 0 & B_z & -B_y \\ y & -B_z & 0 & B_x \\ z & B_y & -B_x & 0 \end{pmatrix}$$

where the components B_x, B_y and B_z are related to the *magnetic field* associated with the spin of the black hole. Then I put the Kerr null vector field (4.7) into the eigenvalue equation. With additional requirement $B_x \sin\phi = B_y \cos\phi$ due to symmetry (ϕ is the azimuthal angle associated with the z-axis), it turns out that there is only (5.4) and the eigenvalue is $-1/R$.

Hence to construct l_μ on $\tilde{\Sigma}_0$, I use Minkowski electrodynamics as a model problem in the following way.

5.4.2 The new procedure

Assume we want the initial data set to represent n black holes with initial coordinate positions $\mathbf{r}_i = (x_i, y_i, z_i)$, mass parameters m_i, momentum parameters $\mathbf{P}_i = (P^i_x, P^i_y, P^i_z)$ and spin parameters $\mathbf{S}_i = (a^i_x, a^i_y, a^i_z)m_i$. By the *coordinate position of a black hole* I mean the coordinate position of that point on $\tilde{\Sigma}_0$ where the divergence of l_μ becomes infinite. Now, in analogy with the single Kerr black hole case, set for each black hole on $\tilde{\Sigma}_0$ the electromagnetic field tensor of a moving spinning charge of type eq. (5.4). This means the following.

First introduce a coordinate frame in Minkowski space (t', x', y', z') in which one of the charges (associated with one of the black holes) at initial position $(t'_0, 0, 0, 0)$ is at rest with the electromagnetic field tensor

$$(\tilde{F}^{i\mu'}{}_{\nu'}) := \begin{pmatrix} 0 & x' & y' & z' \\ x' & 0 & -a^{i\prime}_z & a^{i\prime}_y \\ y' & a^{i\prime}_z & 0 & -a^{i\prime}_x \\ z' & -a^{i\prime}_y & a^{i\prime}_x & 0 \end{pmatrix}, \tag{5.5}$$

the coupling factor Q/r'^3 in electrodynamics will be discussed below.

Now change to a coordinate frame in which the charge has velocity v. So one has to apply a Lorentz transformation and the Lorentz matrix is [33] (here as an example for a boost in z-direction; this can be easily generalized by spatial coordinate rotations)

$$(\Lambda(v)^\mu{}_\nu) = \begin{pmatrix} \Gamma(v) & 0 & 0 & v\Gamma(v) \\ 0 & 1 & 0 & 0 \\ 0 & 0 & 1 & 0 \\ v\Gamma(v) & 0 & 0 & \Gamma(v) \end{pmatrix} \tag{5.6}$$

with

$$\Gamma = \frac{1}{\sqrt{1-v^2}}.$$

In this frame the electromagnetic field tensor of the charge is (standard matrix multiplication)

$$F^i := \Lambda(\mathbf{P}) \cdot \tilde{F}^i \cdot \Lambda^{-1}(\mathbf{P}) \tag{5.7}$$

with

$$\mathbf{v} = \frac{\mathbf{P}}{\sqrt{M^2 + P^2}} \tag{5.8}$$

and the inverse Lorentz matrix

$$\Lambda^{-1}(\mathbf{P}) = \Lambda(-\mathbf{P}).$$

In Minkowski space $\tilde{M}$ the coordinate quadruple (position vector) transforms as a tangent vector under Lorentz transformation, so at $t = 0$ (which does not imply $t'_0 = 0$!)

$$x = x', \quad y = y', \quad z = \Gamma z'. \tag{5.9}$$

Finally in this coordinate frame, where the charge is boosted with a momentum $\mathbf{P}$, we shift the frame to put the charge on its initial position, i.e.

$$x \to x - x_0, \quad y \to y - y_0, \quad z \to z - z_0.$$

Electromagnetism is our model problem in Minkowski space; charges represent black holes on $\tilde{\Sigma}_0$. Now I propose to superpose the black holes, i.e. the associated electromagnetic field tensors, in the following way. I set the total electromagnetic field tensor to be

$$F := \sum_{i=1}^{n} \frac{m_i}{\rho_i^k} F^i \tag{5.10}$$

with the Euclidean separation

$$\rho_i^2 = d(\mathbf{r}' - \mathbf{r}'_i, \mathbf{r}' - \mathbf{r}'_i)$$

measured in the coordinate frame where the ith charge is at rest. $k = 3$ is in full analogy with Minkowski electrodynamics and will be used later because in the case of non-boosted and non-spinning black holes it reduces to Bishop's initial data [10] (Section 5.6).

Higher k correspond to black holes which are more and more undistorted in a neighborhood of their positions (in the meaning described above) because the superposition functions of the other black holes tend to zero faster and faster. This is why k can be called **shielding parameter**. For any k this ansatz for the superposition has the property that two non-boosted black holes with opposite angular momenta on the same coordinate position reduce to a single Schwarzschild black hole. This is not the case if for example one uses the Boyer-Lindquist radial coordinate R eq. (4.8) instead of ρ.

I stated before that to obtain l_μ in the case of a single Kerr black hole one can solve the eigenvalue problem of eq. (5.4) and take l_μ as the eigenvector associated with the negative real eigenvalue (corresponding to *ingoing* Kerr-Schild coordinates). I propose to do the same in the multiple black hole case. Hence after one has computed the total electromagnetic field tensor as described before one can take l_μ from the equation

$$F^\mu{}_\nu l^\nu = \lambda l^\mu \tag{5.11}$$

where λ is the associated eigenvalue. Existence and uniqueness of solutions of this equation for real and negative λ will be discussed in Section 5.5.

If l^μ on $\tilde{\Sigma}_0$ in Minkowski space is constructed this way then it is automatically null with respect to $\eta_{\mu\nu}$ because $F_{\mu\nu} = \eta_{\mu\rho}F^\rho{}_\nu$ is antisymmetric, hence

$$\eta_{\mu\nu}l^\mu l^\nu = \frac{1}{\lambda}\eta_{\mu\nu}F^\mu{}_\rho l^\rho l^\nu = \frac{1}{\lambda}F_{\nu\rho}l^\rho l^\nu = 0.$$

Assume now that l_μ on $\tilde{\Sigma}_0$ is constructed this way and the metric is given by eq. (5.1) with the still unknown function V. Then l_μ is also null with respect to $g_{\mu\nu}$ at $t = 0$ in Σ_0 due to eq. (4.4), i.e.

$$g_{\mu\nu}l^\mu l^\nu = 0.$$

So l_μ is automatically consistent with the Kerr-Schild assumptions.

5.5 Eigenvalue Problem of F

I want to discuss the eigenvalue problem of the antisymmetric tensor $F_{\mu\nu}$ and assume that $(\eta_{\mu\nu}) = \mathrm{diag}(-1, 1, 1, 1)$. One can write in general

$$(F^\mu{}_\nu) = \begin{pmatrix} 0 & \Phi_1 & \Phi_2 & \Phi_3 \\ \Phi_1 & 0 & \Phi_4 & \Phi_5 \\ \Phi_2 & -\Phi_4 & 0 & \Phi_6 \\ \Phi_3 & -\Phi_5 & -\Phi_6 & 0 \end{pmatrix}$$

where $\Phi_1, \ldots, \Phi_6$ are arbitrary smooth functions in Minkowski space. The eigenvalues are the roots of the characteristic polynomial, i.e.

$$\det(F - \lambda\,\mathrm{id}) = 0.$$

Introducing

$$\begin{aligned} A &:= -\Phi_1^2 - \Phi_2^2 - \Phi_3^2 + \Phi_4^2 + \Phi_5^2 + \Phi_6^2 \\ B_1 &:= \Phi_3\Phi_4, \quad B_2 := \Phi_2\Phi_5, \quad B_3 := \Phi_1\Phi_6 \\ B &:= B_1 - B_2 + B_3 \end{aligned}$$

one can check (e.g. with Mathematica) that the roots of the characteristic polynomial can be written as

$$\lambda = \pm\sqrt{-\frac{A}{2} \pm \frac{1}{2}\sqrt{A^2 + 4B^2}}.$$

So there are two and only two (except for single points) real eigenvalues and only one which is negative. I choose

$$\lambda = -\sqrt{-\frac{A}{2} + \frac{1}{2}\sqrt{A^2 + 4B^2}}$$

because in analogy with eq. (5.4) this corresponds to *ingoing* Kerr-Schild coordinates.

The corresponding associated normalized ($l^0 = 1$) eigenvector is (obtained with Mathematica)

$$(l^\mu) = \left(1, \frac{\lambda^2 \Phi_1 + B\,\Phi_6 + \lambda\,(\Phi_2\,\Phi_4 + \Phi_3\,\Phi_5)}{\lambda\left(\lambda^2 + {\Phi_4}^2 + {\Phi_5}^2 + {\Phi_6}^2\right)}, \right.$$
$$\frac{\lambda^2 \Phi_2 - B\,\Phi_5 + \lambda\,(\Phi_3\,\Phi_6 - \Phi_1\,\Phi_4)}{\lambda\left(\lambda^2 + {\Phi_4}^2 + {\Phi_5}^2 + {\Phi_6}^2\right)}, \tag{5.12}$$
$$\left. \frac{\lambda^2 \Phi_3 + B\,\Phi_4 - \lambda\,(\Phi_1\,\Phi_5 + \Phi_2\,\Phi_6)}{\lambda\left(\lambda^2 + {\Phi_4}^2 + {\Phi_5}^2 + {\Phi_6}^2\right)} \right)$$

Note that because of the normalization $l^0 = 1$ there are singular points if

$$\lambda\left(\lambda^2 + {\Phi_4}^2 + {\Phi_5}^2 + {\Phi_6}^2\right) = 0.$$

Nevertheless, this normalization is assumed here because the constraint equations become simpler and because one can compare to Bishop's original approach, see the following section. For the future one might want to work with the regularized version of eq. (5.12) which is only singular at the positions of the black holes.

5.6 Compare to Bishop's Construction

In [10] Bishop et al. invented a different construction of l_μ, the free part of the initial data. Nevertheless, in the case of non spinning non boosted black holes and for a special choice of the shielding parameter the same results are obtained.

They construct l_i (the spatial part of l_μ) as the normalized gradient of a potential

$$l_i = C\nabla_i\Phi$$

in the case of vanishing angular momentum with

$$\Phi = \sum_i \frac{m_i}{\rho_i}.$$

My construction procedure in this case leads to a total electromagnetic field tensor

$$(F^\mu{}_\nu) = \begin{pmatrix} 0 & \Phi_1 & \Phi_2 & \Phi_3 \\ \Phi_1 & 0 & 0 & 0 \\ \Phi_2 & 0 & 0 & 0 \\ \Phi_3 & 0 & 0 & 0 \end{pmatrix}.$$

Using the general formula for l^μ eq. (5.12) we get for the spatial part

$$(l^i) = \frac{1}{\lambda}(\Phi_1, \Phi_2, \Phi_3)$$

with

$$\lambda = -\sqrt{\Phi_1^2 + \Phi_2^2 + \Phi_3^2}.$$

We have from the construction procedure

$$\Phi_1 = \sum_i \frac{m^i}{\rho_i^k}(x - x_i)$$
$$\Phi_2 = \sum_i \frac{m^i}{\rho_i^k}(y - y_i)$$
$$\Phi_3 = \sum_i \frac{m^i}{\rho_i^k}(z - z_i).$$

So my construction leads to the same l_μ as in Bishop if the shielding parameter is $k = 3$. Later on I will consider $k = 3$ exclusively.

5.7 Physical Implications

5.7.1 Limit of infinite Coordinate Separations

Let ρ be the typical coordinate separation of the black holes position (in the sense described above) and $d = \alpha\rho$ the radius of a coordinate sphere $\tilde{K} \subset \tilde{\Sigma}_0$ around one black hole position with $\alpha \ll 1$. Look at the limit $\rho \to \infty$ now. The coupling functions of all other black holes in the superposition eq. (5.10) converge to zero in $\tilde{K}$. They fall off faster the higher the shielding parameter k is. So in this limit the total generating tensor in $\tilde{K}$ is that of a single black hole (5.4)[1]. So in $\tilde{K}$ the Kerr-Schild null vector field l_μ is that of a single Kerr black hole[1]. In $\tilde{K}$ it is thus possible to find a solution of the constraint equations which, interpreted on Σ_0, is the data of the initial Kerr-Schild slice of a single Kerr black hole[1] and hence the coordinates are standard single black hole Kerr-Schild coordinates.

Let us call K that region in Σ_0 associated with the region $\tilde{K}$ in $\tilde{\Sigma}_0$. In the limit $\rho \to \infty$, the proper diameter of K is infinite because the metric there is that of a single black[1] hole and so K is asymptotically flat. Hence the notions of ADM-masses, -momenta and -spins on K are well defined.

In this limit the spin-parameter used in the construction of l_μ is the ADM-spin per unit mass because it is the spin parameter of a single Kerr black hole[1]. If the momentum parameter is zero then the metric reduces to a Kerr black hole with ADM-momentum zero (possibly times shifts and rotations of the coordinates). Because by construction the ADM-momentum **P**, defined in the asymptotically flat region of K with Minkowski coordinates, transforms under Lorentz transformation as the Lorentz momentum parameter for a given ADM-mass, the ADM-momentum per unit mass equals the momentum parameter per unit mass in this limit. Only the ADM-mass itself is not fixed by the construction procedure of l_μ alone because we use the specific superposition eq. (5.10). Writing $m_i = \alpha_i M$ with M the total ADM-mass the eigenvalue equation eq. (5.11) can be divided by M which only changes the size (but not the sign) of the eigenvalue. So only the relations of the mass parameters, i.e. the α_is, influence the null vector field by construction. The ADM-mass is one of the further freedoms hidden in the constraint equations and is determined by fixing the boundary conditions with which they are solved.

[1] possibly additional coordinate transformations as coordinate shifts, rotations or Lorentz boosts must be applied

5.7.2 Apparent Horizons

In Bishop's original paper [10] it is discussed that surfaces orthogonal to the spatial part of the Kerr-Schild null vector field l_i with $V = -1/2$ are marginally trapped if l_i is surface forming. This is the case described in Section 5.6; more generally from Frobenius's Theorem [52] the surface forming condition is

$$l_{[i}l_{j,k]} = 0.$$

They argue that l_μ is the ingoing normal to such a surface and $k^\mu = 2t^\mu - (1 + 2V)l^\mu$ is the outgoing one and find for the outgoing divergence

$$\Theta_{out} = -(1 + 2V)\Theta_{in}.$$

So $\Theta_{out} = 0$ if $V = -1/2$. Nevertheless the argument does not seem to be good because k_μ is only an outgoing null normal of the surface if $V > -1/2$. So exactly in the case when we have a marginally trapped surface, i.e. $1 + 2V = 0$, we have $k^\mu = 2t^\mu$ and it is not an outgoing normal.

In [46] they claim that they have checked the marginally trapped surface condition eq. (1.8) and came to the same result as Bishop.

Currently no generalization exists for not surface forming l_i.

Chapter 6

Constraint Equations

6.1 Derivation of Kerr-Schild Constraint Equations

Ansatz eq. (5.1) implies that the data and the constraints on the initial hypersurface Σ_0 are fully determined by the Kerr-Schild part of the metric because the components $G^0_{\ 0}$ and $G^0_{\ i}$ of the Einstein tensor do not contain second time-derivatives. So the Einstein tensor defined by metric (5.1) does not contain j-matrices and one can compute the constraint equation at $t = 0$ considering only the Kerr-Schild part.

In [10] they derived the Kerr-Schild constraint equations in Cartesian Kerr-Schild coordinates. I reproduced the computations with Mathematica using the tensor package EinS [29]. This package allows to obtain tensor expression keeping terms together by means of Einstein's summation convention. Standard Mathematica itself is only able to compute the expression and fully evaluate it in terms of all tensor components which is much longer. But to check the computations done with EinS, I compared the resulting equations with those obtained by standard Mathematica which was eventually successful.

The constraint equations were computed from the definition of the Einstein tensor $G^0_{\ 0} = 0$ and $G^0_{\ i} = 0$ directly and not using eq. (2.5) and (2.6). Here is the Hamiltonian constraint

$$\begin{aligned} 0 = &- V_{,ii} + l_i l_j V_{,ij} \\ &+ 2\left(2V\dot{l}_i + (1+2V)a_i + l_i l_{j,j}\right)V_{,i} + 2V^2\dot{l}_{i,i} \\ &+ V^2(\dot{l}_i\dot{l}_i - a_i a_i) + 2V(1+V)a_{i,i} + V(l_{i,i}l_{j,j} - l_{i,j}l_{j,i}), \end{aligned} \tag{6.1}$$

the momentum constraint $G^0_{\ i}l_i = 0$

$$\begin{aligned} 0 = &V_{,ii} - l_i l_j V_{,ij} \\ &+ \left((1-4V)\dot{l}_i - (1+4V)a_i - l_i l_{j,j}\right)V_{,i} + V(1-2V)\dot{l}_{i,i} \\ &+ 2V^2 a_i a_i - V(1+2V)a_{i,i} - V(1-2V)a_i\dot{l}_i + \dot{V}l_{i,i} + Vl_{i,j}(l_{j,i} - l_{i,j}) \end{aligned} \tag{6.2}$$

and the momentum constraints $G^0{}_i z_i = 0$

$$\begin{aligned} 0 =& - l_i V_{,ij} z_j \\ &+ \left([\dot{l}_j l_i - l_{i,j} + 2 l_{j,i}] V_{,i} - l_{i,i} V_{,j} + V l_i \dot{l}_{j,i} - \dot{V}_{,j} \right) z_j \\ &+ \left(\dot{V} a_j + V(l_{j,ii} - l_{i,ij}) + V \dot{l}_j l_{i,i} + 2V^2 a_i (l_{i,j} - l_{j,i}) \right. \\ &\left. + 2V^2 \dot{l}_i l_{i,j} + V(1-2V) \dot{l}_i l_{j,i} \right) z_j . \end{aligned} \tag{6.3}$$

To write down these equations I use Einstein's summation convention for repeated indices with the simplified notation $l^i = l_i$. This is very convenient when dealing with computer algebra but can be dangerous when one wants to change to other than Cartesian coordinates. The vector $\mathbf{z}$ on $\tilde{\Sigma}_0$ is orthogonal to $\mathbf{l}$ with respect to the Euclidean metric (i.e. the induced metric of $\tilde{\Sigma}_0$), so

$$l_i z_i = 0.$$

One has to choose two linearly independent $\mathbf{z}$ because eq. (6.3) represents two equations. I also introduce

$$\dot{l}_i := \partial_t l_i \quad \text{and} \quad \dot{V} := \partial_t V$$

and

$$a_j := l_{j,i} l_i .$$

Beside the normalization $l_i l_i = 1$ the following identities are used

$$\begin{aligned} \dot{l}_i l_i = l_{i,j} l_i = 0, \quad l_i \dot{l}_{i,j} = -\dot{l}_i l_{i,j}, \quad l_i l_j \dot{l}_{i,j} = -a_i \dot{l}_i, \\ l_j l_{j,kk} = -l_{j,k} l_{j,k}, \quad l_k l_{j,kl} = a_{j,l} - l_{k,l} l_{j,k}. \end{aligned}$$

The unknown functions to be solved for are V, $\dot{V}$ and two (linear combinations of the) components of $\dot{l}_i$, obtaining the third component by means of eq. (5.3).

6.2 Schwarzschild Solution

As a first check of the correctness of the constraint equations, I want to derive the Schwarzschild solution, see Section 4.4 for $a = 0$. In this case we have

$$\mathbf{l} = -\hat{r}, a_i = 0, \dot{l}_i = 0, \dot{V} = 0$$

with $\hat{r}$ the radial unit vector and one can assume $V = V(r)$ with $r = \sqrt{x^2 + y^2 + z^2}$ due to symmetry. Here are the equations to be solved

$$\begin{aligned} 0 =& - V_{,ii} + l_i l_j V_{,ij} + 2 l_i l_{j,j} V_{,i} + V(l_{i,i} l_{j,j} - l_{i,j} l_{j,i}) \\ 0 =& V_{,ii} - l_i l_j V_{,ij} - l_i V_{,i} l_{j,j} + V l_{i,j} (l_{j,i} - l_{i,j}) \\ 0 =& - l_i V_{,ij} z_j + \left(-V_{,j} l_{i,i} - V_{,i} l_{i,j} + 2 V_{,i} l_{j,i} \right) z_j + \left(V l_{j,ii} - V l_{i,ij} \right) z_j . \end{aligned}$$

Because l_i is curl free we have $l_{i,j} = l_{j,i}$ and the sum of the first two equations gives

$$l_i l_{j,j} V_{,i} + V(l_{i,i} l_{j,j} - l_{i,j} l_{j,i}) = 0.$$

We have

$$-\frac{\partial}{\partial x}\frac{x}{r} = -\frac{r - x^2/r}{r^2} = -\frac{r^2 - x^2}{r^3},$$

hence

$$l_{j,j} = -\frac{2}{r}.$$

Further on, it is

$$l_{i,j}l_{j,i} = a_{j,j} - l_i l_{j,ij} = -l_i l_{j,ji} = l_i \partial_i \left(\frac{2}{r}\right).$$

In this simple case $l_i\partial_i = -\partial_r$ so we obtain

$$\frac{2}{r}V_{,r} + V\left(\frac{4}{r^2} - \frac{2}{r^2}\right) = 0$$
$$\Rightarrow \quad V_{,r} = -\frac{1}{r}V \quad \Rightarrow \quad V(r) = \frac{C}{r}.$$

C is an integration constant. By comparison with the Newtonian limit, we must set $C = -M$. Of course one has to check that this solution fulfills all three constraint equations individually. In fact this is the case; computations are straight forward and were done with Mathematica.

6.3 Analysis for Surface Forming l_i

6.3.1 Basics

In this section I assume that l_i is surface forming, i.e. there exists a C^3-function $\Phi : \mathbb{R}^3 \to \mathbb{R}$ such that

$$l_i = C\nabla_i\Phi(x, y, z) \quad \text{with} \quad C = \frac{1}{\sqrt{d^{ij}(\nabla_i\Phi)(\nabla_j\Phi)}}$$

and the smoothness condition $\nabla_i\Phi \neq (0, 0, 0)$ everywhere. If this is the case the general condition in Frobenius's Theorem [52]

$$l_{[i}l_{j,k]} = 0$$

is fulfilled. Physically for example consider a Kerr-Schild black hole initial data set with vanishing momentum and spin parameters (Section 5.6) and

$$\Phi(x, y, z) = \sum_i \frac{m_i}{|\mathbf{r} - \mathbf{r}_i|}.$$

6.3.2 Solutions of the Constraints

Existence

The York-Lichnerowicz conformal decomposition described in Section 3.2 results in elliptic constraint equations. Elliptic equations are normally solved as boundary value problems and one can show that the Cauchy problem is ill-posed [27]. Surprisingly and in contrast to that,

the Kerr-Schild constraint equations in the case of surface forming l_i represent a Cauchy problem; they are not elliptic.

The Cauchy problem [27] consists of finding a surface S (in this case embedded into $\tilde{\Sigma}_0$ and giving appropriate data on S such that all derivatives of the solution on S can be computed. Then – for a real analytic surface and real analytic data – there exists a local real analytic solution of the constraint equations by means of the Cauchy-Kowalevski Theorem. Such a surface S is called **non-characteristic**. A real function is called **real analytic** if it has a local power series expansion.

To talk about solutions of the system of equations (6.1) to (6.3) it is convenient to change to adapted coordinates. l_i is orthogonal to the surface S given by $\Phi(x, y, z) = const$. Due to the smoothness condition $l_i \neq 0$ everywhere, we can find an explicit representation of S in terms of two parameters σ and τ locally

$$x = \phi^1(\sigma, \tau), \quad y = \phi^2(\sigma, \tau), \quad z = \phi^3(\sigma, \tau).$$

σ and τ are regular local coordinates on S, so one can define the tangent vectors $\hat{\sigma} = \partial/\partial_\sigma$ and $\hat{\tau} = \partial/\partial_\tau$ which form a local basis of the tangent space of S in any point. Consequently $(\mathbf{l}, \hat{\sigma}, \hat{\tau})$ is a basis of the tangent space of $\tilde{\Sigma}_0$ in each point of the embedding of S with $d_{ij}l^i\hat{\sigma}^j = d_{ij}l^i\hat{\tau}^j = 0$. Hence locally one can introduce coordinates (ρ, σ, τ) in a neighborhood of a point on the embedding of S with $\mathbf{l} = \partial/\partial\rho$. With this, $\hat{\sigma}$ and $\hat{\tau}$ are the natural choices for the two $\mathbf{z}$ in eq. (6.3). Furthermore, because $\dot{\mathbf{l}}$ is orthogonal to $\mathbf{l}$ we can write

$$\dot{\mathbf{l}} = \dot{l}^\tau\hat{\tau} + \dot{l}^\sigma\hat{\sigma}$$

and it is natural to choose $u = (V, \dot{V}, \dot{l}^\sigma, \dot{l}^\tau)$ as the unknown functions to be solved for. Note that l^τ and l^σ are the contravariant components of $\dot{\mathbf{l}}$ with respect to the basis $(\mathbf{l}, \hat{\sigma}, \hat{\tau})$.

To transform the system (6.1) to (6.3) to the coordinates (ρ, σ, τ), we proceed the following way. First, one writes the equations again in covariant form, i.e. one distinguishes between covariant and contravariant components. This is trivial in Cartesian coordinates for we are free to choose which of the factors in a contraction to write with upper and which to write with lower indices. Consider the second order term of eq. (6.1)

$$V_{,ii} - l_i l_j V_{,ij} = \left(d^{ij} - l^i l^j\right)\partial_i\partial_j V = q^{ij}\partial_i\partial_j V$$

with q^{ij} the induced metric of S. To transform the coordinates one substitutes partial derivatives by covariant derivatives (tensors!)

$$V_{,ii} - l_i l_j V_{,ij} = q^{ab}D_aD_bV = q^{ab}(\partial_a\partial_b V - \Gamma^c{}_{ba}\partial_c V)$$

with $a, b = \rho, \sigma, \tau$ and $\Gamma^c{}_{ba}$ the Christoffel symbols associated with the coordinates (ρ, σ, τ) which are known functions on S. Note that $q^{ab} = 0$ if $a = \rho$ or $b = \rho$, so the first term only consists of derivatives tangent to S. The induced metric q^{ab} is a known function on S. In the same equation we also have to look at this term

$$\dot{l}_{i,i} = \dot{l}^a{}_{;a} = \dot{l}^a{}_{,a} + \Gamma^a{}_{ba}\dot{l}^b.$$

Here, there are also only derivatives tangent to S because $\dot{\mathbf{l}}$ has no components orthogonal to S. The second order term of eq. (6.3) is

$$l_i z_j V_{i,j} = (l_i V_{,i})_{,j} z_j - l_{i,j} V_{,i} z_j.$$

Here we can use the fact that by definition $l_i V_{,i} = V_{,\rho}$ and $z_j \partial_j$ is either ∂_σ or ∂_ρ. The second term is canceled by another term in eq. (6.3). Also look at

$$2 l_{j,i} V_{,i} z_j = 2 d^{ik} l_{j,i} V_{,k} z^j = 2 d^{ab} l_{c;a} V_{;b} z^c = 2 d^{ab} l_{c;a} V_{,b} z^c$$

from eq. (6.3) and $l_{c;a}$ is again a known function on S. Finally

$$l_i \dot{l}_{j,i} z_j = l^a \dot{l}^b_{;a} z_b = l^a \dot{l}^b_{,a} z_b + l^a \Gamma^b_{\ ca} \dot{l}^c z_b = l^a (\dot{l}^b z_b)_{,a} - l^a \dot{l}^b z_{b,a} + l^a \Gamma^b_{\ ca} \dot{l}^c z_b.$$

Now we can write the system of equations in the following form

$$\sum_{a,b=\rho,\sigma,\tau} A^{ab} \partial_a \partial_b u + \sum_{a=\rho,\sigma,\tau} B^a \partial_a u + C = 0 \tag{6.4}$$

with A_{ij} and B_i 4×4-matrices for all $a, b = \rho, \sigma, \tau$ and C a 4-vector. We find

$$A^{ab} = \begin{pmatrix} -q^{ab} & 0 & 0 & 0 \\ q^{ab} & 0 & 0 & 0 \\ -\delta^a_\rho \delta^b_\sigma & 0 & 0 & 0 \\ -\delta^a_\rho \delta^b_\tau & 0 & 0 & 0 \end{pmatrix}$$

and

$$B^a = \begin{pmatrix} 2\left(2V\dot{l}^a + (1+2V)a^a + l_{j,j}\delta^a_\rho\right) + q^{cb}\Gamma^a_{\ bc} & 0 & 2V^2\delta^a_\sigma & 2V^2\delta^a_\tau \\ (1-4V)\dot{l}^a - (1+4V)a^a - l_{j,j}\delta^a_\rho - q^{cb}\Gamma^a_{\ bc} & 0 & V(1-2V)\delta^a_\sigma & V(1-2V)\delta^a_\tau \\ \dot{l}^\sigma \delta^a_\rho + 2d^{ab} l_{c;b} \hat{\sigma}^c - l_{i,i}\delta^a_\sigma & -\delta^a_\sigma & V\delta^a_\rho & 0 \\ \dot{l}^\tau \delta^a_\rho + 2d^{ab} l_{c;b} \hat{\tau}^c - l_{i,i}\delta^a_\tau & -\delta^a_\tau & 0 & V\delta^a_\rho \end{pmatrix}.$$

Note that **a** has only components tangential to S. The lower order terms C are of no interest for this analysis.

On S one gives the following data which is assumed to be real analytic in the following

$$\begin{aligned} V &= \nu(\sigma, \tau) \\ \dot{l}^\sigma &= \lambda_1(\sigma, \tau) \\ \dot{l}^\tau &= \lambda_2(\sigma, \tau). \end{aligned}$$

So all σ and τ derivatives of the unknown functions V, $\dot{l}^\sigma$ and $\dot{l}^\tau$ on S can be computed. Hence from the first equation we know $V_{,\rho}$ on S as long as $2l_{j,j} + q^{cb}\Gamma^\rho_{\ bc} \neq 0$. The differential part of the second equation is completely determined. Hence we get V on S explicitly from the lower order part as long as $l_{i,i} \neq 0$. From the third equation one obtains $\dot{l}^\sigma_{,\rho}$ and from the fourth $\dot{l}^\tau_{,\rho}$ on S if $V \neq 0$ (i.e. $\nu \neq 0$) because $V_{,\rho\sigma}$ and $V_{,\rho\tau}$ have already been determined. Consequently all higher derivatives of the unknown functions on S can be constructed. Now the Cauchy-Kowalevski Theorem guarantees existence of a unique analytic solution in a neighborhood of all points of S as long as the conditions above are satisfied.

The existence of local solutions might not be very meaningful physically. To see that consider the example of the Schwarzschild solution with $\rho = r$ so $\mathbf{l} = -\partial/\partial\rho$ (result: $V = -M/r$). With the Cauchy data $V = -1/2$, $\dot{l}^\sigma = \dot{l}^\tau = 0$ on the surface S given by $r = 2M$ one obtains beside $\dot{V} = 0$ the derivatives on S

$$\frac{\partial^n}{\partial r^n} V = (-1)^{n+1} n! \frac{M}{r^{n+1}}\bigg|_{r=2M},$$

all other derivatives vanish. The analytical solution given by the Taylor series

$$V = \sum_{k=0}^{\infty} \frac{1}{k!} \left(\frac{\partial^k}{\partial r^k} V(r) \right)_{r=2M} (r-2M)^k = -\frac{1}{2} \sum_{k=0}^{\infty} (-1)^k \left(\frac{r}{2M} - 1 \right)^k$$

converges only for $0 < r < 4M$ (geometric series). Nevertheless the solution $V = -M/r$ exists for all $r > 0$.

A proof of well-posedness, i.e. existence, uniqueness and continuous dependence of the solution on the Cauchy data, for the Cauchy problem of the system of Kerr-Schild constraints by means of the Cauchy-Kowalevski Theorem is only possible among the analytic solutions. This means that one can be sure that there is exactly one local analytic solution of the constraints which also depends analytically on the Cauchy data if the requirements above are met: $2l_{j,j} + q^{cb}\Gamma^{o}_{\ bc} \neq 0$, $V \neq 0$ and $l_{i,i} \neq 0$ on S. But the Cauchy-Kowalevski Theorem is not a sufficient tool for the general case so there is no general proof of well-posedness.

Numerical Algorithm

Above I described how to construct all derivatives of the solution on S from given Cauchy data. Hence there is the following algorithm to solve the system of constraints numerically. With the first derivatives with respect to ρ obtained from the system of constraints as above one can integrate outwards (or inwards) for a distance $\delta\rho$ (outwards means $\delta\rho < 0$) along the normal of the surface, namely l_i. After this integration step one has the data on another surface S' which is a bit bigger (or smaller) than S. From S' one can proceed the same way and so on. To increase the order of accuracy for a given step-width $\delta\rho$ it is possible to use higher derivatives computed from the system of constraints as well.

I have not implemented this algorithm because it is useless for numerics, see the following section.

6.3.3 Black hole Boundary Conditions and Problems

At a first glance the algorithm which was just described seems to be quite promising. It is even easily possible to guarantee existence of horizons by choosing Cauchy data $V = -1/2$ on the initial surface S (Section 5.7.2). But, one has no control of the asymptotical behavior of the solution. Especially there was no way found to ensure in general that given Cauchy data on S leads to asymptotical flatness which is indeed a crucial ingredient of physical initial data. Only in the linear regime, see below, this can be done analytically. But even then, small numerical errors in the data would excite asymptotically non-flat "modes" which would be exponentially growing and after some finite distance dominate the solution. Hence, due to this instability, the algorithm is useless for numerics.

N. Bishop experimented with this algorithm and said in a private discussion that it produces singular solutions at infinity in nearly all non-trivial cases he tried.

The biggest class of initial data described at the beginning of this thesis use York's conformal decomposition. There, one has to deal with elliptic equations and the Cauchy problem of elliptic equations is ill-posed [27], so one tries to solve it as a boundary value problem. If the system of Kerr-Schild constraint equations was solvable as a boundary value problem then one would have control over both the existence of horizons and the

asymptotical decay of the solution and one would have a better algorithm for numerics. Although for non-linear elliptic partial differential equations there is no general way of proving existence of solutions, whereas in the case of the Kerr-Schild equations this is quite simple (although only locally), from a practical point of view one prefers to have no solutions in some cases than a system of equations with non-controllable solutions. In my thesis I did not try to find a well-posed boundary value algorithm for the Kerr-Schild constraint equations but rather worked out a modification of the Kerr-Schild ansatz leading to elliptic constraints (Part IV of this thesis). Furthermore I spend some time in investigating the linear regime where one has analytical control over the constraint equations (Part III).

Part III

The Linear Regime

Chapter 7

Black Hole Perturbation Theory

7.1 Motivation

In black hole perturbation theory the nature and dynamics of small deviations from a given background metric are investigated, neglecting all terms of higher order in the metric perturbations. In this document it will be assumed that the background metric is the Schwarzschild metric. Below I will describe that one can find a function defined uniquely by the perturbations – the Zerilli and Regge-Wheeler function, respectively – whose evolution equation is linear and strictly hyperbolic, which depends only on the background coordinates and is gauge-independent. Thus this function gives the *physical content* of weak gravitational waves; there is no need to ask if maybe the metric deviations are only associated with a change in the coordinate gauge.

Black hole perturbation theory of a Schwarzschild background is considered here because in the Kerr-Schild framework it turns out to be possible to obtain physically interesting analytic solutions of the constraint equations which otherwise would be very difficult to tackle even numerically. The strict hyperbolicity of the linear – in this case one dimensional – evolution equations makes it possible to set proper boundary conditions for the evolution and compute the gravitational radiation accurately and reliably with a numerical code.

Furthermore small perturbations of a Schwarzschild black hole arise quite naturally in black hole physics if the total angular momentum vanishes (or is infinitesimally small). For example, black holes might be so close initially that they already have a common horizon. The black holes might also be very far away from each other that one is only perturbed a little bit by the other one. These examples are interesting models for the beginning and the final stages of black holes spiraling in from far apart as well as important testbeds for full non-linear numerical codes.

Another motivation to investigate the linear regime is its historical importance for numerical relativity. The perturbation theory of a Schwarzschild background was developed for Schwarzschild background coordinates by Regge and Wheeler [44] in 1957 and Zerilli [56]. Using their formalism, a system of two very close black holes – treated as a weak perturbation of a single black hole – was first considered in [42] using perturbation theory. A little later [5] two equal mass Misner black holes were evolved with a full numerical code and they found agreement with perturbation theory if the separation parameter is small enough. A more comprehensive comparison between perturbation theory and full

non-linear numerical codes for distorted black holes was given in [4]. Perturbation theory of second order was worked out in [24] but will not be used in this thesis. In 2001 the perturbation theory was generalized for general coordinates by Sarbach et al. [45]. I will apply their formalism to Kerr-Schild initial data constructed in the way described before.

Teukolsky [48] developed a formalism of the perturbation of any vacuum Petrov-Type D background; especially of the Kerr metric. From a certain point of view this formalism would have been better adapted to Kerr-Schild initial data but is left for future work.

7.2 Perturbation theory

In [45], a formalism was developed for first order perturbations of a Schwarzschild background which will be explained here only very briefly.

The coordinates of the Schwarzschild background metric are assumed to be adapted to spherical symmetry, i.e. the background metric can be written as

$$\mathbf{g} = \bar{g}_{ab}\mathbf{d}x^a \otimes \mathbf{d}x^b + r^2(x^a)\hat{g}_{AB}\mathbf{d}x^A \otimes \mathbf{d}x^B$$

where bold quantities are abstract, i.e. not written out in a certain coordinate frame, $\mathbf{d}x^a$ and $\mathbf{d}x^A$ are coordinate differentials with respect to the pseudo-Riemannian manifold $\bar{M}$ and the standard metric of the 2-sphere S^2 respectively, i.e. the total background manifold is $M = \bar{M} \times S^2$. The perturbed metric is written as $\mathbf{g} + \delta\mathbf{g}$ with so small perturbation $\delta\mathbf{g}$ that only first order terms are important.

Following Regge-Wheeler and Zerilli the metric perturbations $\delta\mathbf{g}$ can be expanded into **tensor spherical harmonics**; given by the *quantum numbers* l and m. It is beyond the scope of this document to describe them in further detail, but it is important that they are orthonormalized with respect to some scalar product (see [56]) and complete in analogy with the well-known (scalar) spherical harmonics. Besides the quantum numbers l and m, the tensor spherical harmonics are classified by their behavior under parity transformation: the **even parity** ones which transform as $(-1)^l$ and **odd parity ones** which transform as $(-1)^{l+1}$. From the physical point of view odd parity perturbation are associated with infinitesimal rotations. Hence by means of this expansion, one can define a **mode** for each choice of the quantum numbers l and m and parity uniquely in terms of some functions, vector and tensor fields on $\bar{M}$.

7.3 Regge-Wheeler and Zerilli Equation

In the odd and even case for $l \geq 2$ one can construct a quantity – the **Regge-Wheeler**- or **Zerilli-function** respectively – which does not change under infinitesimal odd and respectively even gauge transformations and fulfills a simple evolution equation

$$\ddot{\Psi} - c_1\dot{\Psi}' - c_2\Psi'' - c_3\dot{\Psi} - c_4\Psi' + \alpha^2 V\Psi = 0 \tag{7.1}$$

with (in Kerr-Schild coordinates)

$$c_1 = \frac{4\,M}{r+2\,M} \qquad c_2 = \frac{r-2\,M}{r+2\,M}$$
$$c_3 = -\frac{2\,M}{r\,(r+2\,M)} \qquad c_4 = \frac{2\,M}{r\,(r+2\,M)},$$

the background lapse function

$$\alpha = \sqrt{\frac{r}{r + 2\,M}}$$

and the **Regge-Wheeler-** and **Zerilli-potential** respectively

$$V_{RW} = \frac{-6\,M + l\,(1+l)\,r}{r^3}$$
$$V_Z = \frac{36\,M^2\,(2\,M + r\,\lambda) + r^2\,\lambda^2\,(6\,M + r\,(2+\lambda))}{r^3\,(6\,M + r\,\lambda)^2}$$

defining $\lambda := (l-1)(l+2)$. A dot denotes derivatives with respect to t and a prime with respect to r.

It turns out that in the cases $l = 0, 1$ there are no dynamical modes. For even parity a monopole mode $l = 0$ leads to an infinitesimal change in mass of the background. The dipole mode $l = 1$ for odd parity introduces an infinitesimal angular momentum. The even $l = 1$ and odd $l = 0$ modes are purely gauge.

It is also shown how to compute the energy radiated to null infinity by gravitational waves. In Kerr-Schild coordinates it is

$$E = \frac{1}{16\pi} \lim_{r\to\infty} \int_0^\infty dt \sum_{l,m} \left(|\dot{\Psi}^{\text{odd}}_{lm}|^2 + |\dot{\Psi}^{\text{even}}_{lm}|^2 \right). \tag{7.2}$$

7.4 Characteristic Analysis and Well-Posedness

One wants to use eq. (7.1) to write a code which evolves Kerr-Schild initial data which can be regarded as a distorted Schwarzschild black hole. In numerical computations one always introduces artificial *noise* due to round-off errors and other approximations that can cause quickly growing modes and an eventual crash of the numerical code.

There is a wide range of dangers for a stable numerical code. The reason for this can be on the one hand the numerical method, on the other hand also the equation itself. For example for the parabolic heat equation one can show on the analytical level that little deviations in the initial data grow more than exponentially when integrating backward in time [32] which one calls **ill-posedness**. In contrast to this one calls a Cauchy problem **well-posed** if for given initial data a unique solution exists and if it depends on the initial data continuously. For linear equations with fixed coefficients, for example the wave equation, well-posedness implies that such deviations may grow not stronger than exponentially for all times [32]. This is a result which one obtains by means of the theory of Fourier transformations. If the coefficients are varying one also finds well-posedness but only up to a finite time [32]. Of course even exponential growth, which is allowed for a well-posed Cauchy problem, may kill a numerical code. So from the point of view of stable numerics, well-posedness of a Cauchy problem is rather necessary than sufficient.

Look again at eq. (7.1) but assume for a moment that it is a general quasi-linear equation, i.e. the coefficients are arbitrary but c_1 and c_2 only dependent on the first derivatives of u, u itself and r and t. In [27] such a second order quasi-linear equation is defined as **hyperbolic** if it has two independent non-vanishing **characteristics** which is equivalent to the fact that

the determinant of the coefficients of the **principle part** is strictly negative

$$\det\begin{pmatrix} 1 & -c_1/2 \\ -c_1/2 & -c_2 \end{pmatrix} = -\frac{1}{4}(c_1^2 + 4c_2) < 0. \tag{7.3}$$

By defining $\pi = \dot{\Psi}$ and $\phi = \Psi'$ one obtains an equivalent system of first order partial differential equations. In [32] it is shown that this first order system is well-posed if the coefficient matrix of the spatial derivatives has a complete set of real eigenvectors. In the computations of [45] in Section V it is derived that the hyperbolicity condition (7.3) is equivalent to this well-posedness condition. So eq. (7.1) is a well-posed hyperbolic partial differential equation if condition eq. (7.3) is fulfilled and one calls it **strictly hyperbolic** [32]. In the latter reference it is also shown that the initial-boundary-value problem, i.e. for finite computational domains with some boundary conditions, is well-posed if all characteristics leave the domain.

Going back now to the specific case of the Regge-Wheeler equation eq. (7.1) in Kerr-Schild coordinates. The hyperbolicity condition eq. (7.3) reads

$$c_1^2 + 4c_2 = \frac{4\,r^2}{(2\,M + r)^2} > 0$$

so it is in fact strictly hyperbolic.

The characteristics – also called **modes** – of eq. (7.1) are curves given by [27]

$$\frac{dr^\pm}{dt} = -\frac{1}{2}\left(c_1 \pm \sqrt{c_1^2 + 4c_2}\right) = -\frac{2M \pm r}{2M + r}.$$

Hence outside the background horizon $r > 2M$ there is one outgoing mode with speed $(r-2M)/(2M+r)$ and an ingoing one with speed 1 (speed of light); inside the event horizon $r < 2M$ both modes are going inwards. On these characteristic curves, $\Psi^\pm := \Psi(r^\pm(t), t)$ evolves as follows

$$\frac{d\Psi^\pm}{dt} = \Psi' \frac{dr^\pm}{dt} + \dot{\Psi} \tag{7.4}$$

which is

$$\begin{pmatrix} \frac{d\Psi^+}{dt} \\ \frac{d\Psi^-}{dt} \end{pmatrix} = \begin{pmatrix} \frac{dr^+}{dt} & 1 \\ \frac{dr^-}{dt} & 1 \end{pmatrix} \begin{pmatrix} \Psi' \\ \dot{\Psi} \end{pmatrix}.$$

This can be inverted

$$\begin{aligned} \begin{pmatrix} \Psi' \\ \dot{\Psi} \end{pmatrix} &= \frac{1}{\frac{dr^+}{dt} - \frac{dr^-}{dt}} \begin{pmatrix} 1 & -1 \\ -\frac{dr^-}{dt} & \frac{dr^+}{dt} \end{pmatrix} \begin{pmatrix} \frac{d\Psi^+}{dt} \\ \frac{d\Psi^-}{dt} \end{pmatrix} \\ &= -\frac{r+2M}{2r} \begin{pmatrix} 1 & -1 \\ -\frac{r-2M}{r+2M} & -1 \end{pmatrix} \begin{pmatrix} \frac{d\Psi^+}{dt} \\ \frac{d\Psi^-}{dt} \end{pmatrix}. \end{aligned} \tag{7.5}$$

This gives rise to simple and consistent boundary conditions. We want that at the boundaries of the computational domain there are only modes that leave the domain; modes, that are defined by the data on the domain. Because both modes leave the domain automatically when the inner boundary is placed inside the background horizon ($r < 2M$) we do not have to specify extra boundary conditions there (**excision**). At the outer boundary which is usually placed far away from the black hole horizon we set as a boundary condition

$d\Psi^+/dt = const$. If the constant vanishes than there is no ingoing mode but this condition is not necessarily consistent with the initial data which will be found analytically for all $r > 0$. So as the outer boundary condition, I compute the ingoing mode of the initial data at the outer boundary and leave it constant during evolution.

Chapter 8

Numerical Evolution

8.1 Kerr-Schild Initial Data

Assume we have found initial data using the construction procedure in Chapter 5 which can be considered as a weakly distorted Schwarzschild black hole. In Chapter 9 it will be shown by an example that this is indeed possible. Then we can use eq. (7.1) to evolve the data forward (or backward) in time and compute the radiated gravitational waveforms (the Regge-Wheeler or Zerilli function) and energy according to eq. (7.2). Before we are able to do this we have to convert the initial data in terms of l_μ, V and the time derivatives to perturbations of the Kerr-Schild-Schwarzschild background metric and from that to the Regge-Wheeler and Zerilli function, respectively, and their time derivatives for a given l and m and parity [45]. In Kerr-Schild coordinates this leads to long expressions and I used a Mathematica script to do the computations. As soon as one has converted the initial data in terms of l_μ, V and the time derivatives to initial data for the Regge-Wheeler-Zerilli function, one can use a numerical code to evolve the data by means of eq. (7.1).

8.2 Numerical Implementation of the Evolution Equation

Evolution Equations I implement eq. (7.1) in Fortran-90 in the following way. First one converts it to a first order system defining $\pi = \dot{\Psi}$ and $\phi = \Psi'$ which leads to

$$\begin{pmatrix} \dot{\pi} \\ \dot{\phi} \\ \dot{\Psi} \end{pmatrix} = \begin{pmatrix} c_1 & c_2 & 0 \\ 1 & 0 & 0 \\ 0 & 0 & 0 \end{pmatrix} \begin{pmatrix} \pi' \\ \phi' \\ \Psi' \end{pmatrix} + \begin{pmatrix} c_3 & c_4 & -\alpha^2 V \\ 0 & 0 & 0 \\ 1 & 0 & 0 \end{pmatrix} \begin{pmatrix} \pi \\ \phi \\ \Psi \end{pmatrix}. \tag{8.1}$$

Hence there are three evolution equations for three variables π, ϕ and Ψ.

Discretization I introduce a spatial one-dimensional grid of N points starting at the inner boundary r_{IB} within the background horizon and ending at the outer boundary r_{OB} far away from the black hole. The values of the functions at the ith grid point are denoted as π_i, ϕ_i and Ψ_i. As it turns out [45], to approximate the differential operators by finite differences of second order accuracy leads to a stable code only if one adds additional dissipation terms (see also [32]). Hence I decided to use fourth order finite differencing in space (coefficients

obtained straight forwardly with Mathematica)

$$(\partial_r f_i)\Delta r = \frac{1}{12} f_{i-2} - \frac{2}{3} f_{i-1} + \frac{2}{3} f_{i+1} - \frac{1}{12} f_{i+2} + O(\Delta r^5) \tag{8.2}$$

for a grid function f and a fourth order Runge-Kutta scheme in time [41] with the time discretization parameter Δt.

A necessary condition for stability is that the **Courant-Friedrich-Levy parameter**

$$\lambda = \frac{\Delta t}{\Delta r} < 1.$$

In [43] one finds more about stability of such methods.

At the boundaries where eq. (8.2) cannot be applied, I use extrapolation to obtain data on two grid points beyond each of the boundaries. On the left hand side this is

$$f_i = 5 f_{i+1} - 10 f_{i+2} + 10 f_{i+3} - 5 f_{i+4} + f_{i+5} + O(dr^5)$$

and on the right hand side

$$f_i = 5 f_{i-1} - 10 f_{i-2} + 10 f_{i-3} - 5 f_{i-4} + f_{i-5} + O(dr^5).$$

So after extrapolation eq. (8.2) can be used on the whole computational domain.

Boundary conditions Eq. (7.4) and (7.5) give a one-one correspondence between the grid functions and the two characteristics in each point of the grid. At the outer boundary outside the background horizon where the ingoing mode is not defined by the data on the computational domain (except if it stays constantly equal to the initial ingoing mode there) it is thus possible during an evolution to compute the modes from the extrapolated data, set the ingoing mode to the initial one and recompute the data. So this implements an **outgoing radiation boundary**. At the inner boundary it was shown in Section 7.4 that both modes leave the computational domain automatically so both of them are determined by the data. This means that there is no need to put any boundary condition here.

Radiated Energy The energy radiated to null-infinity is computed by means of eq. (7.2). In principal the integral must be evaluated at $r \to \infty$ and for an infinite amount of time. In practice r needs only to be so large that the metric is *practically* flat and one only needs to integrate long enough that the gravitational waves have already passed the point of the extraction.

The Program The program reads initial data from a text file generated by Mathematica. With an ASCII parameter file the following parameters can be controlled:

- Mass M of the background metric
- Angular momentum quantum number l
- A boolean parameter choosing odd- or even parity (to use the Regge-Wheeler or the Zerilli potential in eq. (7.1))

- Position r_{rad} of the extraction of the radiated energy
- Courant-Friedrich-Levy factor λ
- Time when the evolution is to be stopped
- Additional control of the output

To actually confirm fourth order convergence of the numerical code the program has the capability to run the evolutions obtained with three different resolutions. First, the program takes the resolution determined by the initial data ASCII file. Second, it doubles the grid spacing in space and in time (leaving the Courant-Friedrich-Levy factor constant), i.e. using only every second point in the initial data ASCII file. Third it doubles the grid spacing again. The three different resolutions are put into three different output files. If there is 4th order convergence then at each time step

$$16|\Psi_{HR} - \Psi_{MR}| = |\Psi_{MR} - \Psi_{LR}| \tag{8.3}$$

which can then be checked easily with Gnuplot [2]. Here Ψ_{HR} denotes the result of the high, Ψ_{MR} of the medium and Ψ_{LR} of the low resolution run.

8.3 Code Tests

I set the background mass $m = 1$ and only look for a $l = 2$ even parity mode. As initial data for the Zerilli function I chose a Gaussian

$$\Psi(r) = e^{-(r-30)^2/4}$$

and the first time-derivative

$$\dot{\Psi}(r) = 0.$$

The inner boundary is set to $r = 1.8$ and the outer boundary to $r = 50$ with a grid size of $\Delta r = 0.01$ (of the highest resolution run). The evolution runs until $t = 30$ with a Courant-Friedrich-Levy factor of 0.5. Fig. 8.1 on the next page shows the Zerilli function at different times.

A crucial question is if the code shows fourth order convergence. As was said before it runs three times with the same initial data but coarsening the computational grid in each run by a factor of two. If the convergence is correct, eq. (8.3) holds for the results of the three runs. This is shown in Fig. 8.2 and Fig. 8.3 on page 60 for two different times. The plots confirm that there is fourth order convergence except when the pulse hits the outer boundary. The reason for this is not fully understood. One way out of this problem at the moment is to only trust the evolution in regions causally disconnected from the outer boundary.

Although physically meaningless, for these initial data the program extracted the radiated energy at $r = 30$. For the high resolution it is 0.144721465, for the medium one 0.144721468 and for the low one 0.144721520. This is fourth order converging.

The next test for the program was to show that it can reproduce the results in [46] for the close limit of the unboosted black holes without angular momentum, but it turned out that this was not possible. This problem was solved by a personal discussion with the authors M. Tiglio and O. Sarbach from which I learned that they had an error in their code which they used for the paper. After correcting it, now our codes obtain the same results. My computations are described in Chapter 9 which includes the unboosted case $\Pi = 0$.

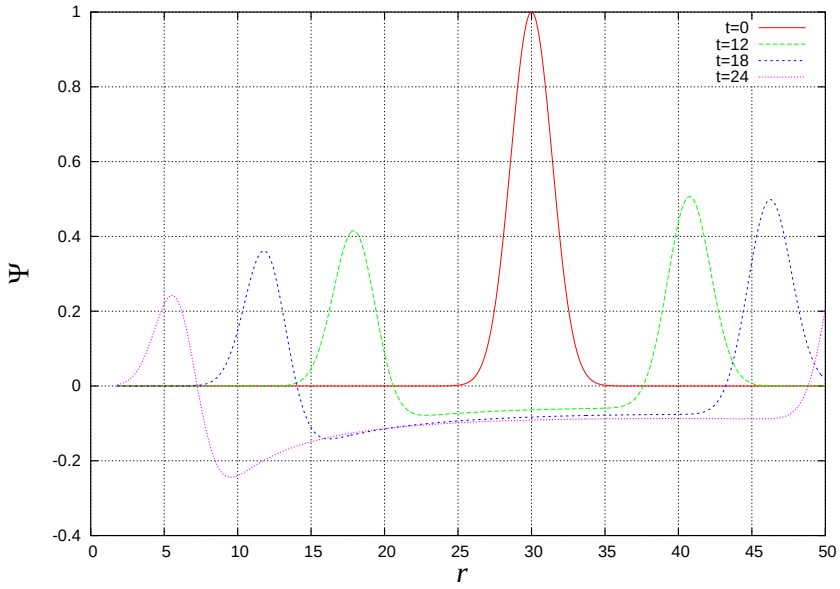

Figure 8.1: Gauß Initial Data: Waveforms at different times, $l = 2$, even parity

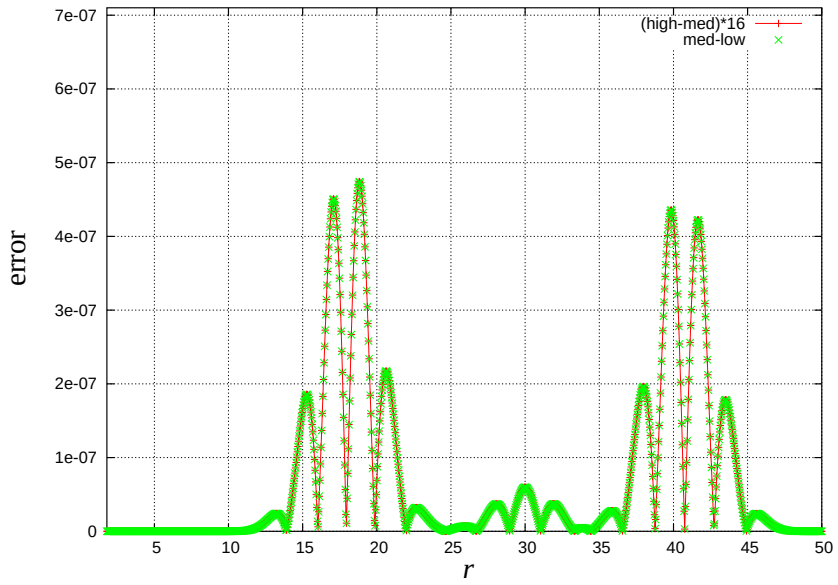

Figure 8.2: Gauß Initial Data: Convergence at $t = 12$, $l = 2$, even parity

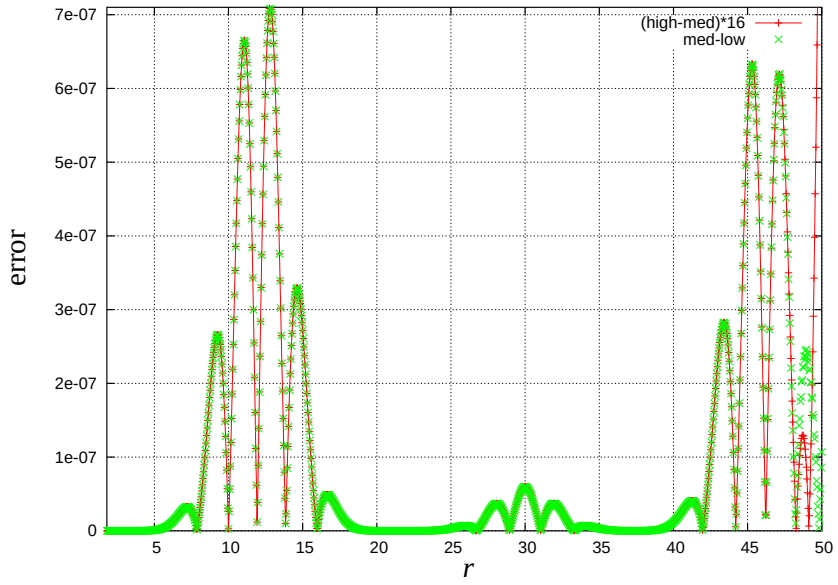

Figure 8.3: Gauß Initial Data: Convergence at $t = 18$, $l = 2$, even parity

Chapter 9

Application: Boosted Schwarzschild like Close Limit

9.1 Initial Data

In [10] analytical initial data for two very close black holes without boosts and spins were found. In [46] these data were evolved and the gravitational energy was computed. With my general framework to construct Kerr-Schild initial data it becomes possible to generalize this simple black hole system for additional boosts.

Consider the following setup for the binary black hole system (Fig. 9.1)

- Mass parameters M_1, M_2 ($M := M_1 + M_2$)
- Coordinate positions $(0, 0, \epsilon M_2)$, $(0, 0, -\epsilon M_1)$
- Momentum parameters $P(0, \sin\chi, \cos\chi)$, $-P(0, \sin\chi, \cos\chi)$
- Vanishing spin parameters

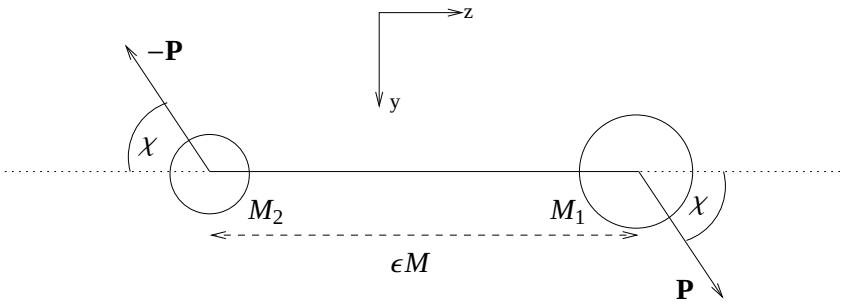

Figure 9.1: Boosted Close Limit Setup

In the following analysis I assume that $\Pi \ll 1$ and $\epsilon \ll 1$ with $\Pi := P/M$. The partly lengthy computations were done with Mathematica.

9.1.1 Electromagnetic Field Tensor

The total *electromagnetic field tensor* is constructed following Section 5.4 with the spin parameters set to zero and the additional generalization that the boosts can show in other directions than the z-axis. With

$$R(\chi) = \begin{pmatrix} 1 & 0 & 0 & 0 \\ 0 & 1 & 0 & 0 \\ 0 & 0 & \cos\chi & \sin\chi \\ 0 & 0 & -\sin\chi & \cos\chi \end{pmatrix}$$

the Lorentz matrix in our case is

$$\Lambda(P,\chi) = R(\chi) \cdot \Lambda(P) \cdot R^{-1}(\chi).$$

The individual electromagnetic field tensors are superposed as in eq. (5.10) using a shielding parameter $k = 3$.

9.1.2 Kerr-Schild Null Vector Field

By means of eq. (5.12) the normalized Kerr-Schild null vector field, i.e. the eigenvector of the total electromagnetic field tensor associated with the only negative eigenvalue, is obtained. It will be printed here in spherical Kerr-Schild coordinates, i.e. in coordinates (r,θ,ϕ) where the induced metric of $\tilde{\Sigma}_0$ is $(d_{ij}) = \mathrm{diag}(1, r^2, r^2\sin^2\theta)$.

To lowest order in ϵ and Π the spatial part of l_μ is

$$\begin{aligned} \mathbf{l} = \mathbf{l}^{(SS)} &+ \epsilon\Pi\, A_{11}(r)\, \underbrace{(S^{1,1}_{\text{odd}}(\theta,\phi) - S^{1,-1}_{\text{odd}}(\theta,\phi))}_{=:R^{1,1}_{\text{odd}}(\theta,\phi)} \\ &+ \epsilon\Pi\, A_{21}(r)\, \underbrace{(S^{2,1}_{\text{even}}(\theta,\phi) + S^{2,-1}_{\text{even}}(\theta,\phi))}_{=:I^{2,1}_{\text{even}}(\theta,\phi)} \\ &+ (\epsilon^2\, A^{\epsilon}_{20}(r) + \epsilon\Pi\, A^{\Pi}_{20}(r))\, S^{20}_{\text{even}}(\theta,\phi). \end{aligned}$$

with

$$A^{\epsilon}_{20}(r) = \sqrt{\frac{\pi}{5}}\,\frac{12M^2\mu}{r}, \qquad A^{\Pi}_{20}(r) = -\sqrt{\frac{\pi}{5}}\,12M\cos\chi,$$

$$A_{21}(r) = -3i\sqrt{\frac{6\pi}{5}}\,M\sin\chi, \qquad A_{11}(r) = \sqrt{\frac{2\pi}{3}}\,M\sin\chi$$

using

$$\mu := \frac{M_1 M_2}{M^2}.$$

Note that there is the symmetry of the simultaneous transformations $\chi \to \pi+\chi$ and $\Pi \to -\Pi$ as is expected from Fig. 9.1.

$S^{l,m}(\theta,\phi)$ are standard vector spherical harmonics [45]. In Kerr-Schild spherical coordinates they are

$$S^{l,m}_{\text{even}}(\theta,\phi) = \mathbf{d}Y^{l,m}(\theta,\phi)$$
$$= \begin{pmatrix} 0 \\ m\,Y^{l,m}(\theta,\phi)\cot\theta + \sqrt{l\,(l+1) - m\,(m+1)}\,Y^{l,m+1}(\theta,\phi)e^{-i\,\phi} \\ i\,m\,Y^{l,m}(\theta,\phi) \end{pmatrix}$$

and

$$S^{l,m}_{\text{odd}}(\theta,\phi) = *\mathbf{d}Y^{l,m}(\theta,\phi)$$
$$= \begin{pmatrix} 0 \\ -i\,m\,Y^{l,m}(\theta,\phi)\csc\theta \\ m\,Y^{l,m}(\theta,\phi)\cos\theta + \sqrt{l\,(l+1) - m\,(m+1)}\,Y^{l,m+1}(\theta,\phi)e^{-i\,\phi}\sin\theta \end{pmatrix}$$

where * is the **Hodge-Operator** associated with the metric on S^2 [45].

This is a perturbation of Schwarzschild Kerr-Schild null vector field to lowest order in ϵ and Π. If the black holes are sitting on top of each other ($\epsilon = 0$), $\mathbf{l}$ reduces to the Schwarzschild one $\mathbf{l}^{(SS)} = -(1,0,0)$ for all values of Π. This means that there is no change of the total background linear momentum. Note [46] that the expansion in ϵ and Π makes no sense if $r < r_0 \sim \epsilon M$.

Now I try to find solutions of the constraint equations in terms of the same modes. Afterwards the physical meaning of the modes will be discussed.

9.1.3 Solution of the Kerr-Schild Constraint Equations

Derivation of the Kerr-Schild Constraint Equations

Eq. (6.1) to (6.3) are the Kerr-Schild constraint equations in Cartesian Kerr-Schild coordinates. I rederived them in spherical Kerr-Schild coordinates to make use of the symmetries in our problem. I applied the same Mathematica code which before successfully derived the Cartesian ones above. For an additional check I also used the RG-TC-package [11][1].

Separation Ansatz

The unknown functions which we have to solve for are $V(r,\theta,\phi)$, $\dot{V}(r,\theta,\phi)$ and $\dot{l}_i(r,\theta,\phi)$ at $t = 0$. All the following computations are very long and only the results are printed. They were done using Mathematica.

[1] Website given in the reference was not active when I finished this thesis, alternative address: http://library.wolfram.com/infocenter/MathSource/4484/

To separate the constraint equations (Section 6.1) the following ansatz is made

$$V(r,\theta,\phi) = -\frac{M}{r} + \epsilon\,\Pi\, v_{11}^{\Pi}(r)\left(Y^{1,1}(\theta,\phi) - Y^{1,-1}(\theta,\phi)\right)\sin\chi + i\,\epsilon\,\Pi\, v_{21}^{\Pi}(r)\left(Y^{2,-1}(\theta,\phi) + Y^{2,1}(\theta,\phi)\right)\sin\chi + \left(\epsilon^2\,\mu\, v_{20}^{\epsilon}(r) + \epsilon\,\Pi\, v_{20}^{\Pi}(r)\right) Y^{2,0}(\theta,\phi), \tag{9.1}$$

$$\dot{\mathbf{I}}(r,\theta,\phi) = \epsilon\,\Pi\, l_{11}^{\Pi}(r)\, R_{\text{odd}}^{1,1}(\theta,\phi)\,\sin\chi + i\,\epsilon\,\Pi\, l_{21}^{\Pi}(r)\, I_{\text{even}}^{2,1}(\theta,\phi)\,\sin\chi + \left(\epsilon^2\,\mu\, l_{20}^{\epsilon}(r) + \epsilon\,\Pi\, l_{20}^{\Pi}(r)\right) S_{\text{even}}^{2,0}(\theta,\phi), \tag{9.2}$$

$$\dot{V}(r,\theta,\phi) = \epsilon\,\Pi\,\tilde{v}_{11}^{\Pi}(r)\left(Y^{1,1}(\theta,\phi) - Y^{1,-1}(\theta,\phi)\right)\sin\chi + i\,\epsilon\,\Pi\,\tilde{v}_{21}^{\Pi}(r)\left(Y^{2,-1}(\theta,\phi) + Y^{2,1}(\theta,\phi)\right)\sin\chi + \left(\epsilon^2\,\mu\,\tilde{v}_{20}^{\epsilon}(r) + \epsilon\,\Pi\,\tilde{v}_{20}^{\Pi}(r)\right) Y^{2,0}(\theta,\phi). \tag{9.3}$$

Reducing the Number of Unknown Functions

The constraint equations lead to the following relations. For simplicity one introduces the mass scaled radial coordinate $x := r/M$.

The unknown radial functions for the odd (1,1)-mode are given by

$$v_{11}^{\Pi}(x) = 0, \quad \tilde{v}_{11}^{\Pi}(x) = 0, \quad l_{11}^{\Pi}(x) = \frac{C}{x}, \tag{9.4}$$

with an arbitrary constant C.

In the even 21-sector the constraints allow to express the three unknown functions in terms of $v_{21}^{\Pi}(r)$, eventually obtaining one ordinary differential equation for it (see next section)

$$\tilde{v}_{21}^{\Pi}(x) = \frac{3\,\sqrt{30\,\pi} + 10\,x^2(1+2\,x)v_{21}^{\Pi}(x) + 5x^3(2+x)v_{21}^{\Pi\,\prime}(x)}{10\,x^3}, \tag{9.5}$$

$$l_{21}^{\Pi}(x) = \frac{x^2}{6}\left(4\,v_{21}^{\Pi}(x) + x\,v_{21}^{\Pi\,\prime}(x)\right). \tag{9.6}$$

As long as $v_{21}^{\Pi}(x)$ is invariant under the simultaneous transformations $\chi \to \pi + \chi$, $\Pi \to -\Pi$, the 21-mode is also invariant.

In the even (2,0)-sector there are two sets of functions, one related to $\epsilon\Pi$

$$\tilde{v}_{20}^{\Pi}(x) = \frac{12\,\sqrt{5\,\pi}\,\cos\chi + 10\,x^2(1+2x)\,v_{20}^{\Pi}(x) + 5x^3(2+x)v_{20}^{\Pi\,\prime}(x)}{10\,x^3}, \tag{9.7}$$

$$l_{20}^{\Pi}(x) = \frac{x^2}{6}\left(4\,v_{20}^{\Pi}(x) + x\,v_{20}^{\Pi\,\prime}(x)\right) \tag{9.8}$$

and one related to ϵ^2

$$\tilde{v}_{20}^{\epsilon}(x) = \frac{12\,\sqrt{5\,\pi}(x-1) + 10x^3(1+2x)v_{20}^{\epsilon}(x) + 5\,x^4(2+x)v_{20}^{\epsilon\,\prime}(x)}{10\,x^4}, \tag{9.9}$$

$$l_{20}^{\epsilon}(x) = \frac{12\,\sqrt{5\,\pi}(x-1) + 20\,x^4\,v_{20}^{\epsilon}(x) + 5\,x^5\,v_{20}^{\epsilon\,\prime}(x)}{30\,x^2}. \tag{9.10}$$

If one wants the 21-mode to be invariant under $\chi \to \pi + \chi$ and $\Pi \to -\Pi$ then one has to require that $v_{20}^{\Pi}(x) \to -v_{20}^{\Pi}(x)$, see below.

Solving the Remaining Equations

With these last relations there are only three unknown functions left $v_{21}^{\Pi}(x)$, $v_{20}^{\Pi}(x)$ and $v_{20}^{\epsilon}(x)$. Each of them fulfills an ordinary linear differential equation and it is possible to find analytic solutions which lead to asymptotic flatness of the total metric.

Even 21-Mode $v_{21}^{\Pi}(r)$ has to satisfy the following second order linear inhomogeneous ordinary differential equation

$$-3\sqrt{\frac{6\pi}{5}} - 6\,x^2\,v_{21}^{\Pi}(x) + 5\,x^4\,v_{21}^{\Pi}{}'(x) + x^5\,v_{21}^{\Pi}{}''(x) = 0. \tag{9.11}$$

A particular solution is

$$v_{21}^{\Pi}(x) = -\sqrt{\frac{\pi}{30}}\frac{3 - 2\,x + x^2}{x^2}.$$

When the homogeneous equation

$$-6\,x^2\,v_{21}^{\Pi}(x) + 5\,x^4\,v_{21}^{\Pi}{}'(x) + x^5\,v_{21}^{\Pi}{}''(x) = 0$$

is transformed the following way

$$v_{21}^{\Pi}(x) = \frac{u(x)}{x^2}$$

and afterwards

$$z = \sqrt{\frac{24}{x}}$$

it reduces to

$$z^2u''(z) + zu'(z) - (16 + z^2)u(z) = 0$$

which is the **modified Bessel equation**[2] for $n = 4$ and is solved by the **modified Bessel functions**. So the general solution of eq. (9.11) is

$$v_{21}^{\Pi}(x) = -\sqrt{\frac{\pi}{30}}\frac{3 - 2\,x + x^2}{x^2} + \frac{C_{21}^1\,I_4\left(\sqrt{\frac{24}{x}}\right)}{x^2} + \frac{C_{21}^2\,K_4\left(\sqrt{\frac{24}{x}}\right)}{x^2} \tag{9.12}$$

with two arbitrary coefficients C_{21}^1 and C_{21}^2. One of them will be fixed later by the additional requirement of asymptotic flatness.

[2] see for example http://mathworld.wolfram.com/ModifiedBesselDifferentialEquation.html

Even 20-Mode We find the general solutions of $v_{20}^{\Pi}(x)$ and $v_{20}^{\epsilon}(x)$ in a very similar way.

The first function $v_{20}^{\Pi}(x)$ has to fulfill

$$-12\,\sqrt{\frac{\pi}{5}}\,\cos\chi - 6\,x^2\,v_{20}^{\Pi}(x) + 5\,x^4\,v_{20}^{\Pi}{}'(x) + x^5\,v_{20}^{\Pi}{}''(x) = 0$$

with the general solution

$$v_{20}^{\Pi}(x) = -2\,\sqrt{\frac{\pi}{5}}\,\frac{3-2\,x+x^2}{3\,x^2}\,\cos\chi + \frac{C_{\Pi}^{1}\,I_4\left(\sqrt{\frac{24}{x}}\right)}{x^2} + \frac{C_{\Pi}^{2}\,K_4\left(\sqrt{\frac{24}{x}}\right)}{x^2}. \tag{9.13}$$

For $v_{20}^{\epsilon}(x)$ we have to solve

$$-12\,\sqrt{\frac{\pi}{5}}\left(3-\frac{2}{x}\right) - 6\,x^2\,v_{20}^{\epsilon}(x) + 5\,x^4\,v_{20}^{\epsilon}{}'(x) + x^5\,v_{20}^{\epsilon}{}''(x) = 0$$

and obtain

$$v_{20}^{\epsilon}(x) = -4\,\sqrt{\frac{\pi}{5}}\,\frac{3+3\,x-2\,x^2+x^3}{3\,x^3} + \frac{C_{\epsilon}^{1}\,I_4\left(\sqrt{\frac{24}{x}}\right)}{x^2} + \frac{C_{\epsilon}^{2}\,K_4\left(\sqrt{\frac{24}{x}}\right)}{x^2}. \tag{9.14}$$

9.1.4 Asymptotic Flatness

For the initial data to be physically relevant one requires that $g_{\mu\nu}$ and its first time derivative are initially asymptotically flat, i.e. it converges to the Minkowski metric for $r \to \infty$. For this it is sufficient to show that all radial functions, which we have just obtained, converge to zero in this limit. This is not the case for arbitrary choices of the free parameters because $\lim_{z\to 0} K_4(z) = \infty$.

Even 21-mode

Using $z = 1/x$, the Taylor expansion of $v_{21}^{\Pi}(1/z)$ at $z \to 0$ is

$$\begin{aligned} v_{21}^{\Pi}(1/z) = &\left(\frac{C_{21}^2}{12} - \sqrt{\frac{\pi}{30}}\right) + \left(\frac{-C_{21}^2}{6} + \sqrt{\frac{2\,\pi}{15}}\right) z + \left(\frac{C_{21}^2}{4} - \sqrt{\frac{3\,\pi}{10}}\right) z^2 - \frac{C_{21}^2\,z^3}{2} \\ &+ \left(\frac{3\,C_{21}^1}{2} + 576\,C_{21}^2\left(\frac{\frac{25}{12} - 2\,\gamma}{768} + \frac{\log(2) - \log(2\,\sqrt{6}) - \frac{\log(z)}{2}}{384}\right)\right) z^4 + \ldots. \end{aligned}$$

Because $\lim_{z\to 0} z^n \log z = 0$ we obtain the right limit if

$$C_{21}^2 = 12\,\sqrt{\frac{\pi}{30}}. \tag{9.15}$$

Hence to leading order ($z^4 \log z$ goes faster to zero than z^3) we have

$$v_{21}^{\Pi}(x) \xrightarrow{x\to\infty} -\sqrt{\frac{6\pi}{5}}\,\frac{1}{x^3}.$$

Because of this we find that both $\tilde{v}_{21}^{\Pi}(x)$ and $l_{21}^{\Pi}(x)$ go to zero for $x \to \infty$, by looking at eq. (9.5) and (9.6).

Even 20-mode

The same can be done for the remaining modes. The requirement of asymptotically flatness leads to

$$C_{\Pi}^{2} = 8\,\sqrt{\frac{\pi}{5}}\,\cos\chi \tag{9.16}$$

and

$$C_{\epsilon}^{2} = 16\,\sqrt{\frac{\pi}{5}}. \tag{9.17}$$

9.1.5 Final Solution

Eventually we have the following solutions of the constraint equations, using ansatz eq. (9.1) to (9.3). From eq. (9.12) and the asymptotic flatness requirement eq. (9.15) one gets

$$\begin{aligned} v_{21}^{\Pi}(x) = &-\sqrt{\frac{\pi}{30}}\,\frac{3-2\,x+x^{2}}{x^{2}} + 2\,(8\gamma+K_{3})\,\sqrt{\frac{\pi}{5}}\,\frac{I_{4}\left(\sqrt{\frac{24}{x}}\right)}{x^{2}} \\ &+ 2\,\sqrt{\frac{6\,\pi}{5}}\,\frac{K_{4}\left(\sqrt{\frac{24}{x}}\right)}{x^{2}}, \end{aligned} \tag{9.18}$$

where there is the additional definition

$$C_{21}^{1} =: 2\,(8\,\gamma+K_{3})\,\sqrt{\frac{\pi}{5}}$$

for consistency with the different definition of the Bessel functions used in [46] and γ is the **Euler number**. The other unknown functions in this sector can be obtained from eq. (9.5) and eq. (9.6).

In the same manner I computed

$$\begin{aligned} v_{20}^{\epsilon}(x) = &-4\,\sqrt{\frac{\pi}{5}}\,\frac{\left(3+3\,x-2\,x^{2}+x^{3}\right)}{3\,x^{3}} + 2\,(8\,\gamma+K_{1})\,\sqrt{\frac{\pi}{5}}\,\frac{I_{4}\left(\sqrt{\frac{24}{x}}\right)}{x^{2}} \\ &+ 16\,\sqrt{\frac{\pi}{5}}\,\frac{K_{4}\left(\sqrt{\frac{24}{x}}\right)}{x^{2}} \end{aligned} \tag{9.19}$$

and

$$\begin{aligned} v_{20}^{\Pi}(x) = \sqrt{\frac{\pi}{5}}\,\frac{2}{x^{2}}\Bigg[&(8\,\gamma+K_{2})\,I_{4}\left(\sqrt{\frac{24}{x}}\right) \\ &-\frac{3-2\,x+x^{2}}{3}+4\,K_{4}\left(\sqrt{\frac{24}{x}}\right)\Bigg]\cos\chi. \end{aligned} \tag{9.20}$$

where I defined

$$C_{\Pi}^{1} =: 2\,(8\,\gamma+K_{2})\,\sqrt{\frac{\pi}{5}}\cos\chi$$

because with this the 20-mode has the desired transformation behavior for $\chi \to \pi+\chi$ and $\Pi \to -\Pi$.

For the odd 11-mode there is only l_{11}^{Π} which is not necessarily vanishing, see eq. (9.4).

9.1.6 Regge-Wheeler-Zerilli Function

For each of the modes with $l \geq 2$ one can compute the initial Regge-Wheeler-Zerilli function and its first time-derivative [45]. Then one uses the Regge-Wheeler-Zerilli equation eq. (7.1) to evolve that data, compute waveforms and the radiated energy by means of eq. (7.2). The $(1,1)$-mode is not dynamical and there exists no Regge-Wheeler-Zerilli function.

One obtains with the help of Mathematica

$$\Psi_{21}(x) = i\,\epsilon\,\Pi\,\frac{3\,\sqrt{30\,\pi} + 5\,x^2\,v_{21}^{\Pi}(x)}{15(3+2\,x)}\,\sin\chi \tag{9.21}$$

and

$$\dot{\Psi}_{21}(x) = i\,\epsilon\,\Pi\,\frac{3\,\sqrt{30\,\pi} + 10\,x^2(1-2x)\,v_{21}^{\Pi}(x) + 5\,x^3\,(2-x)v_{21}^{\Pi}{}'(x)}{30x\,(3+2\,x)}\,\sin\chi. \tag{9.22}$$

The 20-mode is

$$\Psi_{20}(x) = \epsilon^2\,\mu\,\frac{-12\,\sqrt{5\,\pi} + 5\,x^3\,v_{20}^{\epsilon}(x)}{15\,x\,(3+2\,x)} + \epsilon\,\Pi\,\frac{12\,\sqrt{5\,\pi}\,x\,\cos\chi + 5\,x^3\,v_{20}^{\Pi}(x)}{15\,x\,(3+2\,x)}$$

and

$$\begin{aligned}\dot{\Psi}_{20}(x) = &-\epsilon^2\,\mu\,\frac{12\,\sqrt{5\,\pi}(x-1) - 10\,x^3(1-2x)\,v_{20}^{\epsilon}(x) - 5\,x^4(2-x)\,v_{20}^{\epsilon}{}'(x)}{30\,x^2\,(3+2\,x)} \\ &+\epsilon\,\Pi\,\frac{12\,\sqrt{5\,\pi}\,x\,\cos\chi + 10\,x^3\,(1-2x)v_{20}^{\Pi}(x) + 5\,x^4\,(2-x)v_{20}^{\Pi}{}'(x)}{30\,x^2\,(3+2\,x)}.\end{aligned} \tag{9.23}$$

Because the Regge-Wheeler functions are gauge-independent, the free parameter K_1, K_2 and K_3 cannot be just gauge-parameters but must have an impact on the physics of the initial data.

9.2 Results & Interpretation

9.2.1 Modes

We have found a solution of the constraint equations in terms of three modes: odd-(1,1), even-(2,1) and even-(2,0). With the help of [45], even without evolutions this gives rise to physical interpretations.

First there is no even monopole mode. This means that to lowest order in the perturbation parameters the total ADM-mass is M.

Second there is a non-vanishing odd dipole mode if $\chi \neq 0 \neq \Pi$. So the ADM-angular momentum is not zero but infinitesimally small. When one compares the metric at $t = 0$, switching of the other modes, with the Kerr-metric with spin in x-direction in spherical Kerr-Schild coordinates, i.e. those coordinates described in Section 4.4 with the additional transformation that brings $(\eta_{\mu\nu}) = \mathrm{diag}(-1,1,1,1)$ to $(\eta_{\mu\nu}) = \mathrm{diag}(-1,1,r^2,r^2\sin^2\theta)$, one finds to first order in the spin-parameter a that

$$a = \frac{1}{2}M\epsilon\Pi\sin\chi.$$

In special relativity two particles with initial coordinate positions as the black holes above and momenta have angular momentum

$$L = -M^2 \epsilon \Pi \sin\chi.$$

The different sign shows that there is a distinction between a system with angular momentum on a fixed background spacetime and a system of fixed observers on a *rotating* spacetime.

Third there are two dynamical, i.e. gravitational wave modes: even 20- and 21-mode. The first is present even if there is no angular momentum involved. This implies that it does not carry angular momentum but only energy to null infinity. The 21-mode is only present if there is angular momentum in the spacetime which implies that it not only carries energy but also angular momentum to null infinity.

9.2.2 Apparent Horizon

Coordinate Position

From Section 5.7.2 we know that one can find marginally trapped surfaces as surfaces orthogonal to l_i with $V = -\frac{1}{2}$ if l_i is surface forming. In our black hole system this is the case if $\chi = 0$ which I checked with the Frobenius condition $l_{[i} l_{j,k]} = 0$ with Mathematica. Because our initial data is only a lowest order perturbation of the Schwarzschild metric where $x = 2$ defines such a surface one can proceed the following way. One wants to solve the equation

$$V(2 + \Delta x) = -\frac{1}{2}$$

to first order in Δx. Let η be the amplitude of the perturbation (in our case it has to be substituted by ϵ^2 and $\epsilon\Pi$, respectively) and $f(x, \theta, \phi)$ be the perturbation of V. Then I write

$$\begin{aligned} -\frac{1}{2} &= V_{SS}(2 + \Delta x) + \eta f(2 + \Delta x, \theta, \phi) \\ &= -\frac{1}{2} + \partial_x V_{SS}(2)\Delta x + \eta f(2, \theta, \phi) + \eta\, \Delta x\, \partial_x f(2, \theta, \phi). \end{aligned}$$

The last term is now ignored because it is of second order. Then it follows with $\partial_x V_{SS}(2) = 1/4$

$$\Delta x = -4\eta f(2, \theta, \phi)$$

or finally

$$x^{AH}(\theta, \phi) = 2(1 - 2\eta f(2, \theta, \phi)). \tag{9.24}$$

Due to eq. (9.1) for $\chi = 0$ it is

$$\begin{aligned} x^{AH}(\theta, \phi) &= 2\Big[1 - 2\left(\epsilon^2 \mu\, v^{\epsilon}_{20}(2) + \epsilon\, \Pi\, v^{\Pi}_{20}(2)\right) Y^{2,0}(\theta, \phi)\Big] \\ &= 2 - \frac{1}{2}\sqrt{\frac{5}{\pi}}\left(\epsilon^2 \mu\, v^{\epsilon}_{20}(2) + \epsilon\, \Pi\, v^{\Pi}_{20}(2)\right)(3\cos^2\theta - 1). \end{aligned} \tag{9.25}$$

This means that K_1 and K_2 fix the initial coordinate position of the apparent horizon.

The shape of the apparent horizon in coordinate space is that of an ellipsoid, i.e. the section $\phi = const$ is an ellipse (Fig. 9.2 on the following page). An ellipse is the set of points

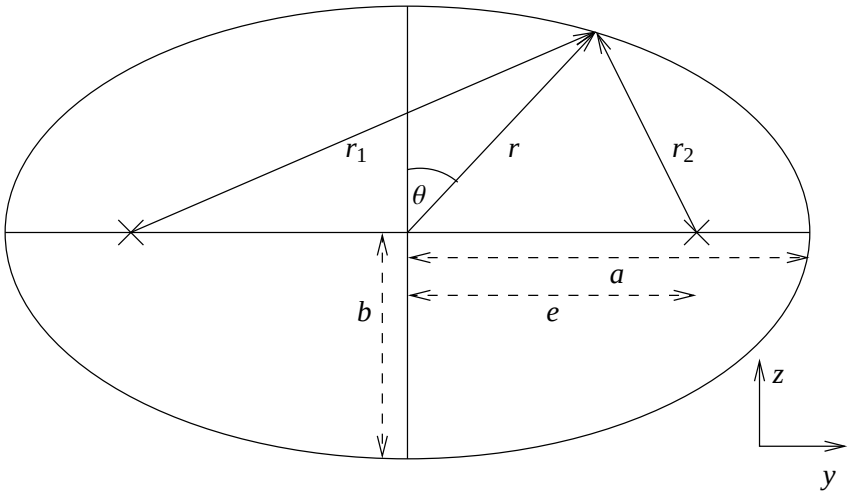

Figure 9.2: Ellipse

such that the sum of the distances from two foci are twice the major semiaxis $r_1 + r_2 = 2a$. If the center of the ellipse is at the coordinate origin and the semiaxes are aligned with the coordinate axes it fulfills the equation

$$\frac{z^2}{b^2} + \frac{y^2}{a^2} = 1$$

where b is the minor semiaxis. The linear eccentricity is the distant e of the center to one of the foci, the numerical eccentricity $\eta = e/a$. There is the relation $a^2 = b^2 + e^2$ and in spherical coordinates we obtain

$$r = a\sqrt{\frac{a^2 - e^2}{a^2 - e^2 \sin^2\theta}}.$$

If $e \ll a$ then this becomes to first order

$$r = a - \frac{e^2}{2a}\cos^2\theta.$$

Comparing this with eq. (9.25) we get

$$a = 2 + \frac{1}{2}\sqrt{\frac{5}{\pi}}\left(\epsilon^2\,\mu\,\nu_{20}^{\epsilon}(2) + \epsilon\,\Pi\,\nu_{20}^{\Pi}(2)\right)$$

and

$$e^2 = 6\sqrt{\frac{5}{\pi}}\left(\epsilon^2\,\mu\,\nu_{20}^{\epsilon}(2) + \epsilon\,\Pi\,\nu_{20}^{\Pi}(2)\right)$$

ignoring higher order terms. To see how these values depend on the free parameters (e.g. in the case $\Pi = 0$)

$$\nu_{20}^{\epsilon}(2) = 0.477 + 0.264K_1.$$

Area

The horizon area is an important physical quantity. There is the general – but unproven – **Penrose inequality**

$$M_{ADM} \geq \sqrt{\frac{A}{16\pi}}$$

for the ADM-mass with the equal sign if and only if the geometry is diffeomorphic to Schwarzschild [40]. If this inequality holds then in my case the area of the horizon on the initial slice can only be decreased or unchanged by the lowest order perturbation parameters in ϵ and Π because it was already found that the ADM-mass is constant.

The area of an embedded 2-submanifold S is defined as

$$A = \int\int d\lambda d\sigma \sqrt{\det q(\lambda, \sigma)}. \tag{9.26}$$

λ and ρ are coordinates with coordinates lines tangent to the 2-surface, $\mathbf{q}$ is its induced metric.

Because we only have to deal with the spacelike slice Σ_0 at the moment and thus do not need to care about its embedding into the full spacetime M, all indices are raised/lowered with γ_{ij} in this section for convenience, e.g. in contrast to Section 4.5 on page 31

$$l^i := \gamma^{ij} l_j$$

(and not $\bar{l}^i$) and I will write γ^{ij} instead of $(\gamma^{-1})^{ij}$. Then the induced metric of S is

$$q_{ij} = \gamma_{ij} - (1 - 2V) l_i l_j = d_{ij} - l_i l_j.$$

using eq. (4.10).

$$q^i{}_j = \gamma^{ik} q_{kj} = \delta^i_j - (1 - 2V) l^i l_j$$

is the projection operator onto the (co)tangent space of S.

Now I define the following coordinate basis for the tangent vector space in each point of Σ_0

$$\left(\frac{\partial}{\partial\rho}\right)^i := -l^i, \quad \left(\frac{\partial}{\partial\lambda}\right)^i := q^i{}_j \left(\frac{\partial}{\partial\theta}\right)^j, \quad \left(\frac{\partial}{\partial\sigma}\right)^i := q^i{}_j \left(\frac{\partial}{\partial\phi}\right)^j.$$

With this λ and σ are coordinates on S. If V is a tangent vector field with the components $\bar{V}^a$ associated with the coordinates (ρ, λ, σ) and V^a associated with the coordinates (r, θ, ϕ) then

$$V^a = J^a{}_b \bar{V}^b$$

where the Jacobi matrix is

$$(J^a{}_b) = \begin{pmatrix} -l^r & q^r{}_\theta & q^r{}_\phi \\ -l^\theta & q^\theta{}_\theta & q^\theta{}_\phi \\ -l^\phi & q^\phi{}_\theta & q^\phi{}_\phi \end{pmatrix}.$$

The components of cotangent vectors ω_a transform like

$$\bar{\omega}_a = J^b{}_a \omega_b$$

so

$$\bar{q}_{ab} = J^c{}_a J^d{}_b q_{cd}.$$

A computation with Mathematica shows that

$$\bar{q}_{ab} = \begin{pmatrix} 0 & 0 & 0 \\ 0 & r^2 & 0 \\ 0 & 0 & r^2 \sin^2\theta \end{pmatrix} + \dots$$

to lowest non-vanishing order in the perturbation parameters, so in eq. (9.26) we have to use the standard determinant on S^2, namely $r^4 \sin^2\theta$. Furthermore we have

$$d\lambda d\sigma = \bar{J}^{\lambda}_{\ a} \bar{J}^{\sigma}_{\ b} dx^a dx^b,$$

where $\bar{J}^b_{\ a}$ fulfills

$$\bar{J}^c_{\ b} J^b_{\ a} = \delta^c_a.$$

There is a first order $drd\theta$, a first order $drd\phi$ and a zeroth order $d\theta d\phi$ term. Because dr itself is of first order expressed in terms of $d\theta$ and $d\phi$ using eq. (9.24) there is only

$$d\lambda d\sigma = d\theta d\phi + \dots.$$

Hence the area of the apparent horizon is $16\pi M^2$ as in the unperturbed case to lowest order in perturbation theory.

9.2.3 Energy Formula

The radiated energy can be computed by means of eq. (7.2). For the 21-mode, the initial time-derivative of the Zerilli function is given by eq. (9.22) together with eq. (9.18). This can be written as

$$-i\dot{\Psi}_{21}(r) = \epsilon\Pi[f(r) + K_3 g(r)] \sin\chi,$$

where f and g are some functions. Because of the linearity of the Regge-Wheeler-Equation (7.1) the total radiated energy will be of the form

$$E_{21} = M\epsilon^2\Pi^2 \left(D_1^{21} + K_3 D_2^{21} + K_3^2 D_3^{21}\right) \sin^2\chi, \tag{9.27}$$

where D_1^{21} to D_3^{21} represent integrals over time and space which have to be evaluated numerically by means of the Regge-Wheeler code described in Section 8.2.

The same argument holds for the 20-mode, but it is more complicated, look at eq. (9.23) with eq. (9.20) and (9.19). The initial time-derivative of the Zerilli function can be written as

$$\dot{\Psi}_{20}(r) = \epsilon^2\mu[f_1(r) + K_1 f_2(r)] + \epsilon\Pi[f_3(r) + K_2 f_4(r)] \cos\chi$$

for some functions f_1 to f_4. Then the energy dependence on the parameters is

$$\begin{aligned} E_{20} = M\Big[& \epsilon^4\mu^2\left(D_1^{20} + D_2^{20} K_1 + D_3^{20} K_1^2\right) \\ & + \epsilon^3\Pi\mu\left(D_4^{20} + K_1 D_5^{20} + K_2 D_6^{20} + K_1 K_2 D_7^{20}\right)\cos\chi \\ & + \epsilon^2\Pi^2\left(D_8^{20} + D_9^{20} K_2 + D_{10}^{20} K_2^2\right)\cos^2\chi \Big]. \end{aligned} \tag{9.28}$$

9.2.4 Numerical Evolution

Test Run & Convergence

First one would like to see how the code, which was described and tested in Section 8.2, performs with these initial data. Fig. 9.3 shows Ψ_{20} for $\epsilon = 1$, $\Pi = 0.4$, $K_1 = K_2 = 0$ and $\chi = 0$. The inner boundary is at $x = 1.8$, the outer boundary at $x = 400.0$, there is a

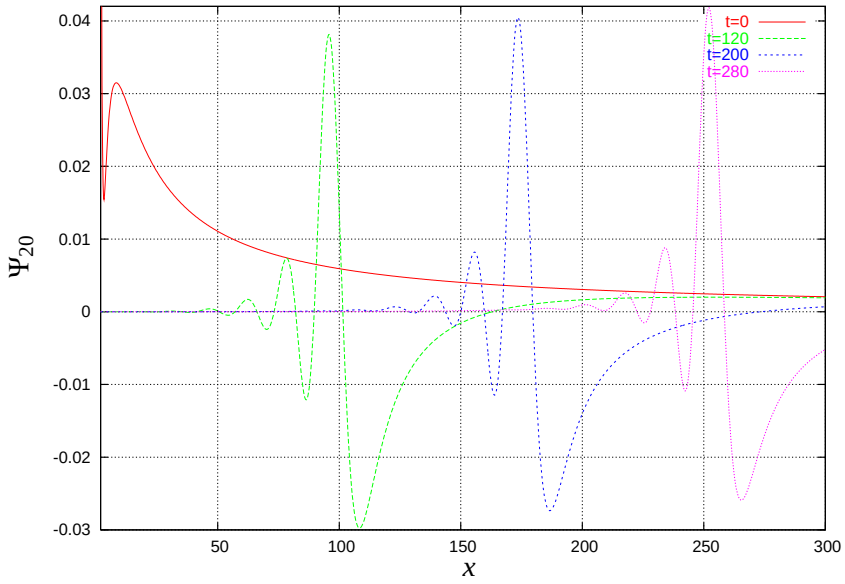

Figure 9.3: Zerilli-function at different times: $K_1 = K_2 = 0$, $\Pi = 0.4$, $\chi = 0$

spatial resolution of $\Delta x = 0.01$ and a CFL-factor of 0.5. The program was run until a time of $250M$.

In Fig. 9.4 on the next page I show a convergence plot at $t = 120M$. According to eq. (8.3) the two curves should sit on top of each other if there is fourth order convergence. First one notes that the difference of the RW-Zerilli-function for the three different resolutions is of the order 10^{-7} so the expected errors are relatively small. Second there actually is fourth order convergence (or a bit less) all the way from the inner boundary up to $x \approx 200$. Looking again at Fig. 9.3 one sees that this point corresponds to a region of the tail of the pulse where the curve flattens out. An interpretation for this point being problematic is that there might be little errors in the propagation speeds of the pulses for the three resolutions so phase errors might be significant there. Again like in the Gaussian test case in Section 8.2 I lose fourth order convergence within a zone propagating to the left from the outer boundary with the speed of light. In Fig. 9.5 on page 75 it is confirmed that this zone corresponds to first order convergence.

So if one wants fourth order convergence in the radiated energy, the point of energy extraction has to be causally disconnected from the outer boundary. In my case I chose $x_{extr} = 100$ which stays in the fourth order regime even after an evolution time of $250M$.

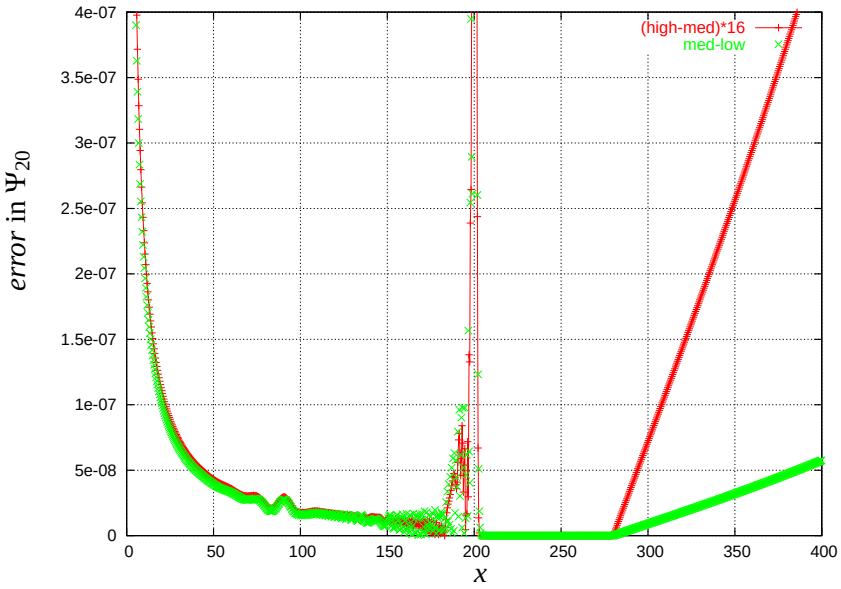

Figure 9.4: Convergence: $t = 120M$, $K_1 = K_2 = 0$, $\Pi = 0.4$, $\chi = 0$

Energy Formula

Coefficients By means of this code the thirteen coefficients in eq. (9.28) and (9.27) are to be determined. Because of the linearity of the evolution equation this can be done in (at least) thirteen runs with different parameters. I start with the 20-mode. The runs were done with the same resolutions as above with $M = 1$, $\epsilon = 1$, $\mu = 1$ and $\chi = 0$. The radiated energy was extracted at $x = 100$ after integrating over a run time of $250M$. In the same way described before I observed fourth order convergence both in the waveforms and in the energy for all runs. The difference in the energies for the three resolutions in each run was smaller than 0.1%; that is why I chose numbers with three digits. The following table shows the results

Π	K_1	K_2	E_{20}
0	0	0	$2.65 \cdot 10^{-4}$
0	100	0	$3.33 \cdot 10^{-3}$
0	−100	0	$7.72 \cdot 10^{-3}$
0.9	0	0	$4.19 \cdot 10^{-3}$
−0.9	0	0	$9.10 \cdot 10^{-3}$
0.9	100	0	$1.62 \cdot 10^{-2}$
−0.9	100	0	$2.34 \cdot 10^{-2}$
0.9	0	100	$1.46 \cdot 10^{-2}$
0.9	0	−100	$2.34 \cdot 10^{-3}$
0.9	10	10	$5.67 \cdot 10^{-3}$

Solving the system of equations for the unknown coefficients with Mathematica, I obtain

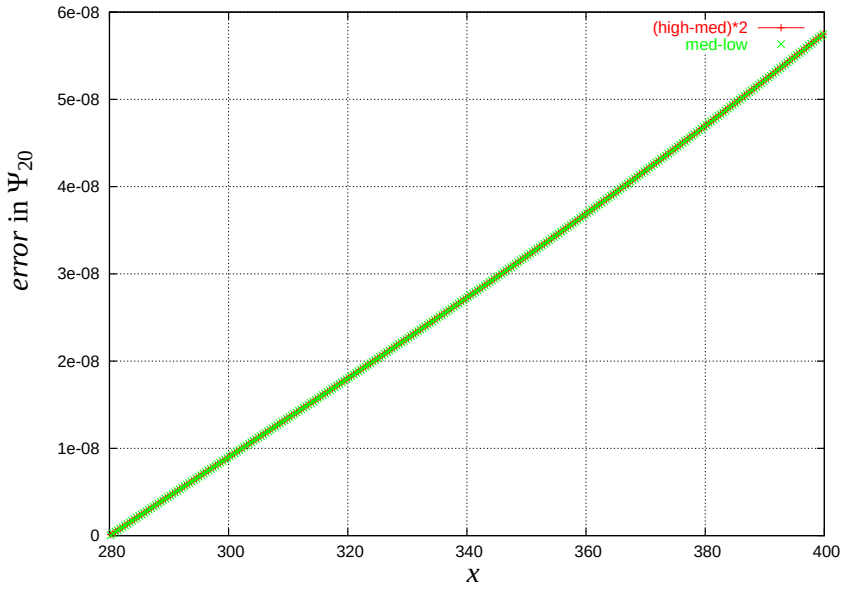

Figure 9.5: Convergence: $t = 120M$, $K_1 = K_2 = 0$, $\Pi = 0.4$, $\chi = 0$

D_1^{20}	$2.65 \cdot 10^{-4}$
D_2^{20}	$-2.20 \cdot 10^{-5}$
D_3^{20}	$5.26 \cdot 10^{-7}$
D_4^{20}	$-2.73 \cdot 10^{-3}$
D_5^{20}	$9.94 \cdot 10^{-5}$
D_6^{20}	$-2.16 \cdot 10^{-5}$
D_7^{20}	$1.07 \cdot 10^{-6}$
D_8^{20}	$7.88 \cdot 10^{-3}$
D_9^{20}	$9.97 \cdot 10^{-5}$
D_{10}^{20}	$5.28 \cdot 10^{-7}$

For the 21-mode there are only three coefficients to be determined. Thus three runs are sufficient with $\Pi = 1.0$

K_3	E_{21}
0	$3.16 \cdot 10^{-3}$
100	$1.49 \cdot 10^{-2}$
-100	$1.97 \cdot 10^{-3}$

So we have

D_1^{21}	$3.16 \cdot 10^{-3}$
D_2^{21}	$6.47 \cdot 10^{-5}$
D_3^{21}	$5.28 \cdot 10^{-7}$

Minima of Energy To understand the physical meaning of the free parameters and maybe be able to find initial data sets with a minimal amount of *artificial* gravitational waves, one wants to find out in what cases an extremal amount of energy is radiated. From the first

derivative with respect to Π of eq. (9.28) one finds that there exists a momentum $\Pi_{\min}$ which extremizes the energy of the 20-mode

$$\Pi^{20}_{\min} = -\frac{\epsilon\mu}{\cos\chi}\,\frac{D^{20}_4 + D^{20}_5 K_1 + \left(D^{20}_6 + D^{20}_7 K_1\right) K_2}{2\left(D^{20}_8 + K_2\left(D^{20}_9 + D^{20}_{10} K_2\right)\right)}.$$

The second derivative with respect to Π gives $2\epsilon^2(D^{20}_8 + D^{20}_9 K_2 + D^{20}_{10} K_2^2)\cos^2\chi$ which is positive $\forall K_2$, $0 \le \chi < \pi/2$ and $\epsilon > 0$ because it is positive for $K_2 = 0$ ($D^{20}_8 > 0$) and has no real roots. In Fig. 9.6 the energy curve is plotted for $K_1 = K_3 = 0$. The 21-mode is

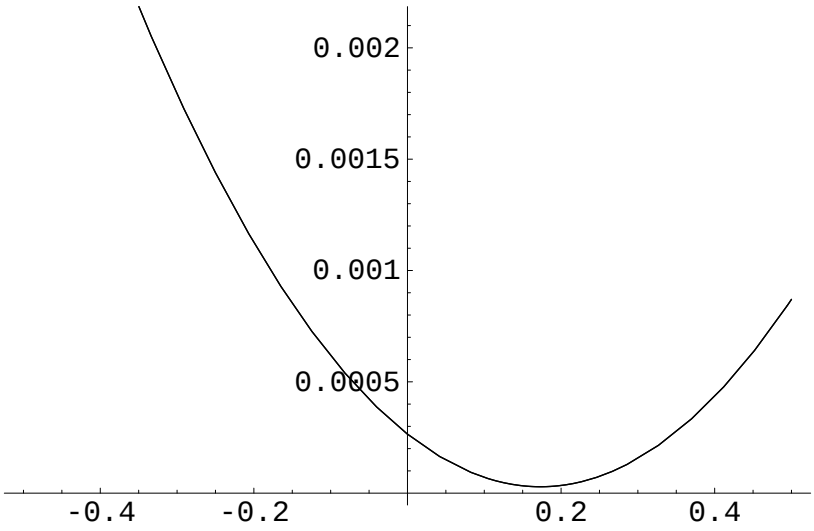

Figure 9.6: Energy vs. Π for $K_1 = K_3 = 0$

minimized by $\Pi = 0$, see eq. (9.27).

One can also ask the question if for a given Π the energy can be minimized by a special choice of K_1, K_2 and K_3. For the 21-mode there is a minimum at

$$K_3 = -\frac{D^{21}_2}{2D^{21}_3} = -61.3.$$

For the 20-mode there is no pair (K_1, K_2) which minimizes the energy except for $\Pi = 0$ (see [46]) because it turns out that the Hesse matrix is indefinite.

Quasi-Normal Ringing Due to lack of time I did not investigate the so called quasi-normal ringing. In [30] one can find a good overview. In general, small perturbations of a Schwarzschild black hole lead to a characteristic radiation and the frequency spectrum is closely related to the mass of the black hole. For the quasi-normal ringing of the close limit of two Misner black holes, see [42] and [7]. Comparing their results to Fig. 9.3 on page 73 it is very convincing that quasi-normal ringing is also present in my data.

9.3 Conclusions

This chapter has shown that it is possible to find analytic solutions of the linearized constraint equations with apparent horizons and asymptotical flatness. One is able to obtain Zerilli functions and evolve them, computing waveforms and the amounts of radiated energy.

In [7] similar things were done for boosted *Misner* black holes and the waveforms with the quasi-normal ringing dominating after some time look very similar to mine.

Initial data of black holes at some finite distance were evolved e.g. in [5]. For late times their waveforms are expected to be similar to those obtained with the close-limit approximation, which is in fact the case. After some time the quasi-normal ringing is dominant in the close-limit approximation as well as in the full non-linear approach. Nevertheless, at early times, it is possible that the close-limit approximation is very *artificial* in terms of gravitational waves entering or leaving the domain. The analysis in this thesis and in the papers cited before is not conclusive in this point. On the one hand I looked for minima of the outgoing radiation and it turns out that there is no such pair (K_1, K_2) for each ϵ and Π except for $\Pi = 0$ that minimizes it as was discussed above. The same should be done for ingoing radiation or alternatively one could evolve backwards in time, but I had to leave this out. On the other hand, I found the surprising result as in [7] that for each (K_1, K_2) one can find a Π leading to minimal energy radiation.

Of course initial data constructed as described in this thesis in the binary black hole close limit should not be considered as astrophysically relevant and thus one should not try to interpret too much. But on the one hand one can learn what can arise in binary black hole initial data sets in general and on the other hand they can serve as testbeds for full non-linear numerical codes. In contrast to that the far limits – which I do not discuss here – are physically relevant because they describe the weak interaction of black holes far away from each other where one has a lot of understanding by means of post-Newtonian theory.

9.4 Other Black Hole Systems

The boosted Schwarzschild like close limit was not the only black hole system which I considered. I chose it as an example to show what can be done with the new construction procedure of black hole initial data in the linear regime and because it was the first simple generalization of [46].

Another interesting system which I looked into is the binary Kerr like close limit where two black holes with opposite spin parameters are very close to each other so that the background metric is still the Schwarzschild one. It will be especially interesting to compare it to [39] where it was already discussed by means of a different construction of the Kerr-Schild null vector field.

Also the binary Schwarzschild far limit will be worth to consider on the one hand to compare it to post-Newtonian techniques and on the other hand to go one step beyond Section 5.7.1 where the *hard* limit of infinite separations was discussed.

Furthermore one can look at the particle limit, i.e. the limit where one black hole has a very small mass compared to the other. This could be compared to work by Zerilli [56] and to recent work by Bishop [9].

Part IV

Bishop’s Modification of the Kerr-Schild Ansatz [8]

Chapter 10

Modification of the Kerr-Schild Ansatz

The Kerr-Schild form of a metric is physically and mathematically nice as was pointed out before. Especially important is the fact that the Kerr metric can be brought to the Kerr-Schild form by a coordinate transformation (see Section 4.4) and I found a new procedure to construct the free part of the superposition of two Kerr like black holes in these coordinates described in Part II. One wants to modify this ansatz to avoid the problems with the Kerr-Schild constraint equations described in Chapter 6. To modify the ansatz we follow a similar route as in the original Kerr-Schild approach; we bring the Schwarzschild metric to a certain form very similar to the Kerr-Schild one to eventually *superpose* two Schwarzschild black holes in those new coordinates.

10.1 New coordinates for the Schwarzschild metric

Consider the Schwarzschild metric in isotropic coordinates eq. (3.3) so that the induced metric on a $t = const$-slice Σ is

$$ds^2 = \left(1 + \frac{m}{2\bar{r}}\right)^4 \left(d\bar{r}^2 + \bar{r}^2 d\theta^2 + \bar{r}^2 \sin^2\theta d\varphi^2\right)$$

and the extrinsic curvature $K_{ij} = 0$. By means of the coordinate transformation on Σ

$$\left(1 + \frac{m}{2\bar{r}}\right)^2 d\bar{r} = dr, \tag{10.1}$$

we obtain

$$\gamma_{ij} = \frac{d_{ij} - 2V l_i l_j}{1 - 2V}, \tag{10.2}$$

with d_{ij} the Euclidean (flat) 3-metric, $\mathbf{l} = \mathbf{e}_r$ the unit radial vector field and

$$V(r) = \frac{1}{2}\left(1 - \left(1 + \frac{m}{2\bar{r}}\right)^{-4} \frac{r^2}{\bar{r}^2}\right), \tag{10.3}$$

where from eq. (10.1)

$$r = \bar{r} + m \ln \frac{2\bar{r}}{m} - \frac{m^2}{4\bar{r}} + \frac{m}{2}. \tag{10.4}$$

The integration constant in this last equation has been chosen such that the event horizon is located at $r = \bar{r} = m/2$. On the event horizon we have $V = 15/32$.

Although the 3-metric is conformally related to a Kerr-Schild metric one has to keep in mind that the slicing is very different than the Kerr-Schild slicing: here the initial slice is an isotropic slice so it has the topology as described in Chapter 3 with Fig. 3.1.

10.2 Multiple Black Holes

Now, for the case of multiple time-symmetric ($K_{ij} = 0$) Schwarzschild like black hole initial data we can – in analogy with the Kerr-Schild ansatz in the special case described in Section 5.6 – introduce a potential $\Phi(\mathbf{r})$ and take l_i as its normalized (Euclidean) gradient, i.e.

$$\mathbf{l} = C\nabla\Phi$$

with C such that

$$d^{ij} l_i l_j = 1.$$

The potential Φ is chosen as

$$\Phi = \sum_i \frac{m_i}{|\mathbf{r} - \mathbf{r}_i|}.$$

The momentum constraints vanish identically and the Hamiltonian constraint can then be solved for the unknown function V. This is a so significantly different decomposition of the free and of the constrained part of the initial data than the York-Lichnerowicz conformal decomposition (Section 3.2) that there is hope that it might lead to very different data and one can learn much from systematic comparisons.

10.3 Constraint Equations

As a first step we only want to construct initial data with axial symmetry and – as was pointed out before – with time-symmetry. With the ansatz just described the momentum constraints vanish identically and the Hamiltonian constraint becomes a single quasi-linear partial differential equation for the only unknown function $V(r, \theta)$ in spherical coordinates defined by

$$(d_{ij}) = \mathrm{diag}(1, r^2, r^2 \sin^2\theta),$$

namely

$$\begin{aligned} c_{20} V_{,rr} + c_{11} V_{,r\theta} + c_{02} V_{,\theta\theta} + c_{1010} (V_{,r})^2 + c_{1001} V_{,r} V_{,\theta} \\ + c_{0101} (V_{,\theta})^2 + c_{10} V_{,r} + c_{01} V_{,\theta} + c_0 V = 0. \end{aligned} \tag{10.5}$$

The coefficients have been computed with both Mathematica and Maple and are functions of r, θ, V, Φ and higher derivatives of Φ. The coefficients of the principal part are

$$c_{20} = -2\frac{(1-2\,V)\;{\Phi_{,\theta}}^2 + 2\,r^2\,{\Phi_{,r}}^2}{(1-2\,V)\left({\Phi_{,\theta}}^2 + r^2\,{\Phi_{,r}}^2\right)}$$
$$c_{11} = -4\frac{(1+2\,V)\;\Phi_{,\theta}\,\Phi_{,r}}{(1-2\,V)\left({\Phi_{,\theta}}^2 + r^2\,{\Phi_{,r}}^2\right)}$$
$$c_{02} = -2\frac{2\,{\Phi_{,\theta}}^2 + r^2\;(1-2\,V)\;{\Phi_{,r}}^2}{r^2\;(1-2\,V)\left({\Phi_{,\theta}}^2 + r^2\,{\Phi_{,r}}^2\right)}$$

so that the determinant of the principal part [27] is

$$\Delta = c_{20}c_{02} - \frac{1}{4}c_{11}^2 = \frac{8}{r^2\;(1-2\,V(r,\theta))}.$$

This means that the equation is elliptic if $V < 1/2$ everywhere.

10.4 Boundary conditions

Because eq. (10.5) is elliptic it is now possible to control the solutions (if they exist) by means of proper boundary conditions; compare to what was said in Chapter 6.

Around each black hole (the inner boundary) we can set the minimal surface condition (1.8). Because we are on a time-symmetric initial slice $K_{ij} = 0$, it reduces to

$$0 = (\mathbf{e}_r)^i_{;i} = \Gamma^i{}_{ri} = \partial_r\left(\ln\sqrt{\det\gamma}\right)$$

for a coordinates sphere. With

$$\sqrt{\det\gamma} = \frac{r^2\sin\theta}{1-2V(r,\theta,\phi)}$$

we obtain the inner boundary condition

$$\partial_r\frac{r^2\sin\theta}{1-2V(r,\theta,\phi)}\bigg|_{r=r_{IB}} = 0. \tag{10.6}$$

The outer boundary can be assumed to be placed far away from the black holes so that the metric *practically* reduces to the single black hole one. Hence we can make use of the asymptotic behavior of the single Schwarzschild V_S eq. (10.3)

$$\lim_{r\to\infty} V_S(r) = \frac{m}{2r}\left(1 - 2\ln\frac{2r}{m}\right).$$

In the binary black hole case there is a point in between where l_i is not defined because $\nabla\Phi = 0$ there. To avoid a singularity (even if it is maybe only a coordinate singularity) we have to postulate that $V = 0$ there. To avoid numerical problems one is probably forced to use an excision region around this point and put meaningful data on its surface. This has to be further investigated in the future; more comments on the binary black hole problem below.

Chapter 11

Perturbation of the Schwarzschild Metric

11.1 Ansatz

As a first step in [8] we explored the case $\Phi = 1/r$ of a single Schwarzschild black hole with $m = 1$. We have already seen that its horizon is located at $r = 1/2$ with $V(1/2) = 15/32$. In this case we can use a simpler inner boundary condition than eq. (10.6) namely

$$V\left(r = \frac{1}{2}, \theta\right) = \frac{15}{32} + \epsilon P_n(\cos\theta) \tag{11.1}$$

to perturb the black hole with the n-th Legendre polynomial P_n. In principle the size of ϵ is only limited by the fact that to preserve ellipticity of eq. (10.5) we have to set

$$|\epsilon| < \frac{1}{32}.$$

On the outer boundary $r = r_{OB}$ we set $V(r, \theta)$ to its unperturbed Schwarzschild value eq. (10.3) which makes physical sense for some large r_{OB}, in principle $r_{OB} \to \infty$.

11.2 Linearized Analysis

For small ϵ we can neglect all terms of order ϵ^2. This linearized approach serves as a testbed for the full non-linear numerical computations below and to obtain an analytical expression of the York tensor. It turns out that the ansatz

$$V(r, \theta) = V_S(r) + \epsilon W(r) P_n(\cos\theta) \tag{11.2}$$

separates the linearized Hamiltonian constraint because the angular part of the equation is equal to that of the Laplace equation in spherical coordinates. To first order in ϵ, I found that one is left with an ordinary differential equation for $W(r)$

$$d_1 W''(r) + d_2 W'(r) + d_3 W(r) = 0 \tag{11.3}$$

where the coefficients are computed with Mathematica and Maple

$$
\begin{aligned}
d_1 =& -r^2\,(1-2\,V_S(r))^2,\\
d_2 =& r\,(1-2\,V_S(r))\,\Big(3-6\,V_S(r)+7\,r\,V_S'(r)\Big),\\
d_3 =& 1-\frac{n(n+1)}{2}+(3n(n+1)-8)\;V_S(r)-2\;(3n(n+1)-10)\;V_S(r)^2\\
&+4\;(n(n+1)-4)\;V_S(r)^3+7\,r^2\,V_S'(r)^2.
\end{aligned}
$$

The fact, that the Schwarzschild solution $V_S(r)$ eq. (10.3) itself is a solution of the Hamiltonian constraint, has been used in the derivation of eq. (11.3).

It seems to be difficult to find analytic solutions of eq. (11.3). That is why I used Mathematica to solve it numerically. Because eq. (10.4) cannot be solved for $\bar{r}$ analytically and $V_S(r)$ is given in terms of $\bar{r}$, the whole equation was transformed to the $\bar{r}$-coordinate using eq. (10.4) analytically. Then it was solved numerically with Mathematica respecting the boundary conditions described above, explicitly

$$W(\bar{r}=\frac{1}{2})=1, \quad W(\bar{r}=\bar{r}_{OB})=0$$

with $\bar{r}_{OB}$ the arbitrary position of the outer boundary. To be explicit I set $r_{OB}=10.0$ and produced the plots Fig. 11.1 for the first three Legendre Polynomials in terms of r.

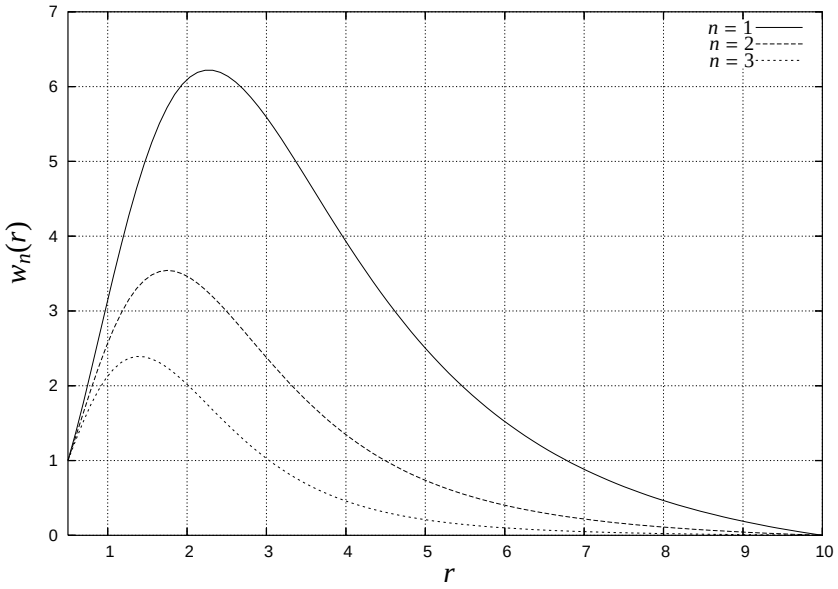

Figure 11.1: Solutions of the linearized Hamiltonian Constraint

11.3 York Tensor

In Chapter 3, I pointed out that there are problems with conformally flat black hole initial data. The motivation for these new data described in this part of the thesis was to obtain

new non-conformally flat data sets which might give new insights into binary black hole physics.

If the York tensor [22, 53]

$$Y_{ijk} = R_{ij;k} - R_{ik;j} + \frac{1}{4}(R_{,j}g_{ik} - R_{,k}g_{ij}) \tag{11.4}$$

does not vanish identically, then the initial slice is not conformally flat. It is sufficient to show that at least one component at one point of the first order York tensor is not zero. With Mathematica I found that

$$Y_{rr\theta} = \frac{2 - n(n+1)}{4\,r^2}\, W(r) P_n'(\cos\theta) + O(\epsilon^2)$$

using the fact that P_n fulfills the Legendre differential equation. So it is proven that these data are not conformally flat if $n > 1$.

11.4 Non-Linear Numerical Computations

11.4.1 Implementation

Here I solve the full non-linear Hamiltonian constraint eq. (10.5) numerically in the perturbed Schwarzschild case $\Phi = 1/r$ applying the boundary conditions eq. (11.1),

$$V(r,\theta)|_{r=r_{OB}} = V_S(r)$$

with $V_S(r)$ given by eq. (10.3) and due to symmetry

$$\left.\frac{\partial V}{\partial n}\right|_{\theta=0,\pi} = 0$$

where n is normal to the $\theta = 0, \pi$-surfaces.

I did the computations with second order finite differencing with the Cactus-Computational-Toolkit [1] and the TAT-Jacobi elliptic solver [47] which is an implementation of the **Jacobi Method** [34]. To solve (non-linear) elliptic partial differential equations

$$\text{Elliptic Operator(V)} = 0$$

using the Jacobi method one first gives an initial guess for the unknown function V chosen to be as close as possible to an actual solution of the elliptic equation. The program computes the left side of the equation which in general leads to a grid function, the so called **residual**, which is not zero everywhere. Then the program adds this residual (multiplied by an arbitrary but adapted factor) to the initial guess point-wise leading to a knew grid function V and after applying the elliptic operator again to a new residual grid function. If one continues like this, one effectively evolves V according to the equation

$$\text{Elliptic Operator(V)} = \frac{\partial V}{\partial t}$$

with an artificial time t. In many cases this parabolic equation converges to a steady state with $\partial V/\partial t = 0$ which is a solution of the original elliptic equation. Thus the Jacobi method is a very simple realization of a **relaxation method**.

For simplicity I implemented the θ-boundary conditions at $\theta = 0 + \eta, \pi - \eta$ with $\eta \ll 1$ and of the order of magnitude of the accuracy up to which eq. (10.5) is to be solved. This is necessary because at $\theta = 0, \pi$ there are coordinate singularities and it is – beside other techniques – also a common procedure to avoid numerical problems at the singular points for instance of the Laplace equation in spherical coordinates.

Because the Hamiltonian constraint is a non-linear elliptic partial differential equation the choice of the initial guess for $V(r, \theta)$ is crucial. A simple and *working* initial guess turns out to be the unperturbed Schwarzschild solution V_S eq. (10.3) plus a perturbation in terms of the nth Legendre polynomial whose amplitude decreases linearly from the inner to the outer r-boundary consistent with the boundary conditions above.

To actually compute $V_S(r)$ for the initial guess numerically, eq. (10.4) was solved for $\bar{r}$ by a numerical integration of eq. (10.1) which was then substituted into eq. (10.3).

The convergence of TAT-Jacobi is very slow mainly due to dominant non-linear terms in eq. (10.5) close to $r = 1/2$. So I first run the elliptic solver with the residual multiplied by $1 - 2V$, which is small near the horizon. This gives the solver the opportunity to get an accurate solution everywhere else, before in a second run, it solves the original equation without the factor. By means of this technique the convergence speed was increased significantly.

Results

Let us consider the case $n = 2$ which is the lowest Legendre polynomial leading to non-conformally flat data. I set $r_{OB} = 10$ and $\epsilon = 0.005$ for three different resolutions in r- and θ-direction.

	N_r	N_θ	Δ_r	Δ_θ	final resid. of eq. (10.5)
low	97	33	0.098	0.095	$4.0 \cdot 10^{-7}$
medium	193	65	0.049	0.048	$1.0 \cdot 10^{-7}$
high	385	129	0.025	0.024	$2.5 \cdot 10^{-8}$

With *final residual* I mean the residual of eq. (10.5) after the elliptic solver has finished. Fig. 11.2 on the following page shows the three plots together with the solution of the linearized Hamiltonian constraint. The three numerical plots show the difference $V(r, \theta) - V_S(r)$ normalized to unity at $r = 1/2$ for $\theta = 0.59$. The graphs suggest second order convergence which is confirmed by Fig. 11.3.

Nevertheless, it is obvious that the linearized solution is not the limit of infinite resolution. We have shown that our numerics show the right convergence, but it must still be understood why the linearized solution deviates so much from the numerical ones, although $\epsilon = 0.005 \ll 1$. The answer is that higher order terms get large close to the horizon. With Mathematica one is able to substitute the linearized solution back into the non-linear equation and see how well it is fulfilled. Although the linearized Hamiltonian constraint eq. (11.3) is satisfied up to an error of 10^{-6}, the error in the full non-linear equation is much bigger, Fig. 11.4 on page 87. Nevertheless, we see the correct second order behavior because the error decreases by a factor of 100 if ϵ is smaller by a factor of 10, i.e. $\epsilon = 0.0005$. This gives us a measure of how small ϵ should be in order to obtain an accurate linearized solution.

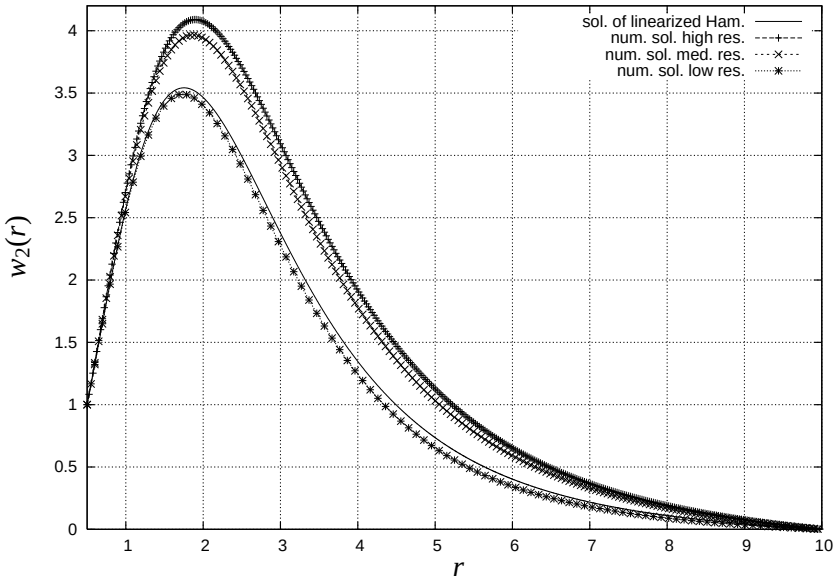

Figure 11.2: Linearized and full numerical solutions for $n = 2$, $\theta = 0.59$

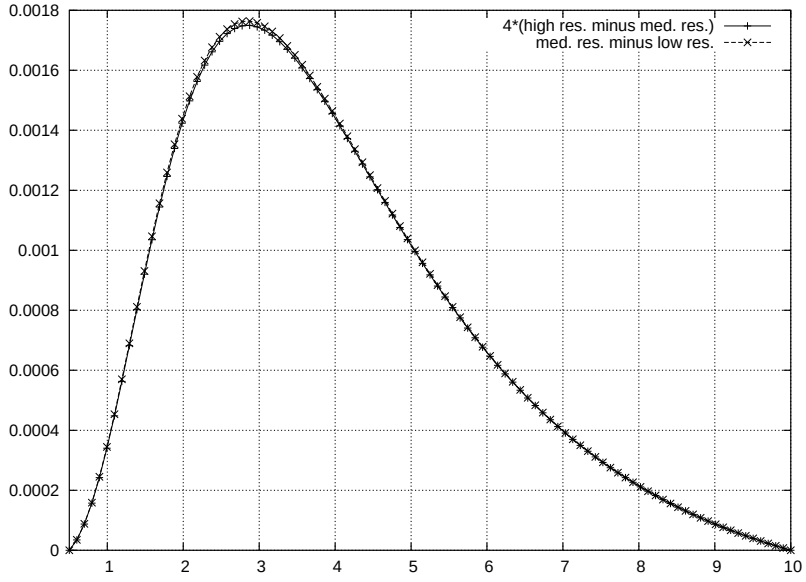

Figure 11.3: Confirmation of second order convergence in the case $n = 2$, $\theta = 0.59$

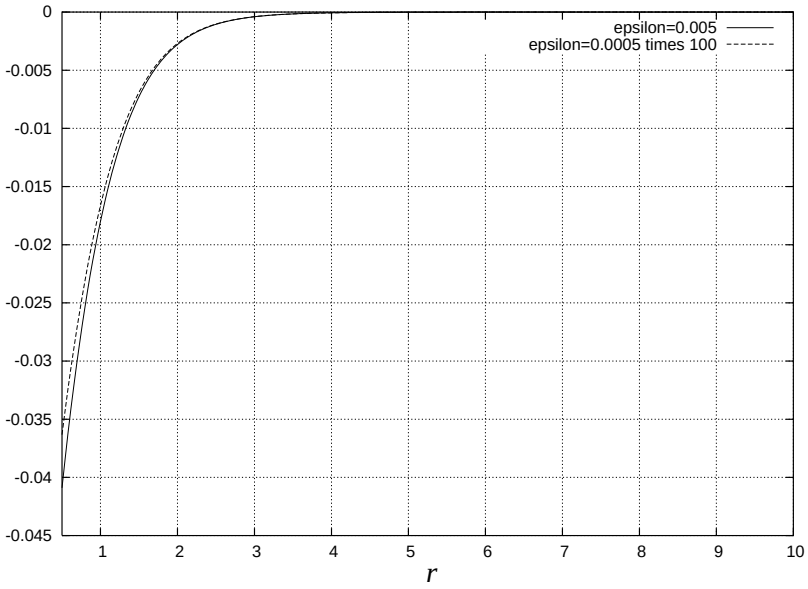

Figure 11.4: Residuum of eq. (10.5) for the linearized solution

Chapter 12

Future Work on the Modified Kerr-Schild Approach

In this part of the thesis I have described a modification of the Kerr-Schild ansatz (introduced in Part II of this thesis) for multiple Schwarzschild like black holes in the case of time-symmetry ($K_{ij} = 0$) using in analogy with the Kerr-Schild ansatz a normalized surface forming vector field l_i. The only non-vanishing constraint equation is the Hamiltonian constraint which has been worked out in the case of axisymmetry and turns out to be elliptic if the only unknown function $V < 1/2$. Then a specific perturbation of a single Schwarzschild black hole was investigated by linearizing the constraint equation on the one hand and by finding numerical solutions of the full non-linear constraint on the other hand. I have confirmed second order convergence of the numerical code and the nature of the deviation from the linearized solutions. Furthermore I argued that the initial data of this specific perturbation of Schwarzschild is not conformally flat.

Everything that was done up to now has to be considered as a first step which is needed to show that the procedure works in principle. The next steps will be first to evolve the initial data of the perturbed Schwarzschild black hole, measure the waveforms and radiated gravitational waves and especially to compare with the results of perturbed conformally flat Schwarzschild black holes; work is in progress. Second the binary Schwarzschild like black hole problem will be tackled. The basic problem for this has already been mentioned: the singularity of l_i between the black holes. With a little luck one can simply put that point between two grid points and obtains convergence of the elliptic solver without further effort. But it is more likely that one has to place an excision region around that point with meaningful data on its surface. Then there is the problem to find a working initial guess for the elliptic solver. When the black holes are far away from each other it might be sufficient to superpose two isolated black solutions linearly for this, but this may lead to problems at the singular point. Furthermore for the equal mass black hole case there is a symmetry surface right between the black holes where a symmetry boundary condition has to be applied when solving the Hamiltonian constraint. But in spherical coordinates this boundary is curved which is difficult to implement numerically. This will make it necessary to use sophisticated interpolation techniques but fortunately these have already been implemented into Cactus. If a solution for the binary black hole problem can be obtained it should be compared with conformally flat initial data in terms of radiated gravitational energies and waveforms.

Part V

Final Summary & Conclusions

In this thesis I worked on Bishop's way [10] of constructing multiple black hole initial data because I was motivated to obtain very different initial data sets than those using the standard conformal decomposition (Chapter 3).

Because the construction of the free part of the initial data had only been worked out for certain cases, I invented a new general procedure (Chapter 5.4) and applied it. But the Kerr-Schild constraint equations turned out to be problematic what had not been pointed out in [10], basically because this system of partial differential equations is not elliptic; it is a Cauchy problem in space, so there is no control over the outer (or the inner) boundary behavior of the solutions. Explicitly this means that it is possible (at least if the spatial part of l_μ is surface forming) to guarantee existence of apparent horizons, but one cannot be sure to obtain asymptotically flat solutions. Nevertheless, in the linear regime (Part III), i.e. when solutions are considered which are only a little perturbation of the Schwarzschild metric, one has analytical control and one can find explicit solutions of the linearized constraints with the right asymptotical behavior. As a special example I considered a system of two very close black holes with vanishing spin-parameter which are infinitesimally boosted in an arbitrary direction. This is a model for the late stages of a binary black hole coalescence. Although I could not draw the conclusion that the Kerr-Schild close-limit initial data are an astrophysically relevant model because it was not conclusive how much *artificial* gravitational radiation is on the initial slice, by evolving the data one could see the characteristic quasi-normal ringing already found by [42] and [7] before in the case of Misner black holes.

In the linear regime, many more interesting systems can be studied which I had to skip due to lack of time; suggestions are given in Section 9.4.

Beyond the linear regime, the Kerr-Schild ansatz has to be modified to make it useful for numerical relativity. One possible way is described in Part IV and leads to an elliptic Hamiltonian constraint in the case of time- and axisymmetry. As a first step it was applied for a special perturbation of a Schwarzschild black hole and one could show that these data are not conformally flat. Work is in progress to evolve these data and compare to other perturbations of the Schwarzschild metric. Furthermore, I am working on the binary black hole problem in this framework. Problematic are the singular point of l_i and the curved symmetry boundary, see above.

The modification above is not the only possible one. One can also think of constructing a Kerr-Schild metric as the conformal metric and then use the standard conformal decomposition. This would lead to elliptic constraints and naturally to not conformally flat data. Because up to now we are only able to control the Kerr-Schild constraint equations in the linear regime, one possibility would be to use the analytic solution of the far-limit approximation which has to be worked out, i.e. two very far separated black holes. Such a conformal metric would be a solution of the constraints alone if the separation is big enough and the conformal factor would be close to one everywhere; it would act as a correction factor when the black holes are closer. A similar procedure has been used in [50] for post-Newtonian initial data.

In summary, there are a number of options to make use of the Kerr-Schild ansatz. But before one can do systematic comparisons and say which initial data set is better in a certain situation than another, one has to obtain a binary black hole solution. After having finished this thesis these kind of conclusions cannot be drawn yet.

Bibliography

[1] 'Cactus Computational Toolkit'. URL `http://www.cactuscode.org/`

[2] 'Gnuplot'. URL `http://www.gnuplot.info/`

[3] **A. A. Abramovici et al.** 'Ligo: The laser interferometry gravitational-wave observatory'. *Science*, 256, p. 325, 1992

[4] **G. Allen, K. Camarda and E. Seidel**. 'Evolution of Distorted Black Holes: A Perturbative Approach'. 1998. `gr-qc/9806014`

[5] **P. Anninos, D. Hobill, E. Seidel, L. Smarr and W. Suen**. 'Head-on collision of two equal mass black holes'. *Phys. Rev. D*, 52, pp. 2044–2058, 1995

[6] **A. Ashtekar and B. Krishnan**. 'Dynamical horizons and their properties'. *Phys. Rev. D*, 68, no. 104030, 2003

[7] **J. Baker, A. Abrahams, P. Anninos, S. Brandt, R. H. Price, J. Pullin and E. Seidel**. 'The collision of boosted black holes'. *Phys. Rev. D*, 55, pp. 829–834, 1997

[8] **N. Bishop, F. Beyer and M. Koppitz**. 'Black hole initial data from a non-conformal decomposition'. October 2003. `gr-qc/0310011`

[9] **N. Bishop, R. Gomez, S. Husa, L. Lehner and J. Winicour**. 'A numerical relativistic model of a massive particle in orbit near a Schwarzschild black hole'. *Phys. Rev. D*, 68, no. 084015, 2003

[10] **N. Bishop, R. Isaacson, M. Maharaj and J. Winicour**. 'Black Hole data via a Kerr-Schild approach'. *Phys. Rev. D*, 57, no. 10, p. 6113, 1998

[11] **S. Bonanos**. 'Riemannian geometry & tensor calculus'. URL `http://www.inp.demokritos.gr/~sbonano/SB.html`

[12] **J. M. Bowen and J. W. York**. 'Time-asymmetric initial data for black holes and black-hole collisions'. *Phys. Rev. D*, 21, no. 8, April 1980

[13] **S. Brandt and B. Brügmann**. 'A simple construction of initial data for multiple black holes'. *Phys. Rev. Lett.*, 78(19), pp. 3603–3609, May 1997

[14] **S. Brandt and E. Seidel**. 'The Evolution of Distorted Rotating Black Holes III: Initial Data'. *Phys. Rev. D*, 54, pp. 1403–1416, 1996

[15] **D. R. Brill and R. W. Lindquist**. 'Interaction energy in geometrostatics'. *Phys. Rev.*, 131(1), pp. 471–476, July 1963

[16] **S. Chandrasekhar**. *The Mathematical Theory of Black Holes*. Oxford University Press, New York, 1983

[17] **G. B. Cook**. 'Initial data for numerical relativity'. *Living Rev. Relativity*, 3, no. 5, 2000. URL `http://www.livingreviews.org/lrr-2000-5`

[18] **T. Damour, P. Jaranowski and G. Schaefer**. 'On the determination of the last stable orbit for circular general relativistic binaries at the third post-Newtonian approximation'. *Phys. Rev. D*, 62, no. 084011, 2000

[19] **B. deWitt**. 'Quantum theory of gravity i., the canonical theory'. *Phys. Rev.*, 160, no. 5, August 1967

[20] **P. Diener**. 'A new general purpose event horizon finder for 3d numerical spacetimes'. *Class. Quant. Grav.*, 20, pp. 4901–4918, 2003

[21] **A. Einstein and N. Rosen**. 'The particle problem in the general theory of relativity'. *Phys. Rev.*, 48, p. 73, July 1935

[22] **L. P. Eisenhart**. *Riemannian Geometry*. Princeton University Press, 1926

[23] **A. Garat and R. H. Price**. 'Nonexistence of conformally flat slice of the Kerr spacetime'. *Phys. Rev. D*, 61, no. 124011, May 2000

[24] **R. Gleiser, O. Nicasio, R. Price and J. Pullin**. 'Second order perturbations of a Schwarzschild black hole'. *Class. Quant. Grav.*, 13, pp. L117–L124, 1996

[25] **M. Gürses and F. Gürsey**. 'Lorentz covariant treatment of the Kerr-Schild geometry'. *J. Math. Phys.*, 16, no. 12, December 1975

[26] **S. W. Hawking and G. F. R. Ellis**. *The large scale structure of space-time*. Cambridge University Press, 1973

[27] **F. John**. *Partial Differential Equations*. Applied mathematical sciences. Springer, 1982

[28] **R. Kerr**. 'Gravitational field of a spinning mass as an example of algebraically special metrics'. *Phys. Rev. Lett.*, 11, no. 5, September 1963

[29] **S. Klioner**. 'EinS'. URL `http://rcswww.urz.tu-dresden.de/~klioner/eins.html`

[30] **K. Kokkotas and B. Schmidt**. 'Quasi-normal modes of stars and black holes'. *Living Rev. Relativity*, 2, 1999. URL `http://www.livingreviews.org/lrr-1999-2`. Cited on 19 Jan 2004

[31] **D. Kramer, H. Stephani and E. Herlt**. *Exact solutions of Einstein's field equations*. Cambridge University Press, 1980

[32] **H. Kreiss and J. Lorenz**. *Initial-Boundary Value Problems and the Navier-Stokes Equations*. Academic Press, 1989

[33] **L. Landau and E. Lifshitz**. *The Classical Theory of Fields*, volume 2 of *Course of Theoretical Physics*. Butterworth and Heinemann, 1975

[34] **H. P. Langtangen**. *Computational Partial Differential Equations*, chapter D.3. Lecture Notes in Computational Science and Engineering. Springer, 1991

[35] **R. Lind and E. Newman**. 'Complexification of the algebraically special gravitational fields'. *J. Math. Phys.*, 15, no. 7, December 1974

[36] **R. A. Matzner, M. F. Huq and D. Shoemaker**. 'Initial data and coordinates for multiple black hole systems'. *Phys. Rev. D*, 59, no. 024015, pp. 1–6, January 1999

[37] **C. W. Misner**. 'The method of images in geometrostatics'. *Ann. Phys. (N.Y.)*, 24, pp. 102–117, October 1963

[38] **C. W. Misner, K. S. Thorne and J. A. Wheeler**. *Gravitation*. Freeman, San Francisco, 1973

[39] **C. Moreno, D. Nunez and O. Sarbach**. 'Kerr-Schild type initial data black holes with angular momenta'. *Class. Quantum Grav.*, 19, pp. 6059–6073, November 2002. `gr-qc/0205060`

[40] **R. Penrose**. *Ann. N.Y. Acad. Sci.*, 224, no. 125, 1973

[41] **W. Press, S. Teukolsky and W.T.Vetterling**. *Numerical Recipes in FORTRAN*. Cambridge University Press, 1992

[42] **R. H. Price and J. Pullin**. 'Colliding Black Holes: The Close Limit'. *Phys. Rev. Lett.*, 72, pp. 3297–3300, 1994

[43] **S. Reddy and L. Trefethen**. 'Stability of the method of lines'. *Numerische Mathematik*, 62, pp. 235–267, 1992

[44] **T. Regge and J. A. Wheeler**. 'Stability of a Schwarzschild singularity'. *Phys. Rev.*, 108, no. 4, November 1957

[45] **O. Sarbach and M. Tiglio**. 'Gauge-invariant perturbations of Schwarzschild black holes in horizon-penetrating coordinates'. *Phys. Rev. D*, 64, no. 084016, September 2001

[46] **O. Sarbach, M. Tiglio and J. Pullin**. 'Close limit evolution of Kerr-Schild type initial data for binary black holes'. *Phys. Rev. D*, 65, no. 064026, 2002

[47] **E. Schnetter**. 'TATJacobi'. URL `http://www.tat.physik.uni-tuebingen.de/~schnette/tat-arrangement/index.html`

[48] **S. Teukolsky**. 'Perturbation of a Rotating Black Hole. I. Fundamental Equations for Gravitational, Electromagnetic, and Neutrino-Field Perturbations'. *Astrophysical Journal*, 185, pp. 635–647, October 1973

[49] **J. Thornburg**. 'Finding Apparant Horizons in Numerical Relativity'. *Phys. Rev. D*, 54, pp. 4899–4918, 1996. gr-qc/9508014

[50] **W. Tichy, B. Bruegmann, M. Campanelli and P. Diener**. 'Binary black hole initial data for numerical general relativity based on post-Newtonian data'. *Phys. Rev. D*, 67, no. 064008, 2003

[51] **A. Trautmann**. 'On the propagation of information by waves'. In 'Recent Developments in General Relativity', Pergamon Press, 1962

[52] **R. Wald**. *General Relativity*. University of Chicago Press, 1984

[53] **J. W. York**. 'Gravitational degrees of freedom and the initial-value problem'. *Phys. Rev. Lett.*, 26, pp. 1656–1658, 1971

[54] **J. W. York**. 'Initial Data for Collisions of Black Holes and Other Gravitational Miscellany'. In **C. R. Evans, L. S. Finn and D. E. Hobill**, editors, 'Frontiers in Numerical Relativity', pp. 89–109. Cambridge University Press, 1989

[55] **J. W. York and T. Piran**. 'The initial value problem and beyond'. In **R. A. Matzner and L. C. Sheply**, editors, 'Spacetime and Geometry, The Alfred Schild Lectures', University of Texas Press, Austin, 1982

[56] **F. J. Zerilli**. 'Gravitational field of a particle falling in a Schwarzschild geometry analyzed in tensor harmonics'. *Phys. Rev. D*, 2, no. 10, November 1970

Acknowledgements

I would like to thank Prof. Gernot Münster to recommend the Albert-Einstein-Institut to me, to make it possible to get into touch with Prof. Seidel and to supervise me in Münster.

I thank Prof. Edward Seidel for supervising me at the Albert-Einstein-Institut with many stimulations for my work and to let me participate in a couple of conferences all over the world.

I thank Dr. Peter Diener from the Albert-Einstein-Institut for giving the very interesting topic and basic ideas of my thesis, to help me with my daily work and answer my daily questions.

I would also like to thank Prof. Nigel Bishop for letting me participate in his project and giving me the chance to publish my first paper with him.

Furthermore I say thanks to Dr. Sergio Dain, Dr. Manuel Tiglio and Dipl-Phys. Michael Koppitz for fruitful discussions.

Eidesstattliche Erklärung

Hiermit versichere ich, dass ich die vorliegende Arbeit selbstständig angefertigt und die benutzten Hilfsmittel durch Zitate kenntlich gemacht habe.

Datum Unterschrift